Democratic and Popular Republic of Algeria
Ministry of Higher Education and Scientific Research

University Echahid Hamma Lakhdar of EL-OUED

Faculty of Technology

Order N°:
Series:

Department of Mechanical Engineering

Thesis with a view to obtaining the doctorate degree in Mechanical Engineering

Specialty: Energetic

SUBJECT OF THE THESIS

Elaboration and Characterization of Copper Oxide Thin Films on Zinc Oxide Substrates (CuO / ZnO) by Chemical Bath

By:

ALLAG Nassiba

Defended on: 23/09/2020

Jury committee:

President	Ali CHEMSA	MCA	University of El-Oued
Thesis Director	Boubaker BEN HAOUA	Pr	University of El-Oued
Thesis Co-director	Chahinez SIAD	Pr	University of Biskra
Examiners	Abdelouahad CHALA	Pr	University of Biskra
	Saâd RAHMANE	Pr	University of Biskra
	Yacine AOUN	MCA	University of El-Oued
Invited	Omar BEN MYA	MCA	University of El-Oued

Academic year
2019/2020

République Algérienne démocratique et Populaire
Ministère de l'Enseignement Supérieur et de la Recherche Scientifique

Université Echahid Hamma Lakhdar d'El Oued
Faculté de la Technologie

Ordre N°:
Séries:

Département de Génie Mécanique

Thèse en vue de l'obtention du diplôme de doctorat en Génie Mécanique

Spécialité: Énergétique

SUJET DE LA THÉSE

Elaboration Et Caractérisation Des Couches d'Oxyde de Cuivre Sur des Substrats d'Oxyde de Zinc par Bain Chimique

Par:

ALLAG Nassiba

Soutenue le: 23/09/2020

Comité du jury:

Président	Ali CHEMSA	MCA	Université d' El-Oued
Directeur de thèse	Boubaker BEN HAOUA	Pr	Université d' El-Oued
Co- directeur de thèse	Chahinez SIAD	Pr	Université de Biskra
Examinateurs	Abdelouahad CHALA	Pr	Université de Biskra
	Saâd RAHMANE	Pr	Université de Biskra
	Yacine AOUN	MCA	Université d' El-Oued
Invité	Omar BEN MYA	MCA	Université d' El-Oued

Année universitaire
2019/2020

Abstract

The present work deals with the deposition of CuO thin films on substrates of zinc oxide by a simple and cheap technique such as chemical bath (CB). In first, a set of ZnO thin film was prepared using optimized spray pyrolysis conditions in order to devote the films for ions copper adsorption from aqueous solution. Two sources (zinc acetate and zinc chloride) are considered as deposition parameters. $LaCl_3$ $7H_2O$ was used with different rate of doping.The Structural, morphological and optical results confirm that the films are ZnO hexagonal wurtzite structure with a strong orientation along (002) with excellent optical properties. Further, the application of thin films as adsorbent was studied by Cu(II) adsorption from aqueous solution 0.2M. The obtained ZnO:La 1wt .% films are an effective adsorbent for removing Cu(II) with high adsorption capacity (87%). Thin films of copper oxide were obtained after annealing the ZnO:La substrates at temperature ranging between 200 - 350 °C. Structural, morphological, and optical characterizations were performed on the CuO films. The structural analysis of the later shows that the obtained films are polycrystalline, they exhibit a monoclinic structure. The preferential orientation is strongly related to the experimental parameters studies. From the optical characterization, it was inferred that the deposited films have suitable optoelectronic properties for the photovoltaic applications since they present a good absorption in the visible range .

Keywords: Zinc, thin films, XRD, UV-Visible, spray pyrolysis, oxide, copper, heavy metal, chemical bath.

الملخص:

موضوع الرسالة يتناول تحضير ودراسة الشرائح الرقيقة أكسيد النحاس (CuO) باستعمال تقنية سهلة وبسيطة و التي تتمثل في تقنية الحمام الكيميائي (Bath Chemical BC) . فى الجزء الاول من هذا العمل قمنا بتحضير سلسلة من العينات أكسيد الزنك (ZnO) و المحضرة بطريقة الرش الحراري (Spray pyrolysis SP) بتغيير الشروط التجريبية من اجل إيجاد أفضل الشروط التي تؤدى إلى شرائح ذات خصائص جيدة حيث يمكن استعمالها في امتصاص أيونات النحاس في محلول الماء. الوسائط التي قمنا بدراستها كانت على التوالي : نسبة التطعيم و نوعية الملح الأولي . تؤكد نتائج الخصائص الهيكلية والمورفولوجية والضوئية أن أكسيد الزنك (ZnO) له بنية سداسية Wurtzite مع نمو تفضيلي قوي في الاتجاه (002) وكذلك جودة بلورية عالية مع خاصية بصرية ممتازة . علاوة على ذلك ، تمت دراسة تطبيق الشرائح الرقيقة كممتز بواسطة امتزاز(Cu II) من المحلول المائي. إن ركيزة.ZnO: La1wt ٪ عبارة عن ممتز فعال لإزالة (Cu II) بسعة امتصاص عالية. بعد تلدين امساند عند درجة حرارة تتراوح بين 200 إلى 350 درجة مئوية. حصلنا على شرائح رقيقة من أكسيد النحاس . تم إجراء ودراسة الخصائص البنيوية, المورفولوجية والضؤية على شرائح CuO . الخصائص البنيوية وضحت أن التركيب البلوري للشرائح كان ذو تركيبة أحادية (monoclinique) متعددة التبلور بينما الاتجاه البلوري المفضل يتعلق بشروط التحضير. من نتائج التوصيف الضوئي ، استنتجنا أن الشرائح المودعة لها خصائص الكتروضوئية مناسبة للتطبيقات الكهروضوئية لأنها تتميز بامتصاص جيد في النطاق المرئي.

الكلمات المفتاحية:

زنك ، شريحة رقيقة ، انعراج الأشعة السينية ، مرئي للأشعة فوق البنفسجية ، الرش الحراري ، أكسيد ، نحاس ، معدن ثقيل ، حمام كيميائي

ABBREVIATIONS

TCO	Transparent conductive oxide
PVD	Physical Vapor Deposition.
CVD	Chemical Vapo rDeposition.
E_g	Optical band gap(eV)
μ	Mobility($cm^2/(V.s)$)
ρ	Electrical resistivity(Ω.cm).
σ	Electrical conductivity$S.cm^{-1}$or$\Omega^{-1}.cm^{-1}$
n	Carrier concentration cm^{-3}
JCPDS	Jointe Commette Powder Diffraction System.
XRD	X-Ray Diffraction.
SEM	Scanning Electron Microscope.
FTIR	Fourier Transform Infra-Red.
E_{00}	Urbach energy [meV]
FWHM	Full Width at Half Maximum
W-H	Williamson–Hall.
RF	Radio frequency
LED	light-emitting diode

First thanks to ***ALLAH*** for his grace

and for this help to let me completing

my research thesis.

Acknowledgements

I would like to thank my dear father ***Mr. Allag Abdelkrim***, professor at the University of El oued , could not have imagined having a better advisor and mentor for my Ph.D study. I attribute the level of my PhD degree to his encouragement and effort and without him this thesis, too, would not have been completed or written.

I would like to thank my advisor Prof***. Mr. Ben haoua boubaker*** for the continuous support of my Ph.D study and research, for his patience, motivation, enthusiasm, and immense knowledge. His guidance helped me in all the time of research.

I would like also to thank. ***M^{me}. Siad Chahinez,*** professor at the University of Biskra , who has supported me throughout my thesis with her patience and knowledge whilst allowing me the room to work in my own way. I have been amazingly fortunate to have a second advisor who gave me the freedom to explore on my PhD thesis and at the same time the guidance to recover when my steps faltered.

For most, I would like to express my sincere gratitude to thank the director of the laboratory of Physics Thin Films and Applications ***Mr. Chala Abdelouahad***, professor at the University of Biskra ,for the confidence he has placed in me by welcoming me into his laboratory and for his valuable advice and encouragement which enabled me to complete this work. He put at my disposal all the means available in the laboratory and for his acceptance to judge this modest work.

Doctor ***Mr. Chemsa Ali*** kindly agreed to chair the committee jury and to judge this work. I ask him to find here the expression of my sincere thanks.

I address my thanks to ***Mr. Saâd Rahmane***, professor at the University of Biskra, for agreeing to be an examiner for my thesis. I thank him for giving me the benefit of his scientific skills and experiences on thin films and the semiconductor during my studies and pleasant moments of discussion.

I thank to ***Mr. Yacine Aoun ,*** Lecturer at University of El oued ,for his acceptance to judge this modest work.

I great to thank ***Mr. Ben Mya Omar***, Lecturer at University of El oued, who agreed to participate in this jury as an invited member.

The state-of-the equipment and facilities provided by biskra University, has played a major part in achieving my research goals. As such, I would like to thank the technical who work hard to keep these facilities operational. Specifically, ***Mr. Gasmi Brahim & M^{me}. Touhami hanane*** of the Laboratory of Physics Thin Films and Applications, Biskra University for facility their technical expertise and assistance throughout the duration of my candidature.

A big thank you my dear friends for their support, their kindness and their warm welcome during these unforgettable years, with whom I shared good times: ***Dr. Gherbi Aicha, Dr. hafidha Terea, Dr. Laila Segueni, Dr. khaoula Zaiz, Dr. Karima Beloul.***

Finally, I great to thank my family, especially my heart mum, for her support **I love you my life.**

DEDICATION

To my dear grandmother's memory

and a spirit

“ Mostefaoui Mabrouka “

May she rest in peace

Contents

Figures Caption

Chapter 2

Chapter 3

Figures Caption

Figures Caption

Chapter 4

Figures Caption

Tables Caption

Chapter 2

Chapter 3

Chapter 4

Tables Caption

INTRODUCTION

Chapter 1

INTRODUCTION

The two majors and the most problems in our daily life is the pollution of the environment and increasing demand for energy and reduction of hydrocarbons resources that have gone from abundance to depletion ending by environmental problems, economic crises and wars for the simple reason that supply no longer follows demand.

Many research groups have explored several nanoparticles based on semiconductors oxides for heavy metals removal because of the ease of modifying their surface functionality and their high surface area to volume ratio for increased adsorption capacity and efficiency and with the same nanoparticles, the renewable energy production is another ultimate target to achieve with high efficiency and cost effectiveness.

Recently, release of pollutants such as heavy metal ions to the environment becomes one of the most important problems for soil and water. Fishing, electro plating, pigments, mining are different sources for release of heavy metal ions to the environment [1-8]. Different methods were developed to remove the heavy metal ions from aqueous medium such as precipitation, reverse osmosis and ion exchange. The disadvantage of precipitation method is production of sludge that needs further processing after precipitation which is an expensive method [7-11]. The application of nano-structured materials [12,13] as adsorbent is one of the best methods reported for removing of pollutant for increased adsorption capacity and efficiency.

Renewable energies also have emerged as an alternative solution to this problem, and solar energy more precisely remains an excellent solution because the sun is an impressive source of energy, which supplies the earth with 8,000 times more energy than she does not need it. It will therefore become ever more important in the future as an alternative energy source.

In the actual thin film solar cells achieve high efficiencies using very expensive rare earth minerals or contain toxic elements, respectively [1]. Alternatively, the development of earth-abundant inorganic absorbers has received great interest [2-5]. Most of these based compounds are Cu-,Fe-,Zn or Sn which are low-cost. Among them, oxide semiconductors are very attractive because they are chemically and environmentally stable and their synthesis process is relatively easy. However, it is well known that many problems are facing oxide semiconductors is the inability to produce stable p-type oxides.

Goals and objectives

Finding a new and highly efficient nano-material or crystalline thin film technologies that promise a bright future for photovoltaic energy and for the adsorption of heavy metals from waste water is the main objective of this work.

The various semiconductor materials used are ZnO, TiO_2, and SnO_2. However, zinc oxide (ZnO) is a favorite semiconductor among researchers for the possibility of utilizing it in different applications like gas sensors, light emitting diodes, lasers, thin film transistors, solar cells and photo catalytic degradation [19-24]. Besides, ZnO is a unique material that can be synthesized in several forms of nanostructures such as rods, wires, belts, flowers, hexagons, towers, spheres, tubes and pyramids with extraordinary physical properties by using appropriate physical or chemical techniques [25-27]. Thus, the special characteristics of ZnO motivated us to work on it. Further, though the thin film form of ZnO can be obtained by several fabrication techniques (sputtering, thermal evaporation, sol-gel, spray pyrolysis, laser ablation, etc.), we picked spray pyrolysis since it offers numerous advantages: simple exploratory setup, reproducibility, cost and time effective [28-31].

We are also interested in the new trend that is nanotechnology and the formation of nano crystals from the two of the most used Zn precursors to obtain ZnO films by spray pyrolysis are zinc acetate and zinc chloride undoped and doped lanthanum where used to grow zinc oxide(ZnO).

We found that even though the final product of different Zn precursors is ZnO, but the properties of the sprayed films were different and have a strong impact on the final properties. The combination of high electrical conductivity and transparency is not always possible in intrinsic stoichiometric oxides; however, it is investigated by producing them with a non-stoichiometric composition or by adding appropriate dopants [32]

In this work, we discuss the importance and the impact of the type of zinc precursor and the molar level of the solution for the deposition of ZnO thin films by spray pyrolysis, on their structural, morphological, optical and photocatalytic characteristics. X-ray diffraction, UV-Vis absorption and FT-IR spectroscopy, scanning electron microscopy (SEM), were used for physical and chemical characterizations.

The final purpose of our present work is to utilize the prepared thin films of micro-structured zinc oxide doped lanthum for the adsorption of copper ions from aqueous solution and to produce stable p-type CuO oxides after annealing treatment .In order to optimize the

adsorption process, we studied also the effect of the temperature and time on the removal of heavy metal ions (copper ions).

This thesis is organized as follows:

- The first chapter **"Introduction":** we present general introduction about this workt .
- The second chapter **"Background and Literature Review":** we present a bibliographic search exclusively directed to the study of the properties (structural, electrical and optical) of ZnO and CuO in all its forms and some applications.
- The third chapter **"Elaboration and Physico-Chemical Characterization of ZnO Substrates":** we present firstly the description utilize the prepared thin films of zinc oxide doped lanthum(0 to 5 wt.%) at different precursor .Secondly, the different characterization techniques X-ray diffraction, scanning electron microscope (SEM), UV-Visible spectro photometry, IR, will be used. Thirdly , results and discussions on the impact of non-doped ZnO and doped with lanthanum (0 to 5 wt.%) upon the adsorption process of the copper ions will be presented in next chapter.
- The fourth chapter **"Characterization Of CuO Thin Films Prepared by Chemical Bath":** we present, firstly the adsorption of copper ions from aqueous solution by zinc oxide substrate and to produce stable p-type CuO oxides after annealing treatment. Secondly for this, we have characterized the microstructure and optics of our layers by different techniques: scanning electron microscopy (SEM), and X-ray diffraction (DRX) to obtain information on the directions of crystallographic growth and a spectrophotometer (UV-Visible) to obtain information on the transmittance, the energy of gap and the disorder of the deposited layers.
- The fifth chapter **"Conclusion and Future Works":** we present general conclusion about this work.

Bibliography

[1] A. Muthukumar, G. Rey, G. Giusti, V. Consonni, E. Appert, H. Roussel, et al., "Fluorine doped tin oxide (FTO) thin film as transparent conductive oxide (TCO) for photovoltaic applications," in AIP Conference Proceedings, 2013, pp. 710-711.

[2] Y. Lu, "SnO2 thin films-chemical vapor deposition and characterization," 2015.

[3] R. A. Afre, N. Sharma, M. Sharon, and M. Sharon, "TRANSPARENT CONDUCTING OXIDE FILMS FOR VARIOUS APPLICATIONS: A REVIEW," Reviews on Advanced Materials Science, vol. 53, pp. 79-89, 2018.

[4] K. Badeker, "Electrical conductivity and thermo-electromotive force of some metallic compounds," Ann. Phys, vol. 22, p. 749, 1907.

[5] C. G. Granqvist and A. Hultåker, "Transparent and conducting ITO films: new developments and applications," Thin solid films, vol. 411, pp. 1-5, 2002.

[6] A. Thelen and H. König, "ElektrischeLeitfähigkeit und Strukturauf gestäubter Indium oxyds chichten," Naturwissenschaften, vol. 43, pp. 297-298, 1956.

[7] R. Groth and E. Kauer, "Thermal insulation of sodium lamps," Philips Technical Review, vol. 26, pp. 105-&, 1965.

[8] D. S. Ginley and C. Bright, "Transparent conducting oxides," MRS bulletin, vol. 25, pp. 15-18, 2000.

[9] G. J. McCarthy and J. M. Welton, "X-ray diffraction data for SnO2. An illustration of the new powder data evaluation methods," Powder Diffraction, vol. 4, pp. 156-159, 1989.

[10] K. Minegishi, Y. Koiwai, Y. Kikuchi, K. Yano, M. Kasuga, and A. Shimizu, "Growth of p-type zinc oxide films by chemical vapor deposition," Japanese Journal of Applied Physics, vol. 36, p. L1453, 1997.

[11] Y. Lu, J. Jiang, M. Becker, B. Kramm, L. Chen, A. Polity, et al., "Polycrystalline SnO2 films grown by chemical vapor deposition on quartz glass," Vacuum, vol. 122, pp. 347-352, 2015.

[12] M. Afzaal, H. M. Yates, and J. L. Hodgkinson, "Translation effects in fluorine doped tin oxide thin film properties by atmospheric pressure chemical vapour deposition," Coatings, vol. 6, p. 43, 2016.

[13] Y. Kong, D. Yu, B. Zhang, W. Fang, and S. Feng, "Ultraviolet-emitting ZnO nanowires synthesized by a physical vapor deposition approach," Applied Physics Letters, vol. 78, pp. 407-409, 2001.

[14] Z. Y. Banyamin, P. J. Kelly, G. West, and J. Boardman, "Electrical and optical properties of fluorine doped tin oxide thin films prepared by magnetron sputtering," Coatings, vol. 4, pp. 732-746, 2014.

[15] R. Sakhare, G. Khuspe, S. Navale, R. Mulik, M. Chougule, R. Pawar, et al., "Nanocrystalline SnO2 thin films: structural, morphological, electrical transport and optical studies," Journal of Alloys and Compounds, vol. 563, pp. 300-306, 2013.

[16] S. S. Lekshmy, G. P. Daniel, and K. Joy, "Microstructure and physical properties of sol gel derived SnO2: Sb thin films for optoelectronic applications," Applied Surface Science, vol. 274, pp. 95-100, 2013.

[17] E. M. Preiß, T. Rogge, A. Krauß, and H. Seidel, "Gas sensing by SnO2 thin films prepared by large-area pulsed laser deposition," Procedia Engineering, vol. 120, pp. 88-91, 2015.

[18] H. Kim and A. Pique, "Transparent conducting Sb-doped SnO2 thin films grown by pulsed-laser deposition," Applied physics letters, vol. 84, pp. 218-220, 2004.

[19] A. Moholkar, S. Pawar, K. Rajpure, P. Patil, and C. Bhosale, "Properties of highly oriented spray-deposited fluorine-doped tin oxide thin films on glass substrates of different thickness," Journal of Physics and Chemistry of Solids, vol. 68, pp. 1981-1988, 2007.

[20] S. Salaken, E. Farzana, and J. Podder, "Effect of Fe-doping on the structural and optical properties of ZnO thin films prepared by spray pyrolysis," Journal of Semiconductors, vol. 34, p. 073003, 2013.

[21] B. Benhaoua, S. Abbas, A. Rahal, A. Benhaoua, and M. Aida, "Effect of film thickness on the structural, optical and electrical properties of SnO2: F thin films prepared by spray ultrasonic for solar cells applications," Superlattices and Microstructures, vol. 83, pp. 78-88, 2015.

[22] L. Liu, T. Kawaharamura, G. T. Dang, E. K. Pradeep, S. Sato, T. Uchida, et al., "Study on fabrication of conductive antimony doped tin oxide thin films (SnOx:Sb) by 3rd generation

mist chemical vapor deposition," Japanese Journal of Applied Physics, vol. 58, p. 025502, 2019.

[23] K. Murakami, A. Bandara, M. Okuya, M. Shimomura, and R. Rajapakse, "Synthesis and characterization of one-dimensional nanostructured fluorine-doped tin dioxide thin films," in Nanostructured Thin Films IX, 2016, p. 99290X.

[24] T. I. Gandhi, R. R. Babu, K. Ramamurthi, and M. Arivanandhan, "Effect of Mn doping on the electrical and optical properties of SnO2 thin films deposited by chemical spray pyrolysis technique," Thin Solid Films, vol. 598, pp. 195-203, 2016.

[25] D. Chandran, L. S. Nair, S. Balachandran, K. R. Babu, and M. Deepa, "Structural, optical, photocatalytic, and antimicrobial activities of cobalt-doped tin oxide nanoparticles," Journal of Sol-Gel Science and Technology, vol. 76, pp. 582-591, 2015.

[26] A. Murali and H. Y. Sohn, "Plasma-assisted chemical vapor synthesis of indium tin oxide (ITO) nanopowder and hydrogen-sensing property of ITO thin film," Materials Research Express, vol. 5, p. 065045, 2018.

[27] C.-Y. Tsay and S.-C. Liang, "Fabrication of p-type conductivity in SnO2 thin films through Ga doping," Journal of Alloys and Compounds, vol. 622, pp. 644-650, 2015.

[28] F. Aragón, J. A. H. Coaquira, I. Gonzalez, L. Nagamine, W. Macedo, and P. Morais, "Fe doping effect on the structural, magnetic and surface properties of SnO2 nanoparticles prepared by a polymer precursor method," Journal of Physics D: Applied Physics, vol. 49, p. 155002, 2016.

[29] J. Manifacier, M. De Murcia, J. Fillard, and E. Vicario, "Optical and electrical properties of SnO2 thin films in relation to their stoichiometric deviation and their crystalline structure," Thin Solid Films, vol. 41, pp. 127-135, 1977.

[30] F. Ghodsi and J. Mazloom, "Optical, electrical and morphological properties of p-type Mn-doped SnO_2 nanostructured thin films prepared by sol–gel process," Applied Physics A, vol. 108, pp. 693-700, 2012.

[31] M. C. RAO, K. RAVINDRANADH, and R. V. S. S. N. RAVIKUMAR, "Optical and EPR studies of Fe+3 doped tin oxide thin films by spray pyrolysis", OPTOELECTRONICS AND ADVANCED MATERIALS vol. 20, pp. 159-162, 2018.

[32] M.-M. Bagheri-Mohagheghi, N. Shahtahmasebi, M. R. Alinejad, A. Youssefi, and M. Shokooh-Saremi, "Fe-doped SnO2 transparent semi-conducting thin films deposited by spray pyrolysis technique: thermoelectric and p-type conductivity properties," Solid State Sciences, vol. 11, pp. 233-239, 2009.

2 Background and Literature Review

Chapter 2

Background and Literature Review

The present chapter is a brief survey on structural, optical and electrical properties of ZnO, CuO thin films and their most important applications in various technological areas.

2.1 Metal oxide thin films

Metal oxides are an important class of materials: from both scientific and technological point of view. They found huge interesting applications in different technological fields.

Oxide semiconductors are gaining interest as new materials that may challenge the supremacy of silicon. Metal oxide thin films are known for many years ago due to the industrial interest on their unique properties [1].

The physicochemical properties of metal oxide thin layers are closely related to preparation processes and operating conditions. Indeed, it is possible to obtain thin films having an amorphous or crystalline structure. Thereafter, films structural, electrical and optical properties can be tailored by varying the condition and the deposition process. Control of film properties is therefore key parameters of metal oxide films preparation to be used in wide applications such as: fabrication of microelectronic circuits, sensors, piezoelectric devices, fuel cells, coatings against corrosion, and as catalysts. Some metal oxides, their electronic band gap, and conducting nature are listed in table 2. 1.

Earlier, research in the field has been devoted to bulk metal oxides before interest in their thin films aspect. These oxides are zinc oxide (ZnO), tin oxide (SnO_2), titan oxide (TiO_2), tungsten oxide (WO_3), cuprous oxide (Cu_2O) and cadmium oxide (CdO). Recently, several metallic oxide thin films have emerged such as vanadium oxide (V_2O_5), nickel oxide (NiO) molybdenum oxide (MoO_2) and cupric oxide (CuO). Among these oxides, cupric oxide (CuO) thin films exhibit an interesting combination of multifunctional proprieties including: optical, semiconducting, magnetic, electronic, and optoelectronic. CuO thin films find many applications in electronic devices such as: gas sensors, solar cells, catalysts and Li batteries [2].

Table 2. 1 Some metal oxides, their position in the periodic table, band gap, and conducting nature [3].

Name	Position of the metal in the periodic table and nature	Band Gap (eV)	Classification
WO_3	Group 6 (VI); Transition metal	2.6-3.1	Semiconductor (n-type)
MnO	Group 7 (IV); Transition metal	4.1	Semiconductor (n-type)
MnO_3	Group 7 (IV); Transition metal	β 0.26 γ 0.58-0.7	Semiconductor (n-type)
Fe_3O_4	Group 8 (IV); Transition metal	0.1	Metallic
FeO	Group 8 (IV); Transition metal	2.4-2.5	Semiconductor (p-type)
NiO	Group 10 (IV); Transition metal	2.4-2.5	Semiconductor (p-type)
CuO	Group 11 (IV); Transition metal	1.2-1.8	Semiconductor (p-type)
Cu_2O	Group 11 (IV); Transition metal	2.1-2.8	Semiconductor (p-type)
ZnO	Group 12 (IV); Transition metal	3.3-3.4	Semiconductor (n-type)
Al_2O_3	Group 13 (III); Poor metal	6.0-8.8	Insulator

Part I

Zinc oxide *ZnO*

2.2 Zinc Oxide (ZnO)

Zinc oxide has been featured as subject of thousands of research papers, it can be traced the history back as early as 1935 [4]. ZnO has many distinct properties such as high ultra violet absorbance, wide chemistry, large piezoelectricity and strong luminescence at high temperatures. All these unique properties make ZnO being popular in industrial applications. It can be found in paints, cosmetics, plastic and rubber manufacturing, electronics and pharmaceuticals, and so on. ZnO is one of the transparent conductive oxides (TCOs) which are indispensable materials used as electrodes for optoelectronic devices such as flat panel displays and solar cells [5] .

2.3 Film Deposition Techniques

The physical properties of ZnO do not depend solely on its composition chemical, but also of the method used for its preparation The thin layers of ZnO are made using a wide variety of techniques due to the diversity of applications of these materials. They can be obtained by operating in the liquid phase or in the vapor phase and by physical or chemical methods.

- Reactive evaporation [6].
- Laser ablation [7].
- Magnetron sputtering [8].
- Radio frequency [9].
- Reactive sputtering [10].
- Sol gel [11].
- Chemical Vapor Deposition CVD [12].
- Spray [13].
- Hydrothermal

2.4 Fundamental Properties of ZnO

2.4.1 Physical and chemical proprieties

Zinc oxide in mineral form is called “ Zincite ”. It is usually colored red or orange by manganese impurities. The density of zinc oxide is 5.675 g/ cm^3 and insoluble in water. It is melts above 1975 °C with some loss of oxygen. Table 2. 2 regroups some physical and chemical properties of zinc.

Table 2.2 Different properties of ZnO

Zinc Oxide ''ZnO ''	
Chemical names	Zinc Oxide
Mineral	Zincite
Molecular Formula	ZnO
Appearance	White powder
Solubility in water	Insoluble
Molecular Mass	81.38 ± 0.02 g / mol
Density	$\rho' = 5.675$ g / cm^3
Relative permittivity	10.8
Melting point	1800 °C
Boiling point	1975 °C

2.4.2 Crystal Structure

ZnO is a II–VI compound semiconductor, which crystallizes into three different structures viz, würtzite (B4), zinc blende (B3), and rocksalt (B1) under different growth conditions. Where B1, B3, and B4 denote *strukturbericht* designations for the three phases [14]. Among these structures, the würtzite structure is thermodynamically most stable phase under ambient conditions. The zinc blende structure can be stabilized by growing on cubic substrates like MgO and Pt/SiO_2/Si [15]. However, the rocksalt (NaCl) structure can be realized only by applying very high

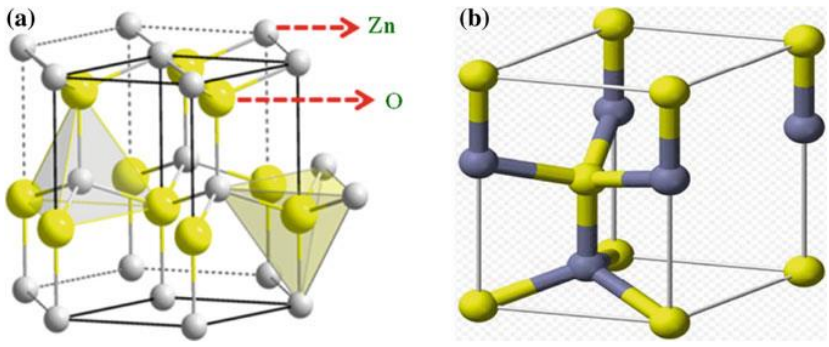

Fig. 2. 1. a) Würtzite crystal structure of ZnO showing the tetrahedral coordination of the Zn and O atoms. b) Unit cell of würtzite structure.

pressures [16]. When compared with zinc blende and rocksalt structures, würtzite ZnO has shown intriguing optical, electrical, and optoelectronic properties in thin film and

nanostructured form. Hence, a lot of research work has been mainly focused on the study of doped and undoped würtzite ZnO thin films and nanostructures.

The würtzite ZnO belongs to the space group of C_{6v}^{4} in the Schoen flies notation and $P6_3mc$ in Hermann-Mauguin notation [17]. Figure 2. 1 shows the crystal structure and unit cell of the würtzite ZnO. The structure is composed of two interpenetrating hexagonal close packed (hcp) sublattices, each of which consists of one type of atom displaced with respect to each other along the three fold c-axis by the amount u = 3/8 = 0.375, where the parameter u is defined as the anion-cation bond length parallel to the c-axis. The measured lattice parameters of the hexagonal würtzite ZnO are a= 3.249Å and c= 5.206Å. In the würtzite ZnO, each sublattice consists of four atoms per unit cell and each atom of one kind is surrounded by four atoms of the other kind. In other words, both Zn and O atoms are tetrahedrally coordinated to each other. This tetrahedral coordination gives rise to polar symmetry along the c-axis.[18]

The polar nature of the ZnO is responsible for many interesting properties viz, piezoelectricity, spontaneous polarization, crystal growth, etching, and defect generation. In ZnO, both Zn terminated (0001) and O terminated $(000\bar{1})$ faces are polar in nature. The other important faces in the würtzite ZnO structure are nonpolar $(11\bar{2}0)$ and $(10\bar{1}0)$. Figure 2. 2 gives the important planes and orientations that are commonly seen in würtzite structure .[18]

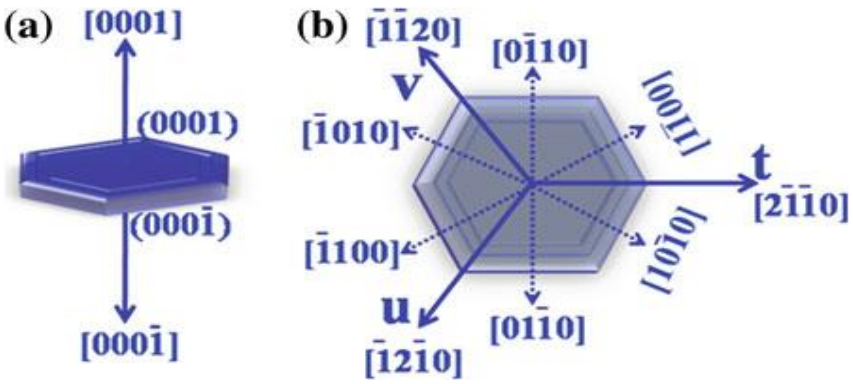

Fig. 2. 2. a, b Various polar and nonpolar planes in ZnO hexagonal würtzite structure [18]

Indeed, the orientation along axis (c) is predominant in many works [19-20] whatever the method of development used while respecting well-defined experimental conditions.

The crystal structure and physical properties of the thin layers of ZnO are sensitive to the deposition method and conditions. In Table 2. 3 we have summarized the structure, the grain size and the preferential orientation reported in the literature for ZnO deposited by different deposition techniques.

Table 2. 3 Structure, grain size and preferential orientation of the thin films of ZnO elaborated by different techniques.

Technical	Parameters studied	Structure	D (nm)	(hkl)
Electron bean evaporation [21]	before annealing	Amorphous		
	annealing 250 °C	Hexagonal	22.5	(002)
	350 °C	Hexagonal	22.8	(002)
	450 °C	Hexagonal	35.3	(002)
	550 °C	Hexagonal	26.1	(002)
PLD [22]	oxygen pressure variation 0.02-0.1 Pa	Wrützite	31- 26	(002)
RF magnetron sputtering [23]	Doped with F Annealing with different temperature	Hexagonal Wrützite	18- 24	(002)
Spray pyrolysis [24]	Change in concentration	Wrützite	75-95	(002) (101) (110)
Sol Gel [25]	Change in Thickness		2.7909	(100)
	Doped with Cd	Hexagonal	2.5899	(002)
			2.4654	(101)

2.4.3 Electronic Band Structure

ZnO is composed of Zinc and Oxygen atoms belonging to II and VI groups of the periodic table. The electronic band structures of oxygen and zinc are:

$$O:\ 1S^2\ 2\ S^2\ 2P^4$$

$$Zn:\ 1S^2 2\ S^2 2\ P^6\ 3\ S^2\ 3\ P^6\ 3\ d^{10} 4S^2.$$

Numerous theoretical calculations have been employed to calculate the band structure of ZnO by a number of groups [26]. Figure 2. 3 shows the calculated band structure of würtzite crystal of ZnO. Location of the Zn 3d levels was unambiguously determined using the local density approximation (LDA) and incorporating atomic self-interaction corrected pseudo-potentials (SIC-PP). In ZnO, both the valence band maxima and the conduction band minima occur at the Γ point k= 0 indicating that ZnO is a direct band gap semiconductor. The bottom 10 bands, occurring around -9eV (not shown in figure), correspond to Zn 3d levels [17].

The next six bands, from -5 to 0eV, correspond to O 2p levels. The first two conduction band states are strongly Zn localized and correspond to empty Zn 3s states. The O 2s bands, associated with core-like energy states, occur around -20 eV. Using the above calculation, the

band gap was determined as 3.77eV. In addition to theoretical calculations, the electronic band structure was experimentally carried out [27], at the surface of würtzite ZnO, using the data obtained from electron energy loss spectroscopy (EELS) and ultraviolet photoelectron spectroscopy (UPS). It was observed that the Zn face possesses more covalent character, arising from the Zn 4s–O 2p states, while the O face is more ionic.

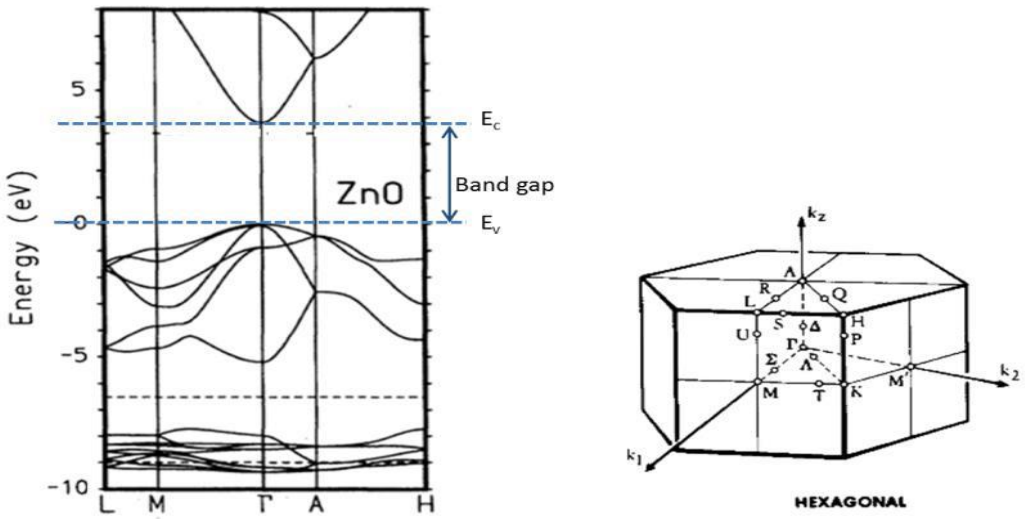

Fig. 2. 3. Local density approximation of the band structure of bulk ZnO.[18]

2.4.4 Electrical properties

The electrical properties of ZnO thin films such as resistivity electrical energy, the concentration of charge carriers and the mobility are determined usually by Hall effect measurements. Resistivity ρ is a physical quantity of interest according to the targeted fields of application. For devices optoelectronic devices like photovoltaic cells, low resistivity is preferable in order to facilitate the transport of the current. For applications of electromechanical transduction, we will favor a greater value of ρ to avoid that the free electrons mask the electric field created by piezoelectric effect.[28]

Table 2. 4 presents the different electrical properties of the thin layers of ZnO performed by different methods of the deposit. We notice that the properties ZnO is depend on the deposit method and the conditions of the preparations (precursor, type of substrate, deposition temperature, environment ...).

The resistivity of ZnO extends over several orders of magnitude, with values ranging from (10^{-4} Ω.cm to 10^{12} Ω.cm) [29,30]. According to the methods of elaborations, we will have films very conductive (ρ= 10^{-4} Ω.cm) or little conductors (ρ= 10^{3} Ω.cm). In the case of ZnO, the electrical conductivity is n-type of the theoretical studies have shown that oxygen deficiency and interstitial zinc are shallow donor defects generating n-type electrical conductivity [31,32]. Other authors argue that interstitial hydrogen is also a donor defect may be responsible for the presence of free electrons [33]. The electrical conductivity of n-type TCO thin film depends on density of electrons (n) in the conduction band and their mobility (μ):

$$\sigma = en\mu_n = \frac{1}{\rho} \qquad (2.\ 1)$$

Mobility μ is a characteristic of conductive and semiconductor media. It is expressed in(cm^2 V^{-1} s^{-1}). Mobility μ varies according to the process and the conditions of growth and post-treatment (Table 2. 4). The spray method has shown that it is able to give thin layers of ZnO with electrical properties of same order of magnitude as those obtained using more sophisticated and after heat treatments .

Table 2. 4 Electrical properties of zinc oxide (ZnO). [33,34….35]

Deposit methods	Deposition temperature(C°)	ρ (Ω.cm)	n_V (cm^{-3})	μ ($cm^2.V^{-1}s^{-1}$)
Spray	350	2.7×10^{-3}	2.4×10^{15}	0.34
	450	2.4×10^{-2}	-	-
	420	1.35×10^{-2}	-	-
	350	47.1×10^{-3}	1.5×10^{19}	4.82
Sputtering	-	2.75×10^{-7}	2.5×10^{17}	-
	150	2.04×10^{-7}	-	3
CVD	300	1.25×10^{-1}	6.4×10^{18}	7.86
	500	3.07×10^{-3}	7.4×10^{20}	1.47
	640	7.31×10^{-4}	-	-
Sol gel	500	2.4×10^{2}	-	-
PLD	400	10^{-4}	1.6×10^{17}	12.3

2.4.5 Optical properties

The optical properties of ZnO thin films depend on the conditions preparation and method of preparation. Table 2. 5 shows the transmission and gap energy of ZnO thin films obtained by

different deposit techniques. ZnO has high optical transparency in the visible and near-infrared; this is due to the wide band gap. In addition to the possibility to emit in the near UV (375nm), the ZnO attracts the interest of the community scientific because it has very robust excitons whose emission persists beyond ambient temperature (binding energy of 60meV). The refractive index of zinc oxide in the massive form is equal to 2.0 [36]. Usually the oxide of Zinc is used in the form of thin films and having a refractive index, which varies between 1.7 and 2.20 depending on the conditions of preparation [37, 38].

Table 2. 5 Optical properties of ZnO [39,40].

deposit methods	deposition temperature(C°)	Thickness (nm)	Transmission (%)	Eg(eV)
Spray	350	335	85	3.31
	350	-	85	3.32
	420	210	~95	3.31
	350	440	~80	3.18
Sputtering	200	-	80	3.1
	-	120	~80	3.25
	200	-	93	3.33
CVD	320	460	85	3.28
	500	-	100	3.44
Sol gel	400	-	87	3.24
	500	-	92	3.26
PLD	400	-	99.8	3.17

2.4.6 ZnO doping

As we pointed out before, the doping of ZnO is necessary for its applications in optoelectronic devices like screens displays, gas detectors and photovoltaic solar cells. Oxide zinc is a würtzite structure wide gap semiconductor (P63mc). However, the ZnO compound can exhibit relatively high conductivity either by existence intrinsic defects (gaps or interstitial atoms), either by the introduction of ions dopants in substitution of zinc or oxygen [37]. The presence of these defect intrinsic leads to n-type conduction .To improve its transparent conductive oxide properties, ZnO must be doped with a group III element (B, Al, In, Ga) and / or a group IV element(Pb, Sn) replacing the zinc or a mono valent element replacing the oxygen. The dopants, the most common, are aluminum, tin, indium and fluorine [38, 39]. So, intrinsic n-type conduction is enhanced by extrinsic doping of the same type. As part of this

study, research focused on diapers Thin zinc oxide doped with tin and aluminum (synthesis routes, dopant level introduced ...). These elements are incorporated into the ZnO network by forming shallow donor levels that contribute to the electrical conduction of ZnO. Paraguay et al. [24] studied the effect of different dopants (Al, Cu, Fe, In and Sn) on the microstructure of ZnO thin films deposited by the spray technique pyrolysis. High electrical conductivity of ZnO thin films with high free electron concentration of about $10^{20}cm^{-3}$ was obtained for doped ZnO Al and Sn doped ZnO [40,41]. N-type ZnO was also realized using Co-dopage by the elements of group 3A and group 4A (Al, Sn). Few works on the ZnO co-doped Al-Sn are reported in the literature. However, lanthanum is considered as one of the most promising of these dopants because it can easily be substitute for Zn because of their similar ionic radii (0.074 nm for Zn^{2+} and 0.069 nm for Sn^{4+}), resulting in a small distortion of the grating [27]. The substitution of Zn results in a large increase in electrical conductivity due to presence of additional free electrons. Doping also plays a role important and Paraguay et al. show that the doping of tin holds the largest sensitivity compared to doping Al, In [27]. Other studies optimize the concentration of tin to increase the sensitivity of ZnO thin films to detect NO_2 [28]. In the literature, the doped ZnO thin films are obtained by solid route [29] or by chemical route sol-gel [29,30] hydrothermal [31,32]. Determining the amount of dopant introduced into the ZnO matrix is carried out either by phase analysis (X-ray diffraction, analyzes EDAX chemicals ...) by indirect methods that consist in measuring .

2.5 Applications of ZnO

The applications of zinc oxide are multiple. For many years they are located in the chemical and pharmaceutical industry. Currently new optoelectronics and spin electronics research routes are of great interest for this material. It can be considered that zinc oxide is one of the few materials multifunctional that can be found today.

2.5.1 Solar cell

Solar cells are systems made of semiconductor materials that have the ability to transform solar energy into electrical energy. This transformation is due to the photovoltaic effect of the material used, which makes it possible to capture the energy of the photons received to release charge carriers from the valence band to the conduction band.

Currently, most solar cells are made from silicon. In this application, zinc oxide can be used as a transparent electrode on the upper "front contact" layer to allow the passage of electric current through the component while letting the light pass through (see Figure 2.4)

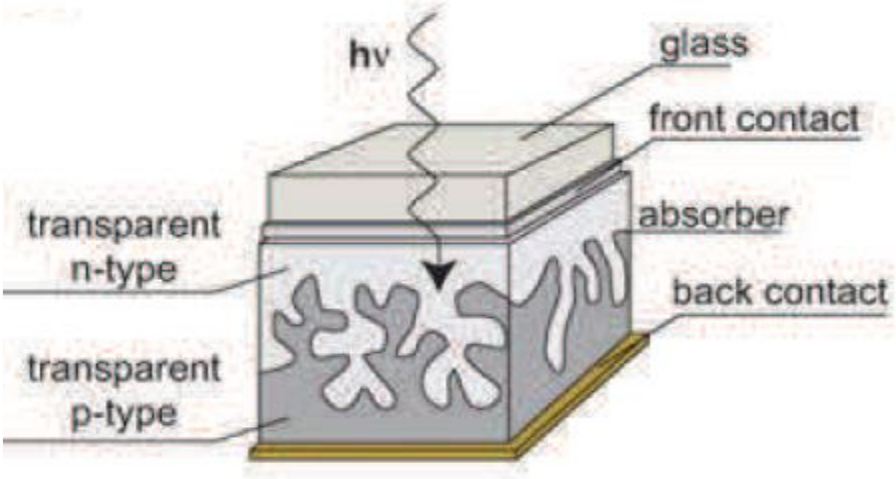

Fig. 2. 4. Schema of the structure of a solar cell [42].

A recent study [43] has shown that the use of ZnO on the surface and under a certain condition can also improve the efficiency of the solar cell. The authors show that depending on the method of production, ZnO can reveal a more or less rough surface. The roughness is an important element for the realization of solar cells. The rougher the surface of the cell, the more light can diffuse into the material (Figure 2. 5). This has the effect of lengthening the path of photons and increasing the chances of absorbing light to free charge carriers. The roughness of ZnO depends on its technological deposition parameters and in this case it is important to control them .

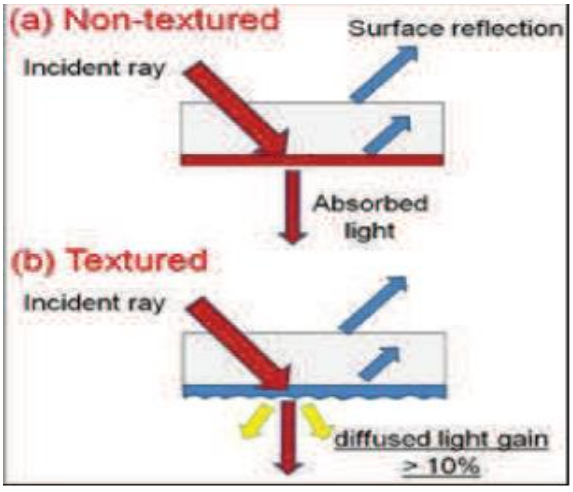

Fig. 2. 5. Influence of the roughness of the layer surface on the absorption of light [43].

2.5.2 Gas sensors

With the development of the industry, and new environmental and safety recommendations, gas sensors have been the subject of research for several years. The semiconductor sensors consist of a layer sensitive to the gas to be detected. The measured parameter is generally the electrical resistance of the sensor, which depends on the composition of the atmosphere around it [44].

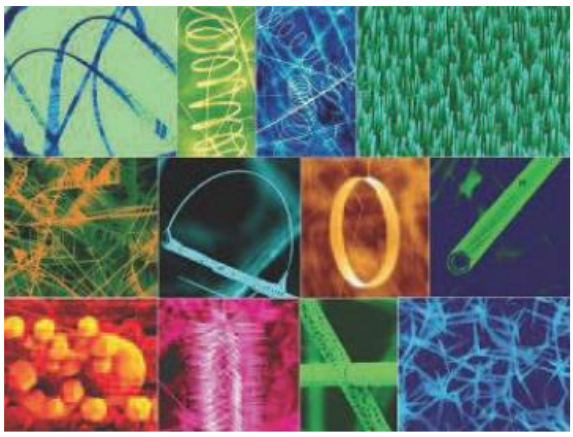

Fig. 2. 6. Examples of ZnO nanostructures [45].

Depending on the preparation method, ZnO can reveal different nanostructures (nanoparticles, nanotubes, nanowires) (Figure 2. 6), and thus offer a morphology adapted to the gas to be detected at the surface. This makes zinc oxide a good candidate for detection applications. We show in Figure 2. 7 the example of a gas sensor consisting of a layer of ZnO on the surface of an alumina tube. The platinum wires are bonded to the Au electrodes to measure the change in sensor voltage. Nickel-chromium alloy heating wires change the temperature of the gas atmosphere to improve the sensitivity of the sensor.

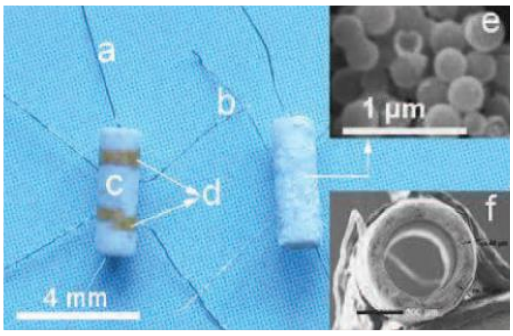

Fig. 2. 7. Photo of a gas sensor: (a) Ni-Cr alloy for heating, (b) Pt wire, (c) Alumina tube, (d) Au electrodes, (e) Hollow ZnO spheres covering the tube and (f) SEM image of the sensor section view [46].

2.5.3 Light emitting diodes

Unlike the solar cell, the principle of the light-emitting diode (LED) is to convert electrical energy into light energy. Like gallium nitride and thanks to its wide forbidden band (3.37 eV), zinc oxide also finds its place in the production of light emitting diodes emitting in particular in blue. These two materials have similar properties, but ZnO has some advantages over GaN. We can cite for example its high exciton binding energy (60 meV against 21 meV for GaN), potentially giving it good light emission capacities at room temperature.

However, unlike GaN, ZnO presents difficulties for the production of stable p-type layers, which are necessary for the production of LEDs. Thus studies are currently focusing on ZnO / GaN heterostructures to take advantage of the advantages of ZnO and GaN.

We show in figure 2. 8 such a heterostructure developed by J.Y. Lee et al. [47]. The authors studied the impact of structure annealing on the light-emitting performance of this diode. They show for example that no light emission could be observed without treatment. On the other hand when the structure is annealed under nitrogen, blue and violet light emissions appear. In contrast, when the structure is annealed in air, there is an emission of yellow light.

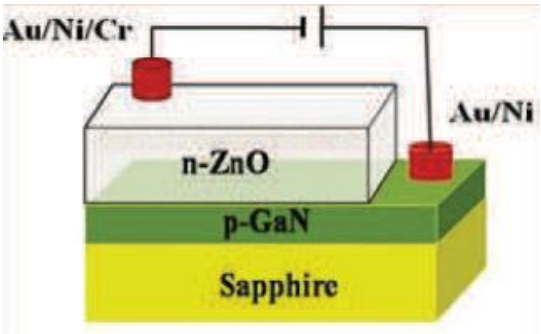

Fig. 2. 8. Schema of an LED cell based on a ZnO layer [47].

These results show us the significant impact of post-deposition treatments of the material on its optical properties.

2.5.4 Other applications

Thanks to the other properties: piezoelectric, ferroelectric, magneto electric and physicochemical, we can also cite other applications of zinc oxide under development in other emerging fields:

1) Surface Acoustic Wave Devices (SAW) [48,49]

Surface acoustic wave devices, based on the piezoelectric effect of the material, are widely used in electronic filters, delay lines and resonators in communication systems. SAWs devices are used not only in the telecommunications sector, but also in the automotive (pressure), medical (biosensor) and industrial (steam, gas, humidity) sectors.

Zinc oxide has a piezoelectric coefficient d_{33} of the order of 5.81pm/V to 28.7pm/V [50], which is higher than that of quartz, d_{11}=2.31pm/V [51]. This effect is closely linked to its crystal structure. When an external electric field is applied to the material, the ions of the elementary meshes of the crystal move by electrostatic forces, which causes the mechanical deformation of the crystal [52]. This property makes ZnO a good candidate for generating acoustic waves.

2) Photocatalysts [53.54]

Photocatalysis is generally used for air purification and water treatment. It is also used in the discoloration of colored aqueous effluents (textile industries), the elimination of odors and the self-cleaning coating of surfaces (glass, metals, concretes, cements).

Photocatalysis is based on an electronic process that occurs on the surface of a catalyst. Its principle includes three stages [55]:

- Production of electron-pairs / positive gap. When the photocatalyst is subjected to photon radiation with an energy at least equal to that of the forbidden band, an electron can pass from the valence band to a vacant orbital of the conduction band. There is then the creation of a hole in the valence band and the release of an electron in the conduction band.
- Separation of electrons and vacancies. The lifetime of the electron-electron pairs is short and their recombination is accompanied by the generation of heat. For photocatalysis to be effective, recombination must be avoided. This is made possible by transferring and trapping free charges to intermediate energy levels.
- Oxidation and reduction reactions. The charges created migrate to the surface of the catalyst and react with adsorbed substances capable of accepting or donating electrons. These are the oxidation or reduction reactions which are interesting for depollution.

Photocatalysis is at the heart of the process. Several semiconductors have a width of the forbidden band sufficient to allow photocatalysis, for example TiO_2, ZnO, ZnS and SnO_2.

Part II

Cupric oxide CuO

2.6. Cupric oxide (CuO)

Copper have two oxidation states +1 and +2, while under special circumstances some compounds of trivalent are also reported. It was shown that this trivalent copper survives not more than few seconds. Consequently, cuprous oxide (Cu_2O) and cupric oxide (CuO) are the two stable forms of copper oxide. However, only cupric oxide (CuO) phase is reported as a gas-sensitive material and exhibits a number of interesting properties.

CuO has attracted particular attention because it is the simplest member of the family of copper compounds and exhibits a range of potentially useful physical properties, such as high temperature superconductivity, electron correlation effects, and spin dynamics .This led to a rapid research expansion in theoretical studies, fabrication, characterization and applications of CuO based devices in the latter half of the 20th century [56].

Cupric oxide can be obtained easily by heating cuprous oxide (Cu_2O) or copper in air at 1273-1373K nearly, cupric oxide is formed as follows:

$$Cu_2O + {}^{1}/_{2}O_2 \longrightarrow 2CuO$$

$$2\,Cu + 2O \longrightarrow 2CuO$$

But in industrial method it is prepared by heating malachite ore, CuO is produced according the reaction below:

$$CuCO_3.Cu(OH)_2 \longrightarrow 2CuO + CO_2 + H_2O + O_2$$

CuO had been studied extensively for a number of decades, with electrical and optical properties reviews, available as early since the 1960's. The first period of notable growth in CuO research interest occurred in the mid of 1980's with a series of highly-cited research works [57]. CuO thin films have been successfully deposited by several deposition techniques including thermal evaporation [58,59], spray pyrolysis (SP) [60], plasma evaporation [61], DC magnetron sputtering [62], electro deposition [63], sol-gel [64] .Work in the early part of the 2000s were mainly focused on growth mechanisms and parameters influence. Several review articles dealing with the state-of the-art of CuO have been published with extensive discussion on band structure, thermal, magnetic, optical and electrical properties, doping, growth and devices.

2.7 Fundamental Properties of cupric oxide

2.7.1 Physical and chemical proprieties

Cupric oxide in mineral form is called “tenorite”. Pure cupric oxide is black solid with a density of 6.32g/cm^3 and insoluble in water. It is melts above 1134 °C with some loss of oxygen. Table 2.6 regroups some physical and chemical properties of cupric oxide.[2]

Table 2.6 Different properties of CuO

Cupric Oxide ‘’CuO ’’	
Chemical names	Copper (II) oxide Cupric oxide Copper monoxide Copper oxide (CuO)
Mineral	tenorite
Molecular Formula	CuO
Appearance	Black powder
Solubility in water	Insoluble
Molecular Mass	79.55 g / mol
Density	ρ'= 6.32 g / cm^3
Relative permittivity	12
Melting point	1134 °C
Boiling point	2000 °C

2.7.2 Crystal Structure

CuO which has a black colour belongs to the monoclinic crystal system, with a crystallographic space group for the unit cell of C2/c. The crystallographic properties of CuO are tabulated in Table 2.7.[65,66] The copper atom is coordinated to four coplanar oxygen atoms situated at the corners of a rectangular parallelogram, which form chains by sharing edges. The oxygen atom is coordinated to four copper atoms situated at the corners of a distorted tetrahedron. The chains traverse the structure in the [110] and [$\bar{1}$10] directions. The two types of chains alternate in the [001] direction and each type is stacked in the [010] direction with a separation between the chains of about 2.7Å.[65,67,68]. Figure 2.9 demonstrates the crystal structure of CuO.

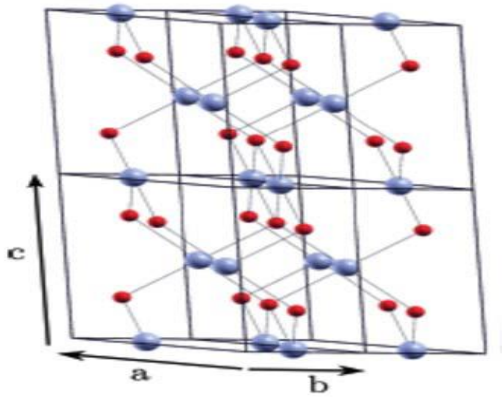

Fig. 2. 9. Crystal structure of CuO shown by four unit cells. The big blue and the small red spheres denote Cu and O atoms respectively.

Table 2. 7 Crystallographic properties of CuO.[2]

CuO	
Unit Cell	Monoclinic a =4.6837 Å b =3.4226 Å c =5.1288 Å β =99.54° α =γ=99.54°
Shortest inter-atomic distance	
Cu-O	1.95 Å
O-O	2.62 Å
Cu-Cu	2.90 Å
Cell volume	81.08 Å^3
Cell content	4 [CuO]

2.7.3 Electronic Band Structure

A schematic representation of the band structure and Brillouin zones of cupric oxide for the monoclinic structure is given in Figure 2. 10.It is recalled that the structures Oxygen and copper band electronics are :

$$O : 1S^2\ 2\ S^2\ 2P^4$$

$$Cu : 1S^2 2\ S^2 2\ P^6\ 3\ S^2\ 3\ P^6\ 3\ d^{10} 4S^1.$$

The reported band gap (Eg) values for CuO, which is a p-type semiconductor, are generally in the range of 1.2 to 2.16eV.[69,70] This wide range is attributed to two factors: interpretation of the nature of the gap (i.e. direct or indirect) and annealing treatment.[71,72,73] According to the Tauc relationship, for photon energies (E) greater than the band gap energy, the light absorption can be approximated using:[74]

$$\alpha E = \alpha_0 (E - E_g)^{\eta} \qquad (2.2)$$

where α is the absorption coefficient, α_0 is a constant, E_g is the band gap energy and η is an exponent that depends on the type of transition involved. The value of η is $^1/_2$ or 2 for direct or indirect transitions, respectively. Rakhshani et al. have reported detailed studies of band gap determination of RF sputtered CuO films.[69]

They found that their CuO films exhibited an indirect transition with a band gap of 1.21 eV. In contrast, Pierson et al. while reporting the same deposition technique (RF sputtering), determined their CuO films exhibited a direct band gap with a value of 1.71eV.[75] The different values of E_g were due to different models $(\alpha E)^2$ or $(\alpha E)^{1/2}$ being used to determine the band gap value. The other significant factor that contributes to the variation of band gap values of CuO films is related to the heat treatment of the films.[73,76] Izaki et al. demonstrated that annealing electrodeposited CuO films altered the Eg value.[76] They reported a reduction of 7.5% in E_g after annealing the as-deposited CuO at 773K. They suggested that the changes in the composition and lattice constant were induced by the annealing process, altering the CuO band gap. [76]

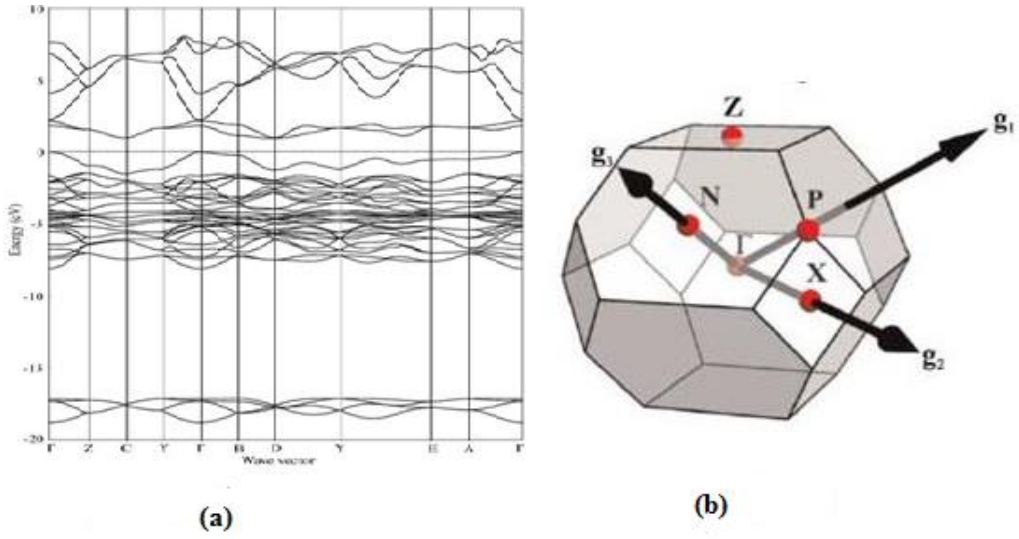

Fig 2. 10. (a) Electronic band structure and density of states from hybrid functional DFT calculations and (b) Brillouin zones with special high symmetry *k* points of cupric oxide Reprinted with permission from ref [68].

2.7.4 Electrical properties

The electrical conductivity and hole density of p-type Cu_2O films vary with copper vacancy density, which act as shallow acceptors.[66] Similarly in CuO, copper deficiencies account for the intrinsic p type semiconducting behaviour.[77] Suda et al. and Young et al. have studied the effect of temperature on electrical conductivity of CuO and Cu_2O films, respectively (Figure 2. 11 a,b).[78,79] They have shown that an increase in temperature increases the conductivity of CuO and Cu_2O due to an increase in hole concentration.[78] It is possible to tune the electrical properties (resistivity, carrier concentration and mobility) of Cu_xO by changing the stoichiometry and crystallinity of the Cu_xO films during the deposition process. Deposition parameters, such as pH of the solution in electro-deposition and hydrothermal methods and ion pressure and concentration in RF sputtering techniques, significantly contribute to changes in stoichiometry and crystallinity.[80,81]

Table 2.8 presents the different electrical properties of the thin layers of CuO performed by different methods of the deposit.

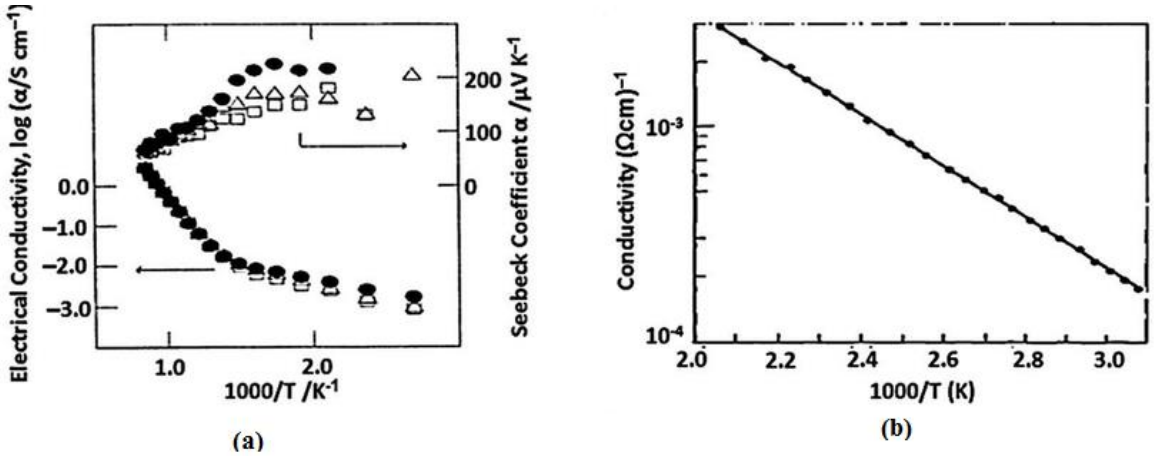

Fig 2. 11. (a) Temperature dependence for electrical conductivity and Seebeck coefficient of CuO in oxygen (●), in air (Δ) and in 3% O_2–Ar (□), (b) Electrical conductivity of Cu_2O single crystal vs 1/T. Reprinted with permission from (a) ref [79] copyright (1992) by The Japan Society of Applied Physics, (b) ref [78] copyright (1969) by Elsevier.

Table 2. 8 Electrical properties of copper oxide (CuO)

Deposit methods	Parameters	ρ (Ω.cm)	n_V (cm^{-3})	μ ($cm^2.V^{-1}s^{-1}$)
Spray	250°C	101.5×10^2	0.9×10^{12}	0.34
	300°C	7.3×10^2	1.27×10^{12}	-
	350°C	0.5×10^2	3.92×10^{12}	-
Sputtering	Oxygen percentage (%)			
	10	0.001×10^3	-	-
	20	0.130×10^3	-	-
	30	0.700×10^3	-	-
Sol gel	400-650 °C	127-371	-	-
Bath Chemical	300°C	2.7×10^5	-	-
	400°C	2×10^5	-	-
	500°C	6.8×10^5	-	-

2.7.5 Optical properties

The optical properties are a crucial parameter for thin films dedicated to optoelectronic devices. The importance of CuO optical proprieties originated from it is useful applications as an absorber layer in solar cells. This application requires the fulfillment of a high absorption in the visible range of solar spectrum.

Since the deposition technique and the experimental parameters affects the structural properties, the film surface morphology, the optical properties are also altered by the

preparation conditions [82,83,84]. Regardless the deposition technique, CuO thin films have a transparency ranged from 0 to 80%. In figure 2. 12 we have reported transmission spectra of CuO thin films deposited by different methods.

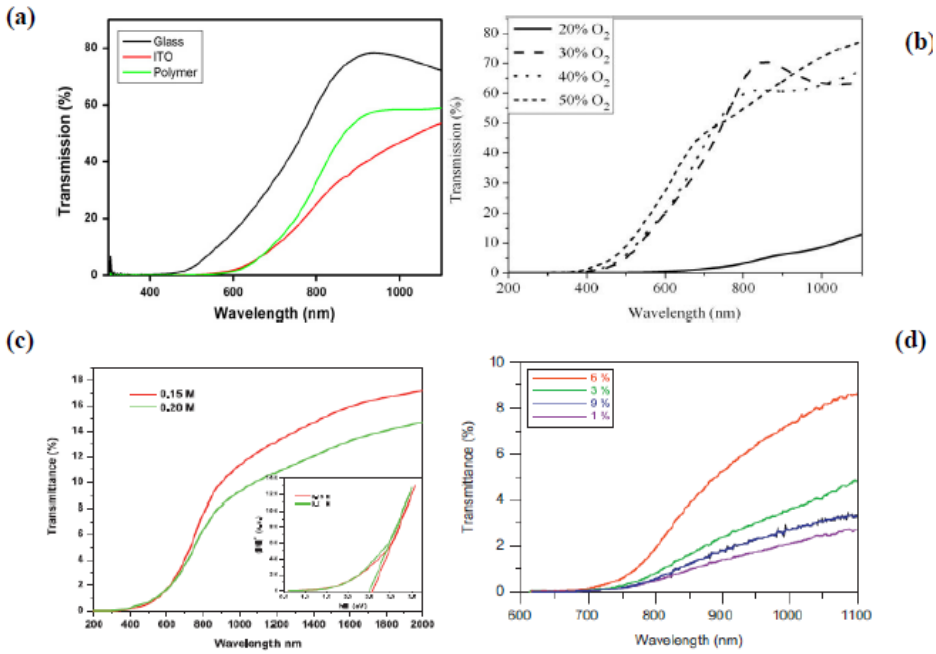

Fig 2. 12. Transmittance spectra reported in CuO thin films prepared by different techniques: (a) sol- gel [64], (b) sputtering [62] (c) spray pyrolysis [60], (d) SILAR method [79].

The optical band gap (Eg) is generally deduced from the optical transmittance. Bulk cupric oxides (CuO) have a direct narrow band gap of 1.2eV. However in CuO thin films the optical band gap can vary in a wide range from 1 to 1.8eV depending on the deposition techniques and parameters.

Numerous experimental studies emphasized that the band gap variation can be due to various factors such as: grain size, substrates temperature, thickness, doping concentration, lattice strain, structural parameters and disorder.

The refractive index of bulk CuO is equal to 2.63. The later is deduced from the ellipsometric measurements. For CuO thin films, the refractive index changes in the range of 1.5 to 3.5 according to the deposition conditions [85,86].

The optical band structure and optical transitions are affected by the presence of localized states in the band gap characterized by a band tail. This tail width is commonly known as Urbach tail or disorder in films network (E_{00}). Basically, Urbach energy depends on the static and induced disorder and deposition temperature .

2.8 Applications of Cu_xO

CuO is a promising material for various applications due to the abundance of its components in nature, low-cost production, good thermal stability, and electrochemical properties. This combined property enables CuO thin films to be a serious candidate for several applications namely: high-temperature superconductors [82], solar cells [82,83], gas sensors [62], magnetic storage media [64], varistors [1] and catalysis [83], antimicrobial activity [62], photoelectron chemical cell [84] and Li batteries [58].

2.8.1 Solar cells and light emitting diodes

Cu_xO films are possible candidates for developing different types of optical devices, including solar cells based on dye-sensitized and heterojunction architectures as well as organic light emitting diodes.

The quest and need for a clean and economical energy source have increased interest in the development of solar applications. Amongst various metal oxide materials for solar energy applications, Cu_xO has attracted increasing interest due to its theoretical power conversion efficiency (PCE) of 18% and an absorption coefficient higher than single crystalline Si.[87]

As described previously Cu_xO is an intrinsically p-type material. However, self-compensation problems and dopant solubility have inhibited the synthesis of n-type Cu_xO to produce efficient homojunctions for photovoltaic applications.[88,89,90] Therefore, heterojunction architectures have been employed with other n-type semiconductors such as ZnO [91,92], CdO [93], TiO_2 [94,95], Ga_2O_3 [96] and GaN. [66] Amongst the aforementioned n-type semiconductors, ZnO has been found to be the most stable and exhibit relatively low lattice mismatch of 7.6% between the (002) ZnO and (111) Cu_2O phase.[91,97,88] Despite the predicted PCE value of 18%, in practice the ZnO-Cu_2O solar systems have yet to reach high efficiencies [88,92,98]. To date, the highest efficiency ever reported for bilayer ZnO-CuO heterojunction solar cells has been 3.83% [99]. This is due to the fact that theoretically their intrinsic electronic band structures do not permit an open circuit voltages larger than 0.7 V [98]. J–V characteristic of this solar cells, in dark and under illumination together with a cross section are reported in figure 2. 13.

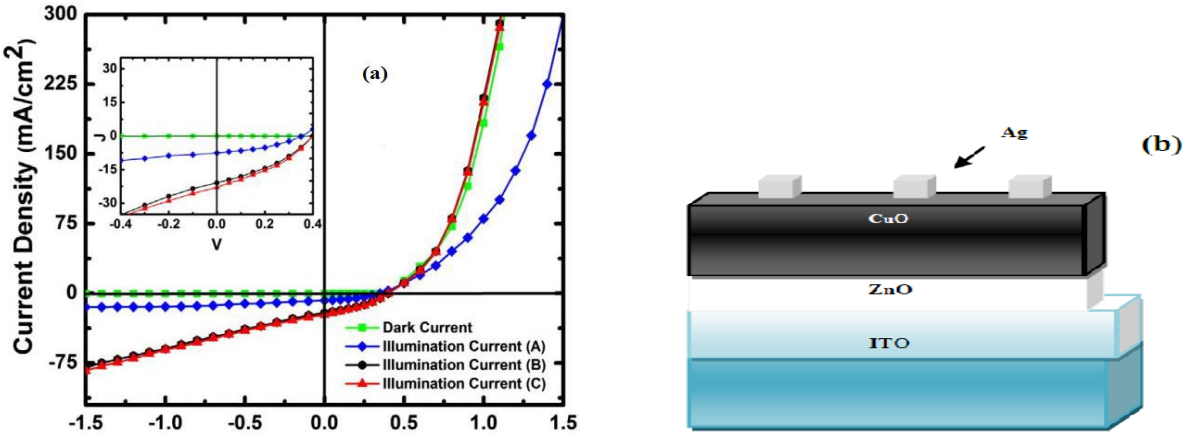

Fig 2. 13. (a) J-V characteristic under dark and illumination and (b) cross section of glass/ITO/ZnO/CuO thin film solar cells.

Cu_xO has also been used in organic light emitting diodes (OLEDs).[99,100] In order to construct efficient OLEDs, it is important to optimize the carrier injection ability at the interface of the active layer and anode materials. The Cu_xO films are commonly used as hole injection layers (HILs) to lower the hole injection barrier.[99,101,102] Kim *et al.* have reported the advantage of using a mixed stoichiometry of CuO and Cu_2O for increasing the performance of OLEDs.[99] Mixed stoichiometry of Cu_xO contains high density of defects such as oxygen vacancies or unbonded oxygen atoms, which act as an extra energy state within the energy gap of the Cu_xO layer. Interestingly, when the energy levels of these gap states are aligned with the highest occupied molecular orbital (HOMO) level of the hole transporting layer, no potential barrier is produced at the anode interfaces ,which can lead to an increase in the hole injection efficiency.[99]

2.8.2 Gas sensor

Cu_xO offers great potential for the development of highly sensitive, yet low cost sensors. This includes optical, gas and bio sensors. Photodetectors are important devices that can be used in various applications, including thermal imaging systems, free-space communications, navigator aids and ozone-layer monitoring.[102,103] Among the semiconductor materials, Cu_xO has proven an attractive material for making photodetectors due to its relatively low band gap and remarkable optoelectronics properties.[103,104]

Cu_xO also offers a great possibility for developing highly sensitive semiconductor-based gas sensors. The sensing properties of Cu_xO can be improved by decreasing its size to nanoscale dimensions (comparable to twice of the Debye length) and by adding appropriate

dopants.[105] Catalytic nanoparticles such as Pd, [106] Pt,[107], Ag[108], and Au [107,109,110] attached to the Cu_xO surface, further increases its sensitivity, mainly due to spill-over effects.[109] Cu_xO thin films have been demonstrated to be highly sensitive towards various gas species including C_2H_5OH [110,103], CO[108], NO_2 [110], and H_2S[111]. Additionally, they have been also tested for organic vapor sensors including: ethanol, methanol and acetone vapor. The performances of CuO-based gas sensor fabricated by various deposition techniques and for various gas, are summarized in table 2.9.

Table 2. 9. CuO-based gas sensor performance fabricated by various deposition techniques and for various gas sensing [112,113].

Sensor and fabrication method	Gas detection	Operation temperature (°C)	Sensitivity y(%)	Response time (s)
Spray pyrolysis CuO	Ethanol 2500ppm	350	29	247
	Methanol 2500ppm	400	15	235
	H_2S 100ppm	200	80	2
Sol-Gel CuO/ZnO	H_2 3000ppm	200	60	250
RF magnetron sputtering CuO-$Cu_xFe_3O_4$	CO 500ppm	400	90	1260
Bath Chemical CuO	H2 1000 ppm	90	16	-
	Gasoline 1000ppm	90	28	-
	CO 1000pmm	90	2	-
Sol-Gel CuO	H_2S 200ppm	200	24	25

2.8.3 Photo-catalytic

Cu_xO is a promising photo–catalyst that is used in many chemical processes, such as organic contamination degradation and water splitting under visible–light irradiation owing to their small band gap and low cost.[114,115] Under illumination, Cu_xO produces electron/hole pairs that can generate hydroxyl radicals (•HO) from water. This radical is capable of mineralizing most organic molecules.[116] For water splitting applications, the majority charge carriers of the Cu_xO (holes) oxidize water to oxygen gas (O_2), while the photo-generated minority charge

carriers (electrons) reduce water to hydrogen gas (H_2).[116,117,118] Significantly, the Cu_xO conduction band is more negative than the redox potential of H^+/H_2, which allows sunlight to produce H_2 from water. [119]

2.8.4 Electrochromic devices

Nanostructured Cu_2O electrochromic based systems, such as smart windows and optical displays, have been studied since the 1990s.[110] It has been found that Cu_2O exhibits cathodic electrochromism, being transparent under visible illumination in their oxidized state and almost black when switched to their reduced state in the presence of an electrolyte containing positive ions such as H^+, Li^+ and Na^+.[83,106,111] Generally, it has been found that the electrochromic process corresponds to the conversion of Cu_2O (transparent) to CuO (black) in a reversible reduction-oxidation process (redox).[106,111] To date, the best coloration efficiency obtained by Cu_2O nanostructures has been up to $37cm^2C^{-1}$, which is only one–fourth of the best of those made from WO_3 nanoporous structures ($141.5cm^2C^{-1}$) .[118,119] Unfortunately, nanostructured Cu_2O requires high coloration voltage and shows poor stability[112], and further work should be carried out to solve such important issues.

2.8.5 Field emission

The field emission (FE) properties of nanostructured Cu_xO are far less reported than other oxides materials such as ZnO, SnO_2 and In_2O_3. Due to its relatively narrow band gap, Cu_xO offers an attractive alternative to serve as a FE emitter.[120,121] In a FE system the emitting capability is believed to be highly dependent on both the properties of the material and configuration of the cathode [23]. It is known that materials with higher aspect ratios and sharp edges generally produce higher FE currents.[120,121,122] Zhu et al. have reported FE measurements of CuO nanowire films with a low turn-on field of 3.5-4.5$V\mu m^{-1}$. They obtained a large current density of 0.45 mA cm^{-2} at an applied electric field of $7V\mu m^{-1}$.[123] Nanostructured Cu_2O also exhibits relatively high FE performance. Shi et al. have demonstrated Cu_2O micro-porous cubes with a low turn'on field of $3.1V\mu m^{-1}$.
They showed a high current density of $1mAcm^{-2}$ at an applied electric field of $11V\mu m^{-1}$.[122] It has also been reported that Cu_2O can be coupled with other metal oxides such as ZnO or TiO_2 to enhance its FE performance (Figure 2. 14).[121,124,125] This enhanced FE is attributed to the alteration in electron affinity of Cu_xO by the other metal oxides forming a nano-heterojunction.[125] Additionally, the presence of the heterojunctions promotes charge separation, where the electrons move to ZnO or TiO_2 and the holes move to Cu_2O, which reduces the recombination of electron-hole pairs.[125]

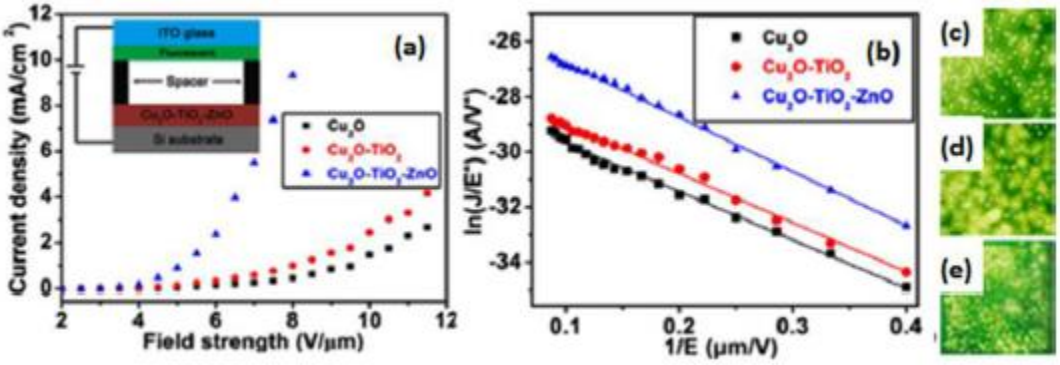

Fig 2. 14. (a) Field emission J−E curves, (b) corresponding F-N plots of the samples. (c)-(e) Electron emission images of the pure Cu_2O nanopines, Cu_2O-TiO_2-ZnO composite samples, respectively. [124]

2.8.6 Other Applications

Nanostructured Cu_xO has also been reported for many applications other than those presented in sections 4.1 to 4.8. Of note, nanostructured CuO has been used in ceramic resistors[126] and super capacitors.[127,128] Nanostructured Cu_2O has also been incorporated in memristors,[125,127] heterogeneous catalysis,[129,130] anti-fouling [131,132] and thin-film transistors.[133] Of course, there are other applications for which Cu_xO has been used, but these are beyond the scope of this research.

Bibliography

[1] E.H. Nicollian,. J.R Brews,"*MOS Physics and Technology*". Wiley, New York (1982) .

[2] Lamri Zeggar Meryem ," *Cupric oxide thin films deposition for gas sensors application*" Ph thesis of the Mentouri-Constantine University , (2016) .

[3] A.S. Grove " *Physics and Technology of Semiconductor Devices*" Wiley, New York (1967) .

[4] Therese, G.H.A. and P.V. Kamath, *Electrochemical Synthesis of Metal Oxides and Hydroxides.* Chemistry of Materials, (2000). 12(5): p. 1195-1204.

[5] Wong Ching Hong., "*Electrosynthesis of oxide films on flexible plastics,*" Ph thesis , The Hong Kong Polytechnic University ,(2010) .

[6] M. Guilloux-Viry, "*Croissance epitaxiale et caracterisations de films minces supraconducteurs a haute temperature critique deposes in-situ par pulverisation cathodique ou ablation laser,*" Ph thesis, University of Rennes I, (1991).

[7] J. Mass, P. Bhattacharya, R.S. Katiyar**,** " *Effect of high substrate temperature on Aldoped ZnO thin films grown by pulsed laser deposition* " Materials Science and Engineering B103 (2003) 9-15.

[8] I. Ozerov, D. Nelson, A.V. Bulgakov, W. Marine, M. Sentis, " *Synthesis and laser processing of ZnO nanocrystalline thin films* ", Applied Surface Science , 212–213 (2003) 349–352.

[9] De la torre Y Ramos J.," *Etudes des propriétés optoélectroniques de structures et de composants à base de nanostructures de Si* " , Ph thesis, Institut national des sciences appliquées de Lyon, (2003).

[10] M. Bender, E. Gagaoudakis, E. Douloufakis, E. Natsakou, N. Katsarakis, V. Cimalla, G. Kiriakidis, E. Fortunato, P. Nunes, A. Marques, R. Martins, " *Production and characterization of zinc oxide thin films for room temperature ozone sensing* ", Thin Solid Films 418 (2002) 45-50.

[11] S. B. Majumder, M. Jain, P. S. Dobal, R.S. Katiyar," *Investigations on Solution Derived Aluminium Doped Zinc Oxide Thin Films*" , Materials Science and Engineering B103 (2003) 16-25.

[12] J. Nishino, Shigeo Ohshio, and Kiichiro Kamata, " *Preparation of Aluminum-Doped Zinc Oxide Films by a Normal-Pressure CVD Method* ", J. Am. Ceram. Soc., 75,3469 (1992)72.

[13] M. Banetoa, A. Enesca, Y. Lare, K. Jondoa, K. Napoa, A Duta, " *Effect of precursor concentration on structural, morphological and opto-electric properties of ZnO thin films prepared by spray pyrolysis* ", Ceramics International 40 (2014) 8397–8404.

[14] H. Morkoc, U. Ozgur, " *Zinc Oxide : Fundamentals* ", Materials and Device Technology , Wiley-VCH Verlag GmbH & Co, Wienheim, (2007) .

[15] S. Choopun, R.D. Vispute, W. Yang, R.P. Sharma, T. Venkatesan, H. Shen, " *Realization of band gap above 5.0 eV in metastable cubic-phase MgxZn1-xO alloy films* ", Appl. Phys. Lett. 80, 1529–1531 (2002).

[16] M. Kunisu, I. Tanaka, T. Yamamoto, T. Suga, T. Mizoguchi," *The formation of a rock-salt type ZnO thin film by low-level alloying with MgO* ". J. Phys.: Condens. Matter. 16, 3801–3806 (2004).

[17] C. Jagadish, S.J. Pearton, " *Zinc Oxide Bulk* " , Thin Films and Nanostructures (Elsevier, New York, 2006).

[18] M.S.Ramachandra Rao, Tatsuo Okada," *ZnO Nanocrystals and Allied Materials*",Springer Series in Materials Science 180, New Delhi , India (2014).

[19] Y.G. Wang, S.P. Lau, X.H. Zhang, H.H. Hng, H.W. Lee, S.F. Yu, B.K. Tay, Journal of Crystal Growth.Vol. 259 (2003) 335–342 .

[20] R. Kaur, A.V. Singh, R.M. Mehra, " *Sol–gel derived highly transparent and conducting yttrium doped ZnO films* ", Journal of Non-Crystalline Solids.Vol. 352(2006)2335- 2338.

[21] F. Yakuphanoglua, Saliha Ilicanb, Mujdat Caglar, Yasemin Caglar, Superlattices and Microstructures 47 (2010) 732- 743.

[22] M. Ghasemi Varnamkhasti, Hamid Reza Fallah , Mehdi Zadsar, " *Effect of heat treatment on characteristics of nanocrystalline ZnO films by electron beam evaporation* " , Vacuum 86 (2012) 871- 875.

[23] X.Q. Gu, L.P. Zhu, L. Cao, Z.Z. Ye, H.P. He, Paul K. Chu," *Optical and electrical properties of ZnO:Al thin films synthesized by low-pressure pulsed laser deposition*", Materials Science Semiconductor Processing 14 (2011) 48–51.

[24] M. Purica, E. Budianu , E. Rusu , M. Danila , R. Gavrila ," *Optical and structural investigation of ZnO thin films prepared by chemical vapor deposition (CVD)* ", Thin Solid Films 403 –404 (2002) 485–488.

[25] Yu-Zen Tsai, Na-Fu Wang, Chun-Lung Tsai,"*Fluorine-doped ZnO transparent conducting thin films prepared by radio frequency magnetron sputtering* " , Thin Solid Films 518 (2010) 4955–4959.

[26] A. Ashrafi, C. Jagadish," *Review of zincblende ZnO: stability of metastable ZnO phases* ". J. Appl. Phys. 102, 071101 (2007) .

[27] I. Ivanov, J. Pollmann, " *Electronic structure of ideal and relaxed surfaces of ZnO: a prototype ionic wurtzite semiconductor and its surface properties* ". Phys. Rev. B. 24, 7275–7296 (1981).

[28] M. Johan . Carlsson,." *A First-Principles Study of Interface Systems: Electronic properties of Metal Quantum Wells and Varistor Materials*.", Ph Thesis, Chalmers University of Technology and Goteborg University, Sweden (2002).

[29] M. Rebien, W. Henrion, M. Bär, Ch.-H. Fischer," *Optical properties of ZnO thin films: Ion layer gas reaction compared to sputter deposition* " , App. Phys. Lett., 80 (2002) 3518.

[30] F. Ng-Cheng-Chin, M. Roslin, Z. H. Gu. T. Z. Fahidy," *On the transmittance properties of electrolytically deposited thin zinc oxide films* " , J.Phys.D Appl.Phy; 31(1998)L71.

[31] Jinzhong Wang, Vincent Sallet, François Journal,And M.Botelho do Rego,Elangovan Elamurugu,Rodrigo Martins, Elvira Fortunato ," *Influence of substrate temperature on N-doped ZnO films deposited by RF magnetron sputtering*" ,Thin Solid Films 515 (2007)8785-8788.

[32] T. L. Chu, S. S. Chu, " Thin film II–VI photovoltaics ,"Solid-State Electronics, 38(1995)5.

[33] Z. Sekkal, Atomeset liaison chimique, edition OPU(1988).

[34] W. Li. D. Mao, F. Zhang, X.Wang, X. Liu, S. Zou, Q. Li, and J. Xu, Nucl.Instrum Methods.Phys.Res., B169 (2000)59.

[35] F. Paraguay D., J. Morales, W. Estrada L.,E. Andrade, M. Miki-Yoshida" *Growth, structure and optical characterization of high quality ZnO thin films obtained by spray pyrolysis*", Thin Solid Films 366 (2000) 16-27.

[36] Dietz, R.E., J.J. Hopfield, and D.G. Thomas, "*Excitons and the Absorption Edge of ZnO"*. Journal of Applied Physics, (1961). 32(10): p. 2282-2286.

[37] Bagnall, D.M., " *Optically pumped lasing of ZnO at room temperature",* Applied Physics Letters, (1997). 70(17): p. 2230-2232.

[38] Ohtomo, A., "*Room temperature ultraviolet laser emission from ZnO nanocrystal thin films grown by laser MBE",* Materials Science and Engineering B-Solid State Materials for Advanced Technology, (1998). 54(1-2): p. 24-28.

[39] Dong, B.Z., "*Effect of thickness on structural, electrical, and optical properties of ZnO :Al films deposited by pulsed laser deposition",* Journal of Applied Physics, (2007). 101(3):p. 7.

[40] Krtschil, A. "*Local p-type conductivity in n-GaN and n-ZnO layers due to inhornogeneous dopant incorporation*", (2005), Awaji Isl, JAPAN: Elsevier Science Bv.

[41] Burstein, M. and J. Loeb, "*Antithrombine naturelle et cofacteur plasmatique de lheparine*", Presse Medicale, 1954. 62(71): p. 1486-1486.

[42] R. Tena-Zaera, M.A. Ryan, A. Katty, G. Hodes, S. Bastide, C. Lévy-Clément, "*Fabrication and characterization of ZnO nanowires/CdSe/CuSCN eta-solar cell",* C.R. Chimie 9 (2006) pp. 717-729.

[43] D. Kim, H. Kim, "*Self-textured transparent conductive oxide film improves efficiency of solar cells",* Proc. of SPIE 7603 (2010) pp. 76030G-1-76030G-8.

[44] M. Debliquy, "*Capteurs de gaz à semi-conducteurs",* Techniques de l'Ingénieur (2006).

[45] Z.L. Wang,"*Nanostructures of zinc oxide",* Materialstoday 7 (2004) pp.26-33, ISSN: 1369- 7021.

[46] J. Zhang, S. Wang, Y. Wang, M. Xu, G. Xia, S. Zhang, W. Huang, X. Guo, S. Wu, "*ZnO hollow spheres: Preparation, characterization, and gas sensing properties",* Sens. Actuator B 139 (2009) pp. 411-417.

[47] J.Y. Lee, J.H. Lee, H.S. Kim, C.-H. Lee, H.-S. Ahn, H.K. Cho, Y.Y. Kim, B.H. Kong, H.S. Lee, "*A study on the origin of emission of the annealed n-ZnO/p-GaN heterostructure LED"*, Thin Solid Films, 517 (2009) pp. 5157-5160.

[48] S. Krishnamoorthy, A.A. Iliadis, "*Properties of high sensitivity ZnO surface acoustic wave sensors on SiO_2/(100) Si substrates"*, Solid-State Electronics 52 (2008) pp. 1710-1716.

[49] Y.C. Lin, C.R. Hong, H.A. Chuang," *Fabrication and analysis of ZnO thin film bulk acoustic resonators"*, Appl. Surf. Sci. (2007) doi:10.1016/j.apsusc.2007.11.059

[50] K.M. Zhang, Y.P. Zhao, F.Q. He, D.Q. Liu, "*Piezoelectricity of ZnO films prepared by sol-gel method"*, Chin. J. Chem. Phys. 20 (2007) pp. 721-726.

[51] D. Royer, V. Kmetik, *Mesure optique de constantes piézoélectriques à l'aide d'une sonde interférométrique hétérodyne*, J. Phys. IV France 02 (1992) pp. C1-785-C1-788.

[52] B. Hannane, "*Elaboration et caractérisation des composites dopes par des agrégats nanométriques de semi conducteurs"*, Ph thesis of the Mentouri-Constantine University (2007) pp. 3-14.

[53] E.S. Elmolla, M. Chaudhuri, "*Degradation of amoxicillin, ampicillin and cloxacillin antibiotics in aqueous solution by the UV/ZnO photocatalytic process"*, J. Hazard. Mater. 173 (2010) pp. 445-449.

[54] N.V. Kaneva, D.T. Dimitrov, C.D. Dushkin," *Effect of nickel doping on the photocatalystic activity of ZnO thin films under UV and visible light"*, Appl. Surf. Sci. 257 (2011) pp. 8113-8120.

[55] A. Laplanche, "*La photocatalyse, une technique prometteuse en emergence"*, La revue trimestrielle du réseau Ecrin, N°60 (2005) pp. 20-26.

[56] F.J. Arregui. "*Sensors Based on Nanostructured Materials*", Berlin Springer (2008).

[57] S. M. Wilhelm,Y. Tananizawa, and N. Hachemn," *A photo-electrochemical investigation of semiconducting oxide films on copper*", Corrosion Science, 22 (1982)791.

[58] Y.S. Gong, C. Lee, C.K. Yang," *Atomic force microscopy and Raman spectroscopy studies on the oxidation of Cu thin films*" , J. Appl. Phys. 77 (1995) 5422.

[59] L.S. Huanga, S.G. Yanga, T. Lia, B.X. Gua, Y.W. Dua, Y.N. Lub, S.Z. Shit, J. Cryst. Growth 260 (2004)130.

[60] J.H. Lee, B.W. Yeo, B.O. Park;" *Effects of the annealing treatment on electrical and optical properties of ZnO transparent conduction films by ultrasonic spraying pyrolysis* ", Thin Solid Films 457 (2004) 333.

[61] K. Santra, C.K. Sarkar, M.K. Mukherjee, B. Ghosh," Copper oxide thin films grown by plasma evaporation method", Thin Solid Films 213 (1992) 226.

[62] B. Balamurugan,B.R. Mehta," *Optical and structural properties of nanocrystalline copper oxide thin films prepared by activated reactive evaporation*", Thin solid films 396 (2001) 90.

[63] E.R. Kari, K.S. Brown, Choi, Chem. Commun 23 (2006) 3311.

[64] N. Serin, T. Serin, S. Horzum, Y. Celik,"*Annealing effects on the properties of copper oxide thin films prepared by chemical deposition*", Semicond. Sci. Technol. 20 (2005) 398.

[65] S. Asbrink and L. J. Norrby, "*A Refinement Of Crystal Structure of Copper(II) Oxide With A Discussion of Some Exceptional ESDS*," Acta Crystall. B-Stru., vol. B 26, pp. 8-&, (1970).

[66] B. K. Meyer, A. Polity, D. Reppin, M. Becker, P. Hering, P. J. Klar, et al., "*Binary Copper Oxide Semiconductors: From Materials Towards Devices*," Phys. Status Solidi B, vol. 249, pp. 1487-1509, (2012).

[67] W. Y. Ching, Y. N. Xu, and K. W. Wong, "Ground-State And Optical- Properties of Cu_2O And CuO Crystals," Phys. Rev. B, vol. 40, pp. 7684-7695, (1989).

[68] C. Frondel, "*Paramelaconite a Tetragonal Oxide of Copper*," Am. Mineral., vol. 26, pp. 657-672, (1941).

[69] A. E. Rakhshani and F. K. Barakat, "*Optical Constants of Reactively Sputtered Cupric Oxide Films*," Mater. Lett., vol. 6, pp. 37-40, (1987).

[70] J. Ghijsen, L. H. Tjeng, J. Vanelp, H. Eskes, J. Westerink, G. A. Sawatzky, et al., "*Electronic-Structure of Cu_2O and CuO*," Phys. Rev. B, vol. 38, pp. 11322-11330, (1988).

[71] M. F. Al-Kuhaili, "*Characterization of Copper Oxide Thin Films Deposited by The Thermal Evaporation of Cuprous Oxide (Cu_2O)*," Vacuum, vol. 82, pp. 623-629, (2008).

[72] A. A. Ogwu, E. Bouquerel, O. Ademosu, S. Moh, E. Crossan, and F. Placido, "*The Influence of RF Power And Oxygen Flow Rate During Deposition on The Optical Transmittance of Copper Oxide Thin Films Prepared by Reactive Magnetron Sputtering*," J. Phys. D Appl. Phys., vol. 38, pp. 266-271, (2005).

[73] K. Nakaoka, J. Ueyama, and K. Ogura, "*Photoelectrochemical Behavior of Electrodeposited CuO and Cu_2O Thin Films on Conducting Substrates*," J. Electrochem. Soc., vol. 151, pp. C661-C665, (2004).

[74] J. C. Tauc, "*Optical Properties of Solids"*. Amsterdam: North-Holland,(1972).

[75] J. F. Pierson, A. Thobor-Keck, and A. Billard, "*Cuprite, Paramelaconite And Tenorite Films Deposited by Reactive Magnetron Sputtering*," Appl. Surf. Sci., vol. 210, pp. 359-367, (2003).

[76] M. Izaki, "*Effects of Annealing on Optical and Electrical Characteristics of P-Type Semiconductor Copper (II) Oxide Electrodeposits*," Thin Solid Films, vol. 520, pp. 2434-2437, (2012).

[77] Y. K. Jeong and G. M. Choi, "*Nonstoichiometry and Electrical Conduction of CuO*," J. Phys. Chem. Solids, vol. 57, pp. 81-84, (1996).

[78] A. P. Young and C. M. Schwartz, "*Electrical Conductivity And Thermoelectric Power of Cu_2O*," J. Phys. Chem. Solids, vol. 30, pp. 249-252, (1969).

[79] S. Suda, S. Fujitsu, K. Koumoto, and H. Yanagida, "*The Effect of Atmosphere And Doping On Electrical-Conductivity of CuO*," Jpn. J. Appl. Phys. 1, vol. 31, pp. 2488-2491,(1992).

[80] K. Mizuno, M. Izaki, K. Murase, T. Shinagawa, M. Chigane, M. Inaba, *et al.*, "*Structural and Electrical Characterizations of Electrodeposited P-Type Semiconductor Cu_2O Films*," J. Electrochem. Soc., vol. 152, pp. C179-C182, (2005).

[81] D. O. Scanlon and G. W. Watson, "*Undoped n-Type Cu_2O: Fact or Fiction?*," J. Phys. Chem. Lett., vol. 1, pp. 2582-2585, (2010).

[82] W. Shockley and H. J. Queisser ," *Detailed Balance Limit of Efficiency of p-n Junction Solar Cells*" , J. Appl. Phys. 32 (1961)510.

[83] L.S. Huang, S.G. Yang, T. Li, B.X. Gu, Y.W. Du, Y.N. Lu, S.Z. Shi," *Preparation of large-scale cupric oxide nanowires by thermal evaporation method*"J. Cryst. Growth 260 (2004) 130.

[84] I. Singha, R.K. Bedi ;" *Studies and correlation among the structural, electrical and gas response properties of aerosol spray deposited self assembled nanocrystalline CuO*", Applied Surface Science 257 (2011)7592.

[85] J. Moralesa, L. Sa´ncheza,, F. Martı´nb, J.R. Ramos-Barradob, M.Sa´nchezb," *Nanostructured Copper Oxide Thin Film for Ethanol Vapor Sensing*", Thin Solid Films 474 (2005)133.

[86] V. Dhanasekaran , T. Mahalingam, R. Chandramohan, Jin-Koo Rhee , J.P. Chu d," *Electrochemical deposition and characterization of cupric oxide thin films* ", Thin Solid Films 520 (2012) 6608.

[87] W. Siripala, A. Ivanovskaya, T. F. Jaramillo, S. H. Baeck, and E. W. McFarland, "*A Cu_2O/TiO_2 Heterojunction Thin Film Cathode For Photoelectrocatalysis*," Sol. Energ. Mat. Sol. C., vol. 77, pp. 229-237, (2003).

[88] K. P. Musselman, A. Marin, L. Schmidt-Mende, and J. L. MacManus- Driscoll, "*Incompatible Length Scales in Nanostructured Cu_2O Solar Cells*," Adv. Funct. Mater., vol. 22, pp. 2202-2208, (2012).

[89] S. Ishizuka and K. Akimoto, "*Control of The Growth Orientation And Electrical Properties of Polycrystalline Cu_2O Thin Films by Group-IV Elements Doping*," Appl. Phys. Lett., vol. 85, pp. 4920-4922, (2004).

[90] R. P. Wijesundera, "*Fabrication of The CuO/Cu_2O Heterojunction Using An Electrodeposition Technique For Solar Cell Applications*," Semicond. Sci. Tech., vol. 25, (2010).

[91] M. Izaki, T. Shinagawa, K.-T. Mizuno, Y. Ida, M. Inaba, and A. Tasaka, "*Electrochemically Constructed P-Cu_2O/N-ZnO Heterojunction Diode for Photovoltaic Device*," J. Phys. D Appl. Phys., vol. 40, pp. 3326-3329, (2007).

[92] K. P. Musselman, A. Marin, A. Wisnet, C. Scheu, J. L. MacManus-Driscoll, and L. Schmidt-Mende, "*A Novel Buffering Technique for Aqueous Processing of Zinc Oxide Nanostructures and Interfaces, and Corresponding Improvement of Electrodeposited ZnO-Cu_2O Photovoltaics*," Adv. Funct. Mater., vol. 21, pp. 573-582, (2011).

[93] Y. Hames and S. E. San, "*CdO/Cu_2O Solar Cells by Chemical Deposition*," Sol. Energy, vol. 77, pp. 291-294, (2004).

[94] D. Li, C.-J. Chien, S. Deora, P.-C. Chang, E. Moulin, and J. G. Lu, "*Prototype of a Scalable Core-Shell Cu_2O/TiO_2 Solar Cell*," Chem. Phys. Lett., vol. 501, pp. 446-450, (2011).

[95] M. Wang, L. Sun, Z. Lin, J. Cai, K. Xie, and C. Lin, "*P-N Heterojunction Photoelectrodes Composed of Cu_2O-Loaded TiO_2 Nanotube Arrays With Enhanced Photoelectrochemical And Photoelectrocatalytic Activities*," Energ. Environ. Sci., vol. 6, pp. 1211-1220, (2013).

[96] T. Minami, Y. Nishi, and T. Miyata, "*High-Efficiency Cu_2O-Based Heterojunction Solar Cells Fabricated Using a Ga_2O_3 Thin Film as N-Type Layer*," Appl. Phys. Express, vol. 6, (2013).

[97] B. M. Fariza, J. Sasano, T. Shinagawa, S. Watase, and M. Izaki, "*Light- Assisted Electrochemical Construction of (111)Cu_2O/(0001)ZnO Heterojunction*," Thin Solid Films, vol. 520, pp. 2261-2264, (2012).

[98] K. P. Musselman, A. Wisnet, D. C. Iza, H. C. Hesse, C. Scheu, J. L. MacManus-Driscoll, et al., "*Strong Efficiency Improvements in Ultra-low- Cost Inorganic Nanowire Solar Cell*s," Adv. Mater., vol. 22, pp. E254-E285, (2010).

[99] T. Minami, Y. Nishi, T. Miyata, and J. Nomoto, "*High-Efficiemcy Oxide Solar Cells with ZnO/Cu_2O Heterjunction Fabricated on Thermally Oxidized Cu_2O sheets*," Appl. Phys. Express, vol. 4, p. 62301, (2011).

[100] G. B. Murdoch, M. Greiner, M. G. Helander, Z. B. Wang, and Z. H. Lu, "*A Comparison of CuO and Cu_2O Hole-Injection Layers for Low Voltage Organic Devices*," Appl. Phys. Lett., vol. 93, (2008).

[101] W. P. Hu, K. Manabe, T. Furukawa, and M. Matsumura, "*Lowering of Operational Voltage of Organic Electroluminescent Devices by Coating Indium-Tin-Oxide Electrodes With a Thin CuO_x Layer*," Appl. Phys. Lett., vol. 80, pp. 2640-2641, (2002).

[102] T. Satoh and H. Fujikawa, "*Copper-Doped Indium Tin Oxide Electrode For Organic Light-Emitting Devices*," Jpn. J. Appl. Phys. 1, vol. 46, pp. 1640- 1642, (2007).

[103] S. B. Wang, C. H. Hsiao, S. J. Chang, K. T. Lam, K. H. Wen, S. C. Hung, et al., "*A CuO Nanowire Infrared Photodetector*," Sens. Actuator A Phys., vol. 171, pp. 207-211, (2011).

[104] S. Sahoo, S. Husale, B. Colwill, T.-M. Lu, S. Nayak, and P. M. Ajayan, "*Electric Field Directed Self-Assembly of Cuprous Oxide Nanostructures for Photon Sensing*," ACS Nano, vol. 3, pp. 3935-3944, (2009).

[105] A. Tricoli, M. Righettoni, and A. Teleki, "*Semiconductor Gas Sensors: Dry Synthesis And Application*," Angew. Chem. Int. Edit., vol. 49, pp. 7632-7659, (2010).

[106] H. Kim, C. Jin, S. Park, S. Kim, and C. Lee, "*H_2S Gas Sensing Properties of Bare and Pd-Functionalized CuO Nanorods*," Sens. Actuator B-Chem., vol. 161, pp. 594-599, (2012).

[107] X. Gou, G. Wang, J. Yang, J. Park, and D. Wexler, "*Chemical Synthesis, Characterisation and Gas Sensing Performance of Copper Oxide Nanoribbons*," J. Mater. Chem., vol. 18, pp. 965-969, (2008).

[108] G. X. Zhu, H. Xu, Y. Y. Xiao, Y. J. Liu, A. H. Yuan, and X. P. Shen, "*Facile Fabrication and Enhanced Sensing Properties of Hierarchically Porous CuO Architectures*," ACS Appl. Mater. Interfaces, vol. 4, pp. 744-751, (2012) .

[109] M. Ando, T. Kobayashi, and M. Haruta, "*Combined Effects of Small Gold Particles on The Optical Gas Sensing by Transition Metal Oxide Films*," Catal. Today, vol. 36, pp. 135-141, (1997).

[110] X.-W. Liu, F.-Y. Wang, F. Zhen, and J.-R. Huang, "*In Situ Growth of Au Nanoparticles on The Surfaces of Cu_2O Nanocubes for Chemical Sensors With Enhanced Performance*," RSC Advances, vol. 2, pp. 7647-7651, (2012).

[111] H. G. Zhang, Q. S. Zhu, Y. Zhang, Y. Wang, L. Zhao, and B. Yu, "*One-Pot Synthesis And Hierarchical Assembly of Hollow Cu_2O Microspheres With Nanocrystals-Composed Porous Multishell And Their Gas-Sensing Properties*," Adv. Funct. Mater., vol. 17, pp. 2766-2771, (2007).

[112] Y. Zhang, X. He, J. Li, H. Zhang, and X. Gao, "*Gas-Sensing Properties of Hollow And Hierarchical Copper Oxide Microspheres*," Sens. Actuator B Chem., vol. 128, pp. 293-298, (2007).

[113] L. Liao, Z. Zhang, B. Yan, Z. Zheng, Q. L. Bao, T. Wu, et al., "*Multifunctional CuO Nanowire Devices: P-type Field Effect Transistors and CO Gas Sensors*," Nanotechnology, vol. 20, (2009).

[114] D. Barreca, P. Fornasiero, A. Gasparotto, V. Gombac, C. Maccato, T. Montini, et al., "*The Potential of Supported Cu_2O and CuO Nanosystems in Photocatalytic H_2 Production*," Chemsuschem, vol. 2, pp. 230-233, (2009).

[115] Z. Zheng, B. Huang, Z. Wang, M. Guo, X. Qin, X. Zhang, et al., "*Crystal Faces of Cu_2O and Their Stabilities in Photocatalytic Reactions*," J. Phys. Chem. C, vol. 113, pp. 14448-14453, (2009).

[116] S. P. Meshram, P. V. Adhyapak, U. P. Mulik, and D. P. Amalnerkar, "*Facile Synthesis of CuO Nanomorphs And Their Morphology Dependent Sunlight Driven Photocatalytic Properties*," Chem. Eng. J., vol. 204–206, pp. 158-168, (2012).

[117] M. Hara, T. Kondo, M. Komoda, S. Ikeda, K. Shinohara, A. Tanaka, et al., "*Cu_2O as a Photocatalyst for Overall Water Splitting Under Visible Light Irradiation*," Chem. Commun., pp. 357-358, (1998).

[118] P. E. de Jongh, D. Vanmaekelbergh, and J. J. Kelly, "*Cu_2O: A Catalyst For The Photochemical Decomposition of Water?*," Chem. Commun., pp. 1069- 1070, (1999).

[119] M.-h. Yao, Y.-g. Tang, L. Zhang, H.-h. Yang, and J.-h. Yan, "*Photocatalytic Activity of CuO Towards HER in Catalyst From Oxalic Acid Solution Under Simulated Sunlight Irradiation*," T. Nonferr. Metal Soc., vol. 20, pp. 1944- 1949, (2010).

[120] S. Ishizuka and K. Akimoto, "*Control of The Growth Orientation And Electrical Properties of Polycrystalline Cu_2O Thin Films by Group-IV Elements Doping*," Appl. Phys. Lett., vol. 85, pp. 4920-4922, (2004).

[121] C. T. Hsieh, J. M. Chen, H. H. Lin, and H. C. Shih, "*Field Emission From Various CuO Nanostructures*," Appl. Phys. Lett., vol. 83, pp. 3383-3385, (2003).

[122] H. Shi, K. Yu, F. Sun, and Z. Zhu, "*Controllable Synthesis of Novel Cu_2O Micro/Nano-Crystals And Their Photoluminescence, Photocatalytic And Field Emission Properties*," CrystEngComm, vol. 14, pp. 278-285,(2012).

[123] Y. W. Zhu, T. Yu, F. C. Cheong, X. J. Xui, C. T. Lim, V. B. C. Tan, et al., "*Large-Scale Synthesis And Field Emission Properties of Vertically Oriented CuO Nanowire Films*," Nanotechnology, vol. 16, pp. 88-92, (2005).

[124] R. C. Wang and C. H. Li, "*Improved Morphologies and Enhanced Field Emissions of CuO Nanoneedle Arrays by Heating ZnO Coated Copper Foils*," Cryst. Growth Des., vol. 9, pp. 2229-2234, (2009).

[125] Y. Wang, K. Yu, H. H. Yin, C. Q. Song, Z. L. Zhang, S. C. Li, et al., "*Facile Synthesis, Enhanced Field Emission And Photocatalytic Activities of Cu_2O-TiO_2- ZnO Ternary Hetero-Nanostructures*," J. Phys. D Appl. Phys., vol. 46, (2013).

[126] S. Tanaka, Y. Sawai, and A. Chiba, "*Electrical Properties And Microstructure of CuO Ceramics Containing Small Amounts of Alkaline Earth Elements*," J. Eur, Ceram. Soc., vol. 24, pp. 289-293, (2004).

[127] K. Nagashima, T. Yanagida, K. Oka, and T. Kawai, "*Unipolar Resistive Switching Characteristics of Room Temperature Grown SnO_2 Thin Films*," Appl. Phys. Lett., vol. 94, p. 242902, (2009).

[128] L. M. Kukreja, A. K. Das, and P. Misra, "*Studies on Nonvolatile Resistance Memory Switching in ZnO Thin Films*," B. Mater. Sci., vol. 32, pp. 247-252, (2009).

[129] A. Shih, W. Zhou, J. Qiu, H.-J. Yang, S. Chen, Z. Mi, et al., "*Highly Stable Resistive Switching on Monocrystalline ZnO*," Nanotechnology, vol. 21, p. 125201, (2010).

[130] M. Janousch, G. I. Meijer, U. Staub, B. Delley, S. F. Karg, and B. P. Andreasson, "*Role of Oxygen Vacancies in Cr-doped $SrTiO_3$ for Resistance- Change Memory*," Adv. Mater., vol. 19, pp. 2232-2235, (2007).

[131] Y. C. Yang, F. Pan, Q. Liu, M. Liu, and F. Zeng, "*Fully Room-Temperature-Fabricated Nonvolatile Resistive Memory for Ultrafast and High-Density Memory Application*," Nano Lett., vol. 9, pp. 1636-1643, (2009).

[132] P. Liu, G. She, W. Shi, and D. Chen, "*Electric-Pulse-Induced Resistance Switching Observed in ZnO Nanotube Point Contact System*," Physica E, vol. 42, pp. 791-794, (2010).

[133] J. W. Seo, J.-W. Park, K. S. Lim, J.-H. Yang, and S. J. Kang, "*Transparent Resistive Random Access Memory and Its Characteristics for Nonvolatile Resistive Switching*," Appl. Phys. Lett., vol. 93, p. 223505, (2008).

3 Elaboration and Physico-Chemical Characterization of ZnO Substrate

Chapter 3

Elaboration and Physico-Chemical Characterization of ZnO Substrates

In this chapter, the conditions for the preparation of thin layers of ZnO by spray pyrolysis and the doping effect on their physico-chemical properties are presented.

ZnO thin layers of with different precursors were deposited on glass substrates by spray pyrolysis. Firstly, the principle briefly will be recall.

In order to obtain the desired characteristics of the developed layers, it is essential beforehand to control and optimize the deposition parameters. For this, we have characterized the microstructure and optics of our layers by different techniques such as scanning electron microscopy (SEM) for the observation of the texture and the surface of the layers. X-ray diffraction (DRX) and a spectrophotometer (UV-Visible) to obtain information on the directions of crystallographic growth and transmittance, energy of gap and disorder of the deposited layers. In the follow we will represent the techniques used in this study, elaboration of the films at optimized conditions and characterization with their formulas. Then discussion of the results will be take plays in this chapter.

3.1 Spray pyrolysis technique

Spray pyrolysis is a processing technique being considered in research to prepare thin and thick films, ceramic coatings, and powders. Unlike many other film deposition techniques, spray pyrolysis represents a very simple and relatively cost-effective processing method (especially with regard to equipment costs). It offers an extremely easy technique for preparing films of any composition. Spray pyrolysis does not require high-quality substrates or chemicals. The method has been employed for the deposition of dense films, porous films, and for powder production. Even multilayered films can be easily prepared using this versatile technique. Spray pyrolysis has been used for several decades in the glass industry and in solar cell production. Typical spray pyrolysis equipment consists of an atomizer, precursor

solution, substrate heater, and temperature controller. The following atomizers are usually used in spray pyrolysis technique: air blast (the liquid is exposed to a stream of air), ultrasonic (ultrasonic frequencies produce the short wavelengths necessary for fine atomization) and electrostatic (the liquid is exposed to a high electric field).

Many studies have been done over about three decades on chemical spray pyrolysis (SP) processing and preparation of thin films, since the pioneering work by Chamberlin and Skarman [1] in 1966 on cadmium sulphide (CdS) films for solar cells. Thereafter, due to the simplicity of the apparatus and good productivity of this technique on a large scale it offered a most attractive way for the formation of thin films of noble metals, metal oxides, spinel oxides, chalcogenides and superconducting compounds. Despite its simplicity, SP has a number of advantages:

- It offers an extremely easy way to dope films with virtually any element in any proportion by merely adding it in some form to the spray solution.
- Unlike closed vapor deposition methods, SP does not require high quality targets and/or substrates nor does it require vacuum at any stage, which is a great advantage if the technique is to be scaled up for industrial applications.
- The deposition rate and the thickness of the films can be easily controlled over a wide range by changing the spray parameters, thus eliminating the major drawbacks of chemical methods such as sol-gel which produces films of limited thickness.
- Operating at moderate temperatures (100±500°C), SP can produce films on less robust materials.
- Unlike high-power methods such as radio frequency magnetron sputtering (RFMS), it does not causes local overheating that can be detrimental for materials to be deposited. There are virtually no restrictions on substrate material, dimension or its surface profile.
- By changing composition of the spray solution during the spray process, it can be used to make layered films and films having composition gradients throughout the thickness.
- It is believed that reliable fundamental kinetic data are more likely to be obtained on particularly well characterized film surfaces, provided the films are quiet compact, uniform and that no side effects from the substrate occur. SP offers such an opportunity.

3.2 Thin film elaboration by spray pyrolysis technique

In the spray deposition process, a precursor solution is pulverized by means of a neutral gas (e.g. nitrogen) so that it arrives at the substrate in the form of very fine droplets. The constituents react to form a chemical compound onto the substrate. The chemical reactants are selected such that the products other than the desired compound are volatile at the temperature of deposition. Figure 3. 1 shows a typical spraying system. It mainly consists of spray nozzle, precursor solution, substrate heater, temperature controller and air compressor or gas propellant. To measure flow of precursor solution and air, liquid and gas flow meters are used. Vertical and slanted spray deposition arrangements with stationary or linearly moving spray nozzle are frequently used in this technique. To achieve uniform deposition the moving arrangements (either nozzle or substrates or both) have been used. Sometimes the spray assembly is mounted on a moving table and is rastered across the substrates using stepping motors. The properties of the film depend upon the anion to cation ratio, spray rate, substrate temperature, ambient atmosphere, carrier gas, droplet size and also the cooling rate after deposition. The film thickness depends upon the distance between the spray nozzle and substrate temperature, the concentration of the precursor solution and the quantity of the precursor solution sprayed. The film formation depends on the process of droplet landing, reaction and solvent evaporation, which are related to droplet size and momentum. An ideal deposition condition is when the droplet approaches the substrate just as the solvent is completely removed.

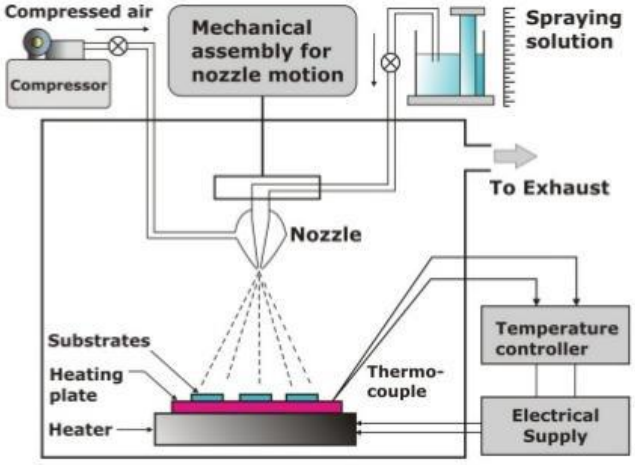

Fig. 3. 1. Schematic set-up for spray pyrolysis technique.

3.3 ZnO thin films preparation

The goal of the present study is the deposition and characterization of ZnO thin films by spray pyrolysis technique. Effect of lanthanum doped and importance of precursor type in fabricating ZnO thin films. Experimental details of films preparation by this techniques and the various characterization techniques used in this thesis will be presented.

In the contrary to the other deposition technique, spray pyrolysis has widely parameters to study. The most important parameters have been investigated in this study namely: different precursor and percentage of lanthanum chloride heptahydrate ($LaCl_3\,7H_2O$) doped .two sets of samples were prepared. In each set only one parameter is varied while the rest of parameters were fixed. For the prepared sets the distance between atomizer and substrate is fixed at 10 cm. substrate temperature 375°C, molarity of the solution 0.5 M . the temperature solution is fixed at room temperature (25°C). The dissolvent used for dissolved the salt source of zinc is (1:1 doble distillate water and methanol) and few drop of acitic acid . The choice of double distilled water is due to this abundance and the low cost. The total volume of the precursor solution is fixed to 20 ml. All the deposited ZnO films are deposited at cleaned glass substrates [2]. The glass substrates are cleaned following these steps:

1. The glass substrate were firstly cleaned ultrasonically in methanol to remove any impurity (grease o dust) stickled in the surface of the substrate three time several and for 10 min.
2. The glass substrates were secondly cleaned ultrasonically in distilled water to remove any trace of the methanol three several times and for 10 min.
3. The cleaned glass substrates are dried with dryer.

In tables 2. 1 (a-b) we have summarized the deposition parameters of each set. we have varied the zinc salt used as source of zinc . The deposition system of spray pyrolysis used for this study is shown in figure 3. 2.

Table 3.1-a Deposition parameters of the first series of ZnO samples.

Sample	Precursor salt	Molarity (M)	Time deposition (min)	Substrate temperature (°C)	Lanthanum ($LaCl_3\,7H_2O$)doping(w.t %)
A					**0**
B	**Zinc acetate**	**0.5**	**12**	**375**	**1**
C	**$C_4H_6O_4.H_2O$**				**4**
D					**5**

Table 3.1-b Deposition parameters of the secondly series of ZnO samples.

Sample	Precursor salt	Molarity (M)	Time deposition (min)	Substrate temperature (°C)	Lanthanum ($LaCl_3$ $7H_2O$)doping(w.t %)
A					**0**
B	**Zinc chloride**	**0.5**	**12**	**375**	**1**
C	**$Zn.Cl_2$**				**4**
D					**5**

Fig. 3. 2. The deposition system of spray pyrolysis.

3.4 Films characterization

Several techniques were used for the structural, morphological, and optical characterization of the films, these techniques are described below:

3.4.1 X-ray diffraction

The structural properties of the films were studied by X-Ray Diffraction (XRD), using Miniflex 600 with Cu-kα radiation of wavelength λ =1.5418 Å. The diffractometer reflections were taken at room temperature and the 2θ value were varied from 20 to 80°. The structural parameters of the all deposited ZnO films are estimated from the XRDML pattern. The crystallites size, lattice strain, dislocation density, texture coefficient and number of crystallites is calculated by the formulas given below:

The principle of the method is based on Bragg's law [3] which interprets the process of diffraction of electromagnetic waves on a crystal

$$n\lambda = 2d\,sin\theta \qquad (3.\,1)$$

n: is an integer called the order of reflection.

λ: the wavelength of X-rays.

d: the characteristic spacing between the crystal planes of a given specimen .

θ: the angle the incident beam and the normal to the reflecting lattice plane.

- The crystallites size was calculated from two formulas the Scherer's and Hall–Williamson equation formula [4] respectively:

$$D = k\lambda/\beta cos\theta \qquad (3.\,2)$$

$$(\beta cos\theta)/_{\lambda} = 1/_{D} + (\varepsilon sin\theta)/_{\lambda} \qquad (3.\,3)$$

where β is the FWHM (full width at half maximum) of diffraction peaks, θ is the Bragg angle, λ is the wavelength of the used X rays, D is the crystallite size and ε is the internal strain. D is estimated from the last square fit of β cos (θ) / λ vs. sin (θ) / λ of different peaks. The intercept of the equation plot with the y axis yields to the crystallite size.

- The texture coefficient (T_c) was calculated, which is defined [5,6]:

$$T_c(hkl) = \frac{I(hkl)/I_0(hkl)}{N^{-1}\sum_n^N I_n(hkl)/I_{0n}(hkl)} \qquad (3.\,4)$$

where I(hkl) and I_0(hkl) are the measured intensity and the standard intensity of the same (hkl) plane according to the JCPDS data whereas N and n are the reflection and the diffraction peaks number, respectively

- The lattice strain is calculated from two fowling equation [4] :

$$\varepsilon = \beta/4tan\theta \qquad (3.\,5)$$

$$(\beta cos\theta)/_{\lambda} = 1/_{D} + (\varepsilon sin\theta)/_{\lambda} \qquad (3.\,6)$$

where β is the FWHM (full width at half maximum) of diffraction peaks, θ is the Bragg angle, λ is the wavelength of the used X rays, D is the crystallite size and ε is the internal strain. The strain is equal to the slope of the plot of β cos (θ) / λ vs. sin (θ) / λ of different peaks.

- the lattice parameters were determined from XRD results using the following equation [7]:

$$1/d_{hkl}^2 = \frac{4}{3}\left(\frac{h^2+hk+k^2}{a^2}\right) + \frac{l^2}{c^2} \qquad (3.\ 7)$$

where d_{hkl}, (*hkl*), (*a*) and (*c*) are the inter-planar space, Miller indices, and the lattice parameters, respectively.

- The dislocation density (ξ) is calculated using this equation [4]:

$$\xi = 1/D^2 \qquad (3.\ 8)$$

where ξ is the dislocation density and D is the crystallite size.

3.4.2 Films morphology

Films morphology was analyzed using scanning electron microscope TESCAN VEGA3 SEM microscope. The grains size is estimated are also used to view the samples in profile and to measure the thickness of the deposited layers by SEM image.

3.4.3 Optical properties

The optical properties of the obtained films were studied using UV Visible transmittance spectroscopy by means of Shimadzu 3101PC double beam spectrophotometer. The optical band gap, disorder (Urbach energy) and absorption coefficient was also measured using the giving expression:

- The absorption coefficient (α): in the spectral region of the light's absorption, was deduced from the Beer-Lambert law using the following expression [8]:

$$\alpha = -\left(1/d\right) ln\left(100/T\right) \qquad (3.\ 9)$$

where α is absorption coefficient, d is the film thickness and T is the transmittance.

- The optical band gap (E_g) : The study of the spectrum of the absorption coefficient α of a semiconductor in the fundamental region and near the fundamental edge provides us with valuable information about the energy band structure of the material [8].

$$(\alpha h\upsilon)^2 = A(h\upsilon - E_g) \qquad (3.\ 10)$$

where α, E_g, and hν are the absorption coefficient, the optical band gap of the thin film and the photon energy where as A is a constant independent on hν., E_g values were deduced by extrapolating $(\alpha h\upsilon)^2 = 0$

- The disorder (E_{00}): the low absorption coefficient α region. The absorption coefficient of films shows a tail for sub-band gap photon energy. This tail is called the Urbach tail. The latter, which is closely related to the disorder in the film network, is expressed as [9]:

$$\alpha = \alpha_0 e^{\left(h\upsilon/E_{00}\right)} \qquad (3.\ 11)$$

where α_o is a constant and E_{00} is interpreted as the width of the tails of localized states in the gap region. To evaluate the values of α_o and E_{00}, one have to plot the variation of absorption coefficient α in logarithmic scale as a function of photon energy hν . The Urbach tail was determined from the slope of the variation of log (α) with the incident photon energy hν [10]. E_{00} can be estimated from the inverse slope of the linear plot of ln(α) versus hν.

3.4.4 Fourier transform infrared spectroscopy

FTIR is a technique based on the absorption of infrared radiation by the material analyzed, which is used to obtain information on the chemical bond in a material and to determine the purity and nature of the materials [11].

3.5 Results and discussion

In this section, we present the results of ZnO films prepared with two different precursors namely: zinc acetate($C_4H_6O_4.H_2O$) , and zinc chloride ($ZnCl_2$.) at various lanthanum doping in order to investigate the effect of this parameter.

- ***Influence of lanthanum doping***

3.5.1 Zinc Acetate

Zinc acetate is used as zinc source with molarity equal to 0.5 M and constant substrates temperature equal 375°C. The samples were deposited with various lanthanum chloride heptahydrate ($LaCl_3\,7H_2O$) doping ranged from: (0-5wt.%) as named in table 3. 1-a.

3.5.1.1 Deposition rate

In figure 3.3 we have reported the variation of growth rate as function of the different concentration of lanthanum. It was seen that the growth rate is very sensitive to the concentration of dopant and the nature of the starting solution. The difference between the behavior of the solutions is due to that of the dissociation enthalpy and the chemical nature of each precursor. It should be remembered that the enthalpy of dissociation of Zinc acetate is equal to 0.1Kcal / mol (0.043eV) [12]. As can be seen, the film thicknesses decrease with the increase in concentration of lanthanum. The films deposition rate starts with 29.07nm/min at the beginning for the undoped and decrease with increase the concentration of the dopant to reach 17.65 nm/min for ZnO films deposited at constant temperature (375°C). The decrease in the growth rate is due to the phenomenon of evaporation which takes place in the boundary layer in the vicinity of the heated substrate. During spray growth, the boundary layer in the vicinity of the substrate plays a very important role, this boundary layer influences the composition of the droplet even before reaching the substrate. The dynamics that are taking place in this region and the exchanges taking place are very complex and difficult to study. To our knowledge, this kind of study is non-existent or at least on an experimental level. The greater the temperature gradient between the substrate and the surrounding medium, the higher the temperature of the substrate. This gradient generates a natural convection, a thermophoretic force resulting which delays the landing of the droplets coming from the nozzle and especially the lighter ones, which cause their dissociation and evaporation before reaching the substrate. For these two reasons, the quantity of solution reaching the substrate is reduced; which explains the reduction in the growth rate in this temperature. This leads to the

reduction of the reactive species quantity on the growing surface. Biglin et al [12] have deposited CdS thin films by spray pyrolysis at different substrate temperature. They observed the same behavior where the evaporation phenomenon was found to cause CdS thin films thickness reduction.

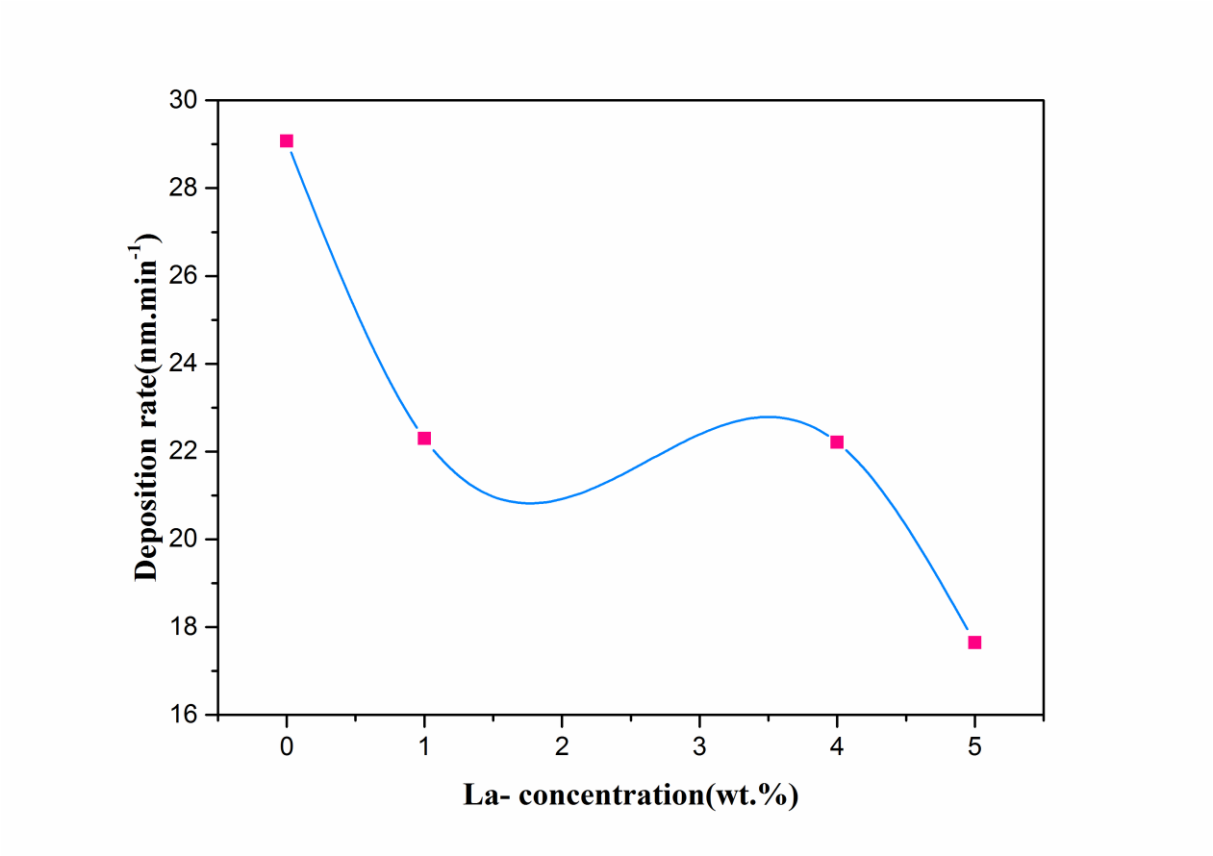

Fig 3. 3. Variation of deposition rate as a function of lanthanum concentration.

3.5.1.2 Structural properties

Shows the XRD patterns of the La-doped ZnO sprayed thin films. The diffraction peaks in the patterns can be assigned to ZnO hexagonal Wurtzite structure according to JCPDS 036-1451 card. The presence of well defined peaks of (100), (002) and (101) orientations which indicate that the films are of polycrystalline nature [13]; Irrespective of the concentration of doping used all the films show (002) plane orientation, corresponding to ZnO hexagonal wurtzite structure indicates that the structures of doped ZnO are not altered by the incorporation of La. It is also worth noting that no peaks related to lanthanum are found in these spectra, which may be due to the low La content and to the limit of XRD detection.

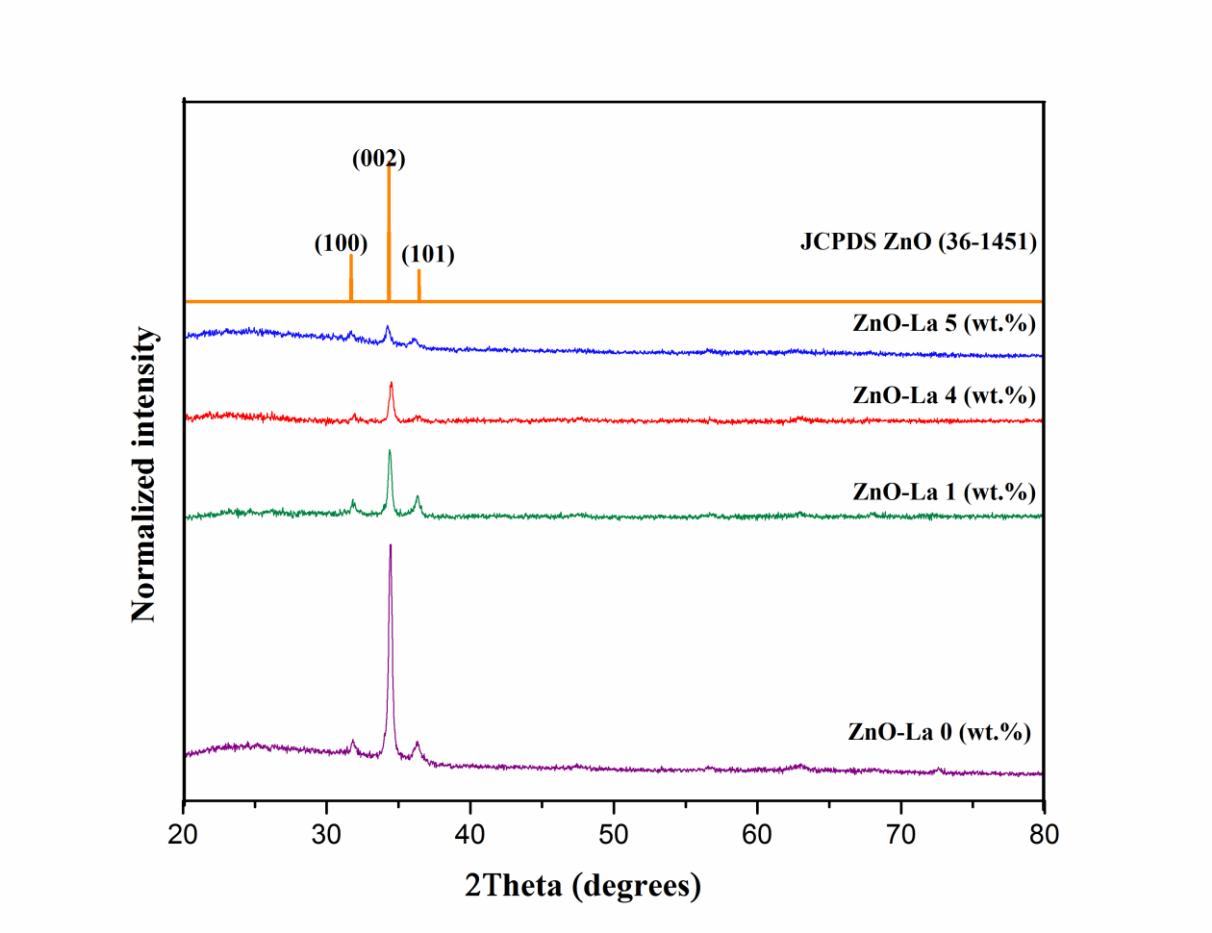

Fig3. 4. X-ray diffraction pattern of La-doped ZnO thin films.

As can perceive from the XRD spectra, the intensity of those peaks are affected by (0-5 wt.%) La doping. The inter planar spacing d_{hkl} values of ZnO:La thin films is calculated via Bragg equation (Eq. 3. 1). Both lattice parameters (a) and (c) for hexagonal phase are calculated with the help of (002) and (101) orientation using (Eq. 3. 7) relation.

Table 3. 2 summarizes the positions of both (002) and (101) peaks and the calculated values of d_{hkl} as well as the lattice parameters (a) and (c). In comparison with undoped ZnO thin film, it can be seen that a little decrease of the lattice parameters (a) and (c) related to La incorporation in ZnO matrix. This result is consistent with that reported by Suwanboon et al. [14], who attributed this decrease in crystal size to the presence of amorphous phase of La_2O_3 due to the solubility limit of La ions in ZnO structure. Thus, small La_2O_3 clusters were dispersed on the surface and compressed the lattice crystal of ZnO depending on a decrease in the lattice parameters. In the same conception, Anandan et al.[15] retained the same explanation and connected this to the difficulty in substituting Zn^{2+} ions by La^{3+} ions because of the great difference between the ionic radius (1.15 Å for La^{3+}, 0.74 Å for Zn^{2+}).

In contrast to results carried out by Zamiri et al. [16] where they have doped ZnO by rare-earth ions (Er^{3+}, La^{3+} and Yb^{3+}) and found that La^{3+} ion cannot be incorporated into ZnO matrix.

Nevertheless, the existence of lanthanum among the grain boundaries and on the surface of ZnO particles retards usually the crystal growth, and then leading a depressed crystallinity. Also, it is noted that c/a ratio is different from the hexagonal wurtzite phase. This difference may be due to the presence of some defects in the deposited films.

Table 3. 2 Peak positions, inter planar spacing d_{hkl} and lattice parameters calculated from (002) peaks.

(wt.%)	$2\theta_{(002)}$ (°)	$2\theta_{(101)}$ (°)	d_{002} (Å)	d_{101} (Å)	a (Å)	c (Å)	c/a	Cell Volume (Å^3)
ZnO	**34.512**	**36.292**	**2.5960**	**2.4737**	**3.230**	**5.1870**	**1.6058**	**47.40**
ZnO:La 1	**34.525**	**36.303**	**2.5959**	**2.4730**	**3.233**	**5.1934**	**1.6063**	**47.38**
ZnO:La 4	**34.527**	**36.314**	**2.5938**	**2.4719**	**3.229**	**5.1847**	**1.6056**	**47.34**
ZnO:La 5	**34.555**	**36.353**	**2.5932**	**2.4686**	**3.233**	**5.1932**	**1.6063**	**47.24**

Moreover, the texture coefficient (T_C), which indicates the maximum preferred orientation of the films along the diffraction plane, means that the increase in the preferred orientation is associated with the increase of the number of grains along that plane. $T_{C(hkl)}$ values were calculated from X-ray data, using the formula (Eq. 3. 4). It is clear that if $T_C > 1$, this implies that the film growth occurs in certain preferred orientation figure (3. 5). These results confirm that (002) plane orientation, corresponding to ZnO hexagonal wurtzite structure, is the preferred orientation as seen in the above section.

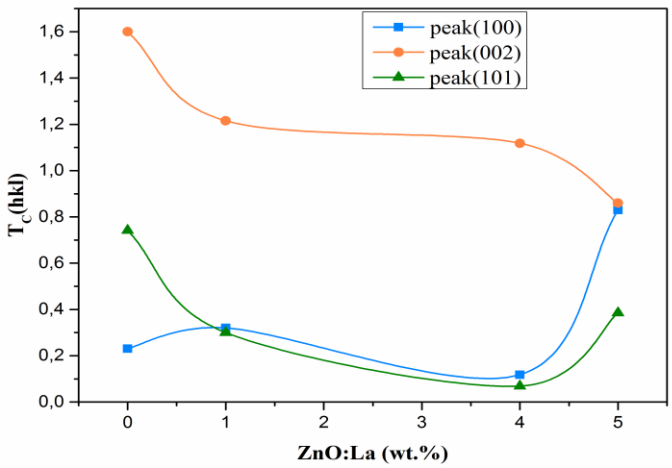

Fig. 3. 5 Variation of texture coefficient as of La-doped ZnO thin layers.

In the following, the structural defects in our samples will be interpreted in terms of crystallite size, micro strain and stress. The full width at half-maximum (FWHM) can be used to estimate the crystallite size along c axis growth. The average crystallite size ***D*** of all ZnO:La thin films is evaluated using Debye Scherer's formula (Eq. 3. 2). Table 3. 3 shows the evolution of crystallite size with La doping concentration.

The crystallite size of undoped and La-doped ZnO thin films is lying in 54.02-45.12nm domain. One decade as appreciable change is observed in crystallite size. The sleazy decrease in crystallite size is probably related to the presence of the secondary phase (La_2O_3),which can be considered as a barrier preventing movement of grain boundaries and limits the growth of crystals.

Table 3. 3 Estimation of crystallite size ,micro strain ,dislocation and stress of ZnO thin films.

(wt.%)	D (nm)	ε x 10^{-4}	ξ x10^{14} (line/m^2)	σ(GPa)
ZnO	54.02	2.42	3.42	-1.10
ZnO:La 1	48.06	3.09	4.32	-1.086
ZnO:La 4	45.22	3.64	4.91	-1.836
ZnO:La 5	49.8	2.45	4.15	-1.1005

The micro stain (ε), which is considered as an interesting structural parameter of ZnO:La sprayed thin films, is calculated using the following relation (Eq.3. 5).

The dislocation density (ξ) values of films are calculated using the expression (Eq.3. 8):

Figure (3. 6) shows a well correlation between micro strain ,dislocation and crystallite size. Their changes, depending on the La concentration, can be explained, as provided by the existence of lanthanum oxide among the grain boundaries and on the surface of ZnO particles which retards the crystal growth and increases the strain. As seen from Table 3. 3, undoped ZnO thin film has the smallest values of micro strain and dislocation density which indicates that La doping deteriorates ZnO crystal structure.

The estimation of stress was performed using the following formulae:

$$\sigma = \left[2C_{13} - \frac{C_{33}(C_{11}+C_{12})}{C_{13}}\right]\varepsilon \qquad (3.\ 14)$$

and

$$\varepsilon = {(C_0 - C)}/{C_0} \qquad (3.\ 15)$$

where,ε is strain, C_{13} ($1.05\times10^{11}N/m^2$), C_{33}($2.1\times10^{11}N/m^2$), C_{11}($2.1\times10^{11}N/m^2$), and C_{12}($1.2\times10^{11}N/m^2$), are the elastic stiffness constants.

The negative values of the stress indicate the presence of compressive stress [17]. This compressive stress occurs usually if there are native defects and distortions in the lattice. It is worth to note that, ZnO:La 1 (wt.%) resulted in less stress. Also, T. P. Rao et al. [18] observed a compressive stress in sprayed ZnO thin films.

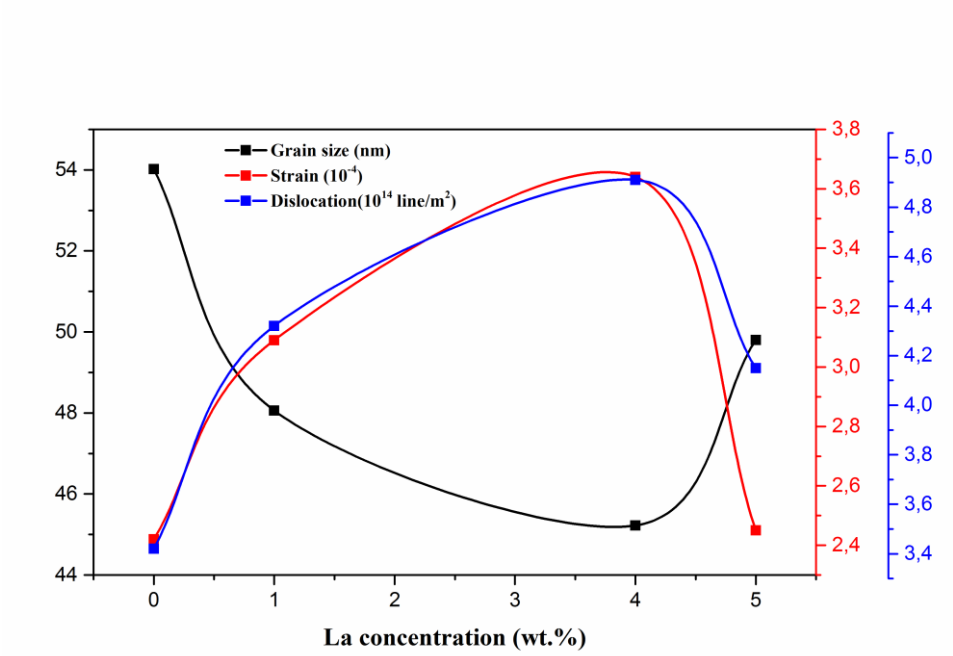

Fig. 3. 6 Correlation between crystallite size, micro strain and dislocation.

3.5.1.3 Surface morphology and composition

- **SEM analysis**

The growth mechanism, shape and size of the particles as well as topography study of the prepared samples were performed by using scanning electron microscopy (SEM). Figure. 3. 7 shows low-magnification SEM images of the La-doped ZnO thin films microstructure. In all films, grains with regular shape and porosity are visible in the surface. The averaged grain size visualized by SEM is higher than the crystallite size deduced with the help of FWHM. As well know SEM visualization allows only seeing grains, which are constituted of more or less disordered atoms and crystallites, while in the XRD method, what is measured is the extent of the crystalline region that diffract X-ray coherently. This is a more stringent criterion and leads to smaller grain size [19].

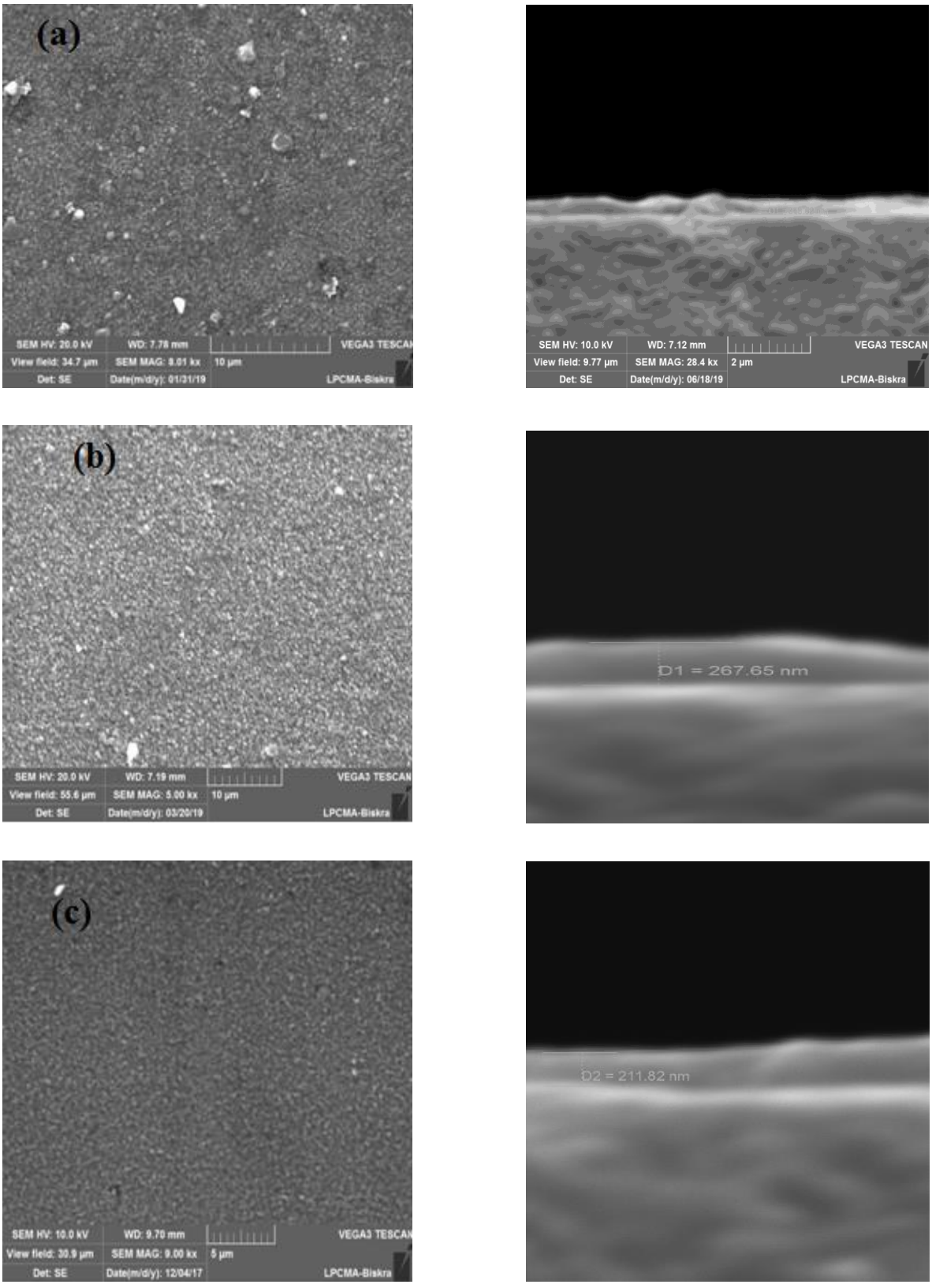

Fig. 3. 7 SEM images of ZnO films and their cross section: a) ZnO, b) ZnO: La 1%, and c) ZnO: La 4%).

The incorporation of lanthanum did not affect the general microstructure and did not significantly affect the grain growth of these materials. This strongly suggests that the ZnO

lattice was not severely disrupted by the La ions. The formation of La_2O_3 may be inferred from the SEM micrograph in the case localized EDAX with absence of Zn but that shows different morphology clusters adhered to the grains, probably consisting of La_2O_3.

- **Film thickness measurement using SEM**

Thickness can be measured by breaking the samples and coating with gold for nonconductive substrates. SEM micrographs of the cross-section for ZnO:La films were obtained at a tilt angle of 80 degrees.

The SEM image in cross section made for the ZnO doped and undoped thin layers is illustrated in figure 3. 7, from which an estimated thickness of thin films are around 210-350nm.

- **EDAX analysis**

The chemical composition of the ZnO thin film was determined by the energy dispersive analysis X-ray spectra. Figure 3. 8 shows the EDAX spectra obtained for two samples of ZnO and ZnO doped with 1% lanthanum.

For the sample (a) The elements identified in the thin layer of ZnO are zinc and oxygen. The EDAX analysis does not reveal the presence of the other peaks which are at the origin of the impurities. This proves the purity of the synthesized ZnO. While in sample (b) the elements identified in ZnO: La 1% the thin layer, It was noted that lanthanum peak in addition to the peaks of mentioned in the previous sample appears.

A peak of carbon is present in EDAX of the whole samples may be come from air as seen in the figure (3. 8 b).

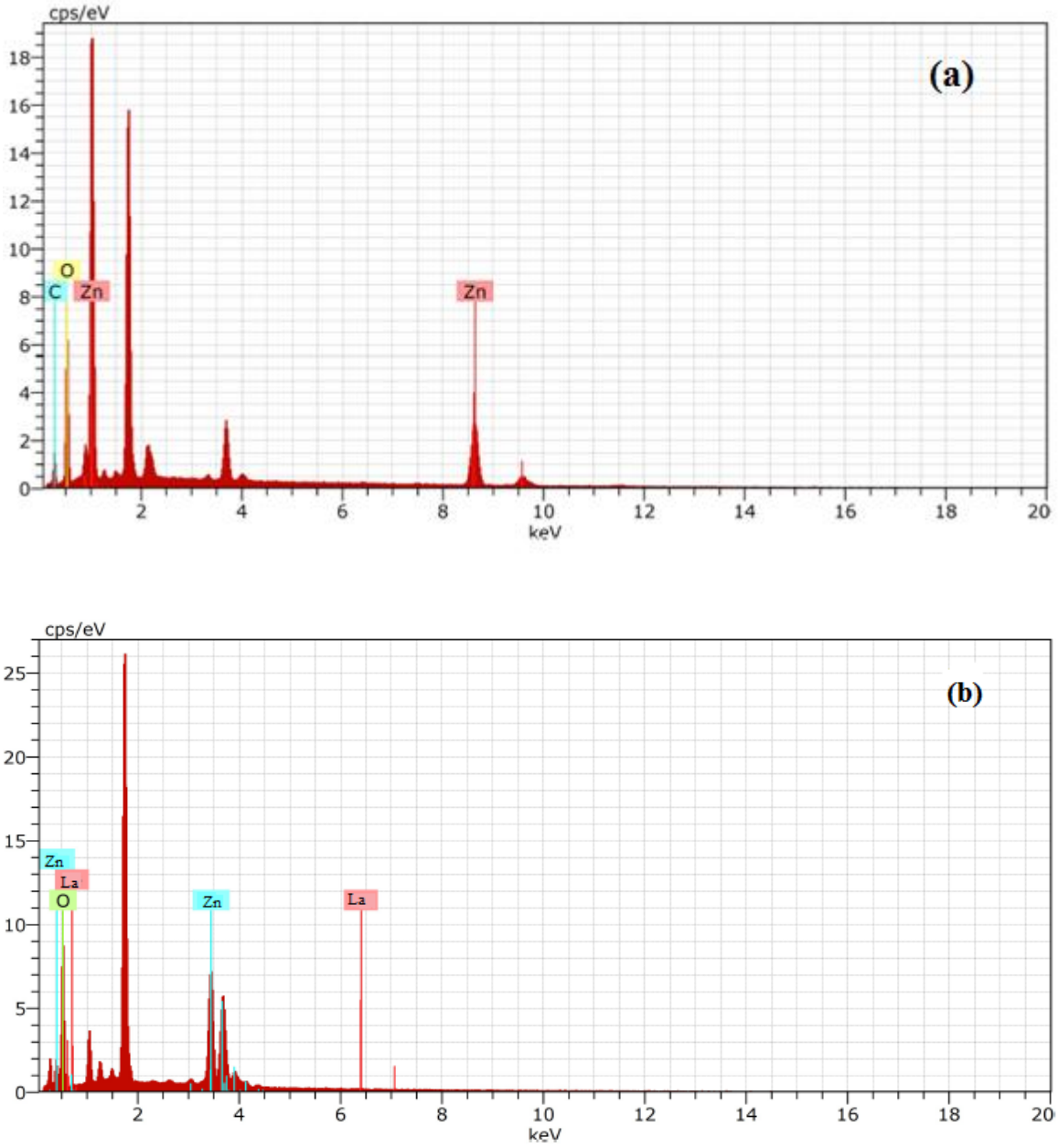

Fig. 3. 8 Typical EDAX spectra for the deposited film ZnO: a) ZnO:La 0%, b) ZnO:La 1%.

3.5.1.4 Optical properties

The optical transmission spectra of ZnO:La films in the wavelength 250-900nm region are shown in figure 3. 9. These spectra show that the prepared films exhibit a high transparency around 95 % in the visible domain. The transmission is found to be maximal for undoped and ZnO 5wt.% La doped film with a little decreased with La content increasing. This may be

attributed to the increased scattering of photons by increase in dislocation at the surface and a structure disorder which dislocation and Urbach energy.

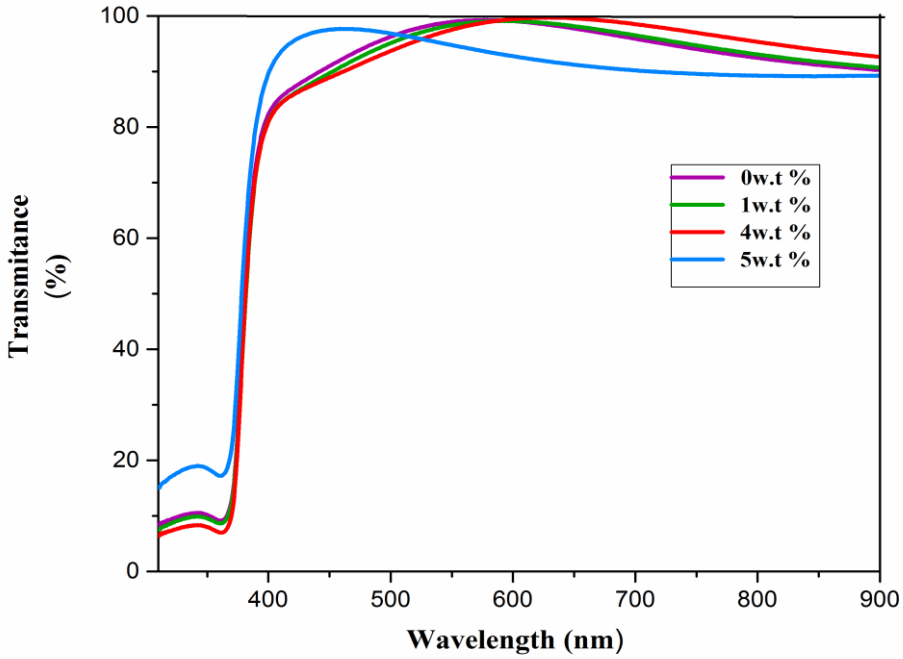

Fig. 3. 9 Transmittance spectra of ZnO:La thin films.

- ***Band gap energy calculation***

To calculate the optical band-gap energy (E_g) of the thin films, the absorption coefficient can be estimated as using the following equation (Eq. 3. 9)

Here, the deposited films are considered as a material having direct band gap energy. For the direct transition, the optical band gap energy of film was determined using the equation (Eq. 3. 10). Therefore, the optical band gap is obtained using Tauc's plot: $(\alpha h\nu)^2$ versus $(h\nu)$ and extrapolating the linear portion to find the intercept with energy axis (Figure. 3. 10).

Calculated values of doped ZnO optical band gap are summarized in Table 3. 4. It can be seen that an increase in optical band gap occurring with doping as it was carried out by Suwanboon at al [5] where they reported that the Eg values of La doped ZnO altered depending on many parameters, for example, imperfection in ZnO crystal, particle shape and particle size.

Table 3. 4 The calculated band gap and Urbach energy values.

	ZnO:La 0%	ZnO:La 1%	ZnO:La 4%	ZnO:La 5%
E_g (eV)	3.24	3.25	3.256	3.27
E_{00} (meV)	84.85	80.02	76.35	56.25

The doping at lower values than 5wt.% results in the rise of additional band tail states, leading to shrinkage of the band gap. Wherase the increase in Eg with 5wt.% La doping as phenomenon may be related in generally to Burstein Moss shift, which phenomenon induces an increase in the band gap with the doping concentration [20,21].

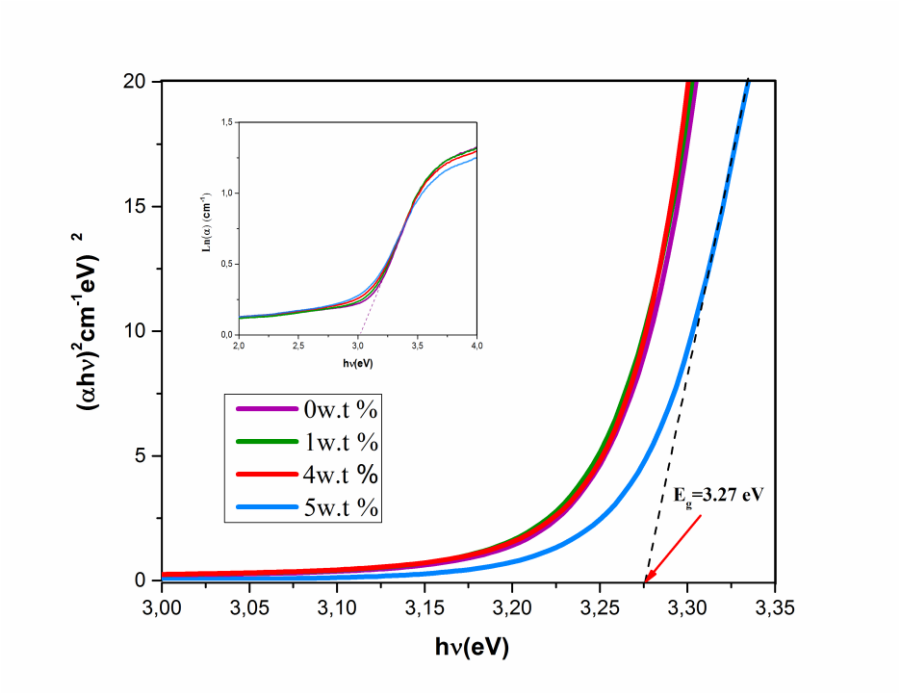

Fig. 3. 10. Plot of $(\alpha h\nu)^2$ versus photon energy of ZnO:La thin films .Inset shows the Urbach energy plot of ln(α) versus(hν).

- ***Urbach energy***

The incorporation of impurity into the semiconductor often reveals the formation of band tailing in the band gap. The optical transitions between occupied states in the valence band tail to unoccupied states of the conduction band edge induce an exponential dependence of the absorption coefficient (α) on photon energy near the band edge.

The band tail energy or Urbach energy (E_{00}), which characterizes the local defects, follows the empirical Urbach law (Eq. 3. 11) [22-25]

E_{00} values are calculated from the inverse of slop of ln(α) versus (hν) as depicted in the insert in figure. 3. 10. The obtained values are shown in Table 3. 4.

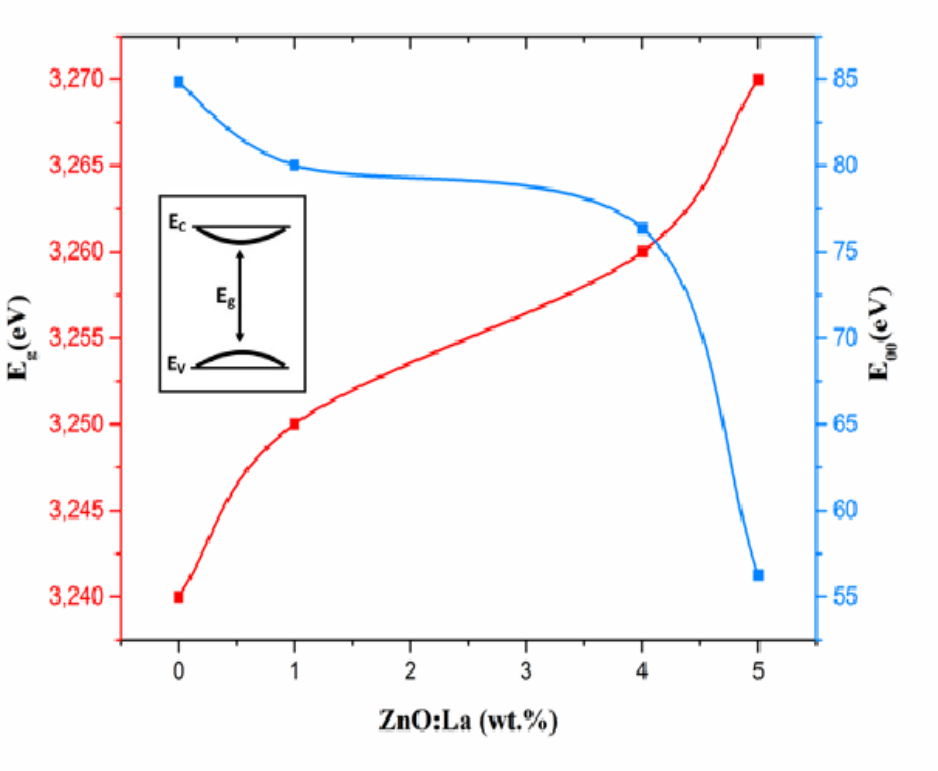

Fig. 3. 11. Variation of E_{00} and E_g with La doping.

Urbach energy of undoped samples is greater than the doped ones. Since this energy is associated to the micro structural lattice disorder, it can be suggested that the incorporation of La ions causes a decrease in disorder and defects in the ZnO:La films. The presence of a band tail for crystalline films indicates that the non homogeneity structural and disorder are significant. On the other hand, Figure 3. 11 giving E_{00} and E_g as a function of La concentration shows that the variations of both E_g and E_{00} correlate very well: It is clear that the optical band gap is inverted to the disorder. As mentioned above, doping at certain level produce localized states in the energy band. As a result, both a broadening of the optical gap and a of stenosis the Urbach tail occurred.

3.5.1.5 FTIR spectroscopy analysis

Vibration modes were determined by Fourier transform infrared (FTIR) spectroscopy. The FTIR spectra were recorded on a PerkinElmer RX spectrometer with KBr as a diluting agent and operated in the wave number range of 400-4000cm^{-1} with 4cm^{-1} resolution.

The products were diluted with potassium bromide in the ratio of 1:100 for FTIR analysis. Figure 3.12 shows FTIR spectra of 0-5 wt.% La-doped ZnO products. A strong absorption bands at 426 and 565cm^{-1} are attributed to the Zn-O stretching vibration of wurtzite hexagonal type ZnO crystal [26,27], belonging to the oxygen sublattice (E_{2H}) vibration and oxygen

vacancies of wurtzite ZnO crystal, respectively [28]. The band at 1629 cm^{-1} is specified as hydrogen-related defects on surface of ZnO [29]. The broad absorption bands at 3013-3633cm^{-1} are the O-H stretching vibration of adsorbed water on ZnO surface [26-28].

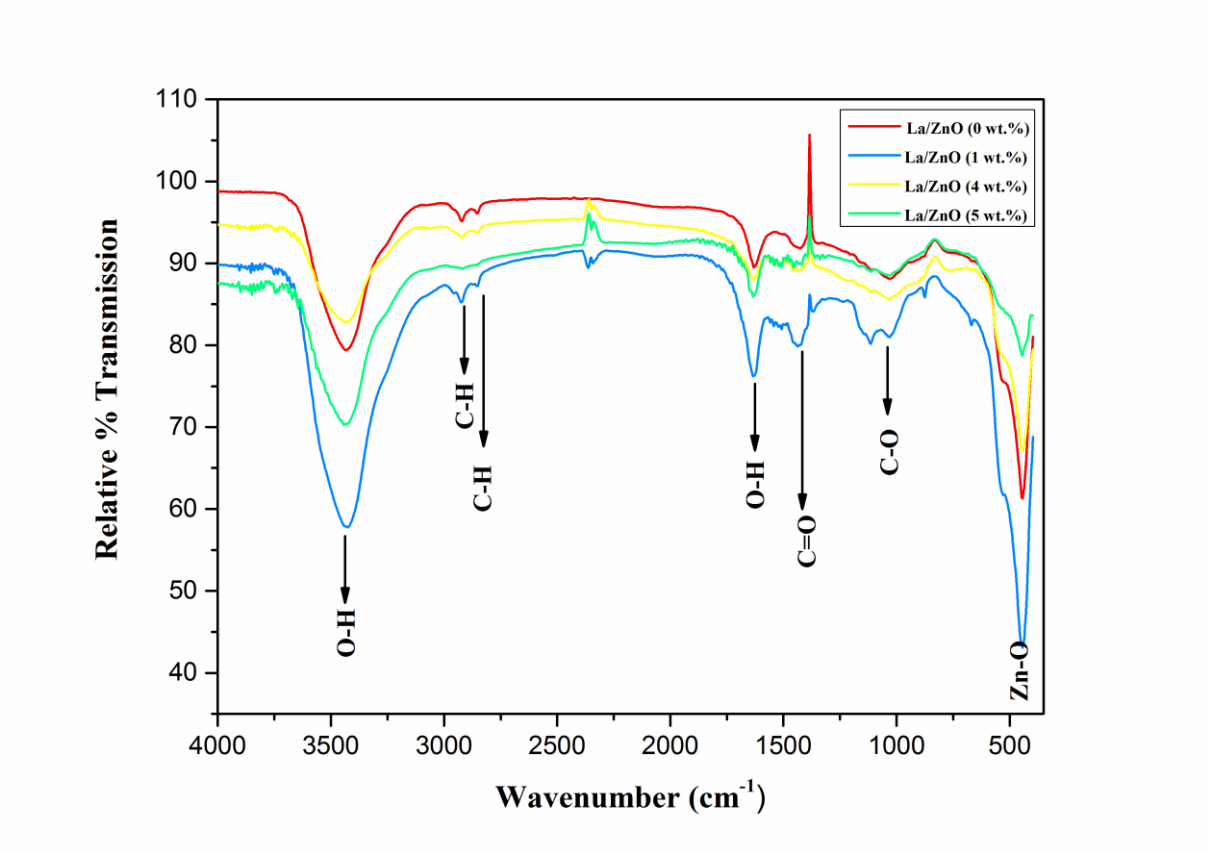

Fig. 3. 12 FTIR spectra of pure ZnO and La-doped ZnO synthesized by spray pyrolysis method.

3.5.2 Zinc chloride

Undoped ZnO thin films were prepared on glass substrates at 375°C, using 0.5M aqueous solution of zinc chloride ($ZnCl_2$). Consecutively, and under similar experimental conditions, lanthanum-doped ZnO thin films solution have been prepared by adding lanthanum chloride heptahydrate ($LaCl_3$,$7H_2O$) to the precursor solution as dopant. The La-to-Zn molar ratios ([La]/[Zn]) were 0%, 1%, 4% and 5%.

3.5.2.1 Growth rate

In figure 3. 13, deposition rate variation was reported as function of 0-5 wt.% La-doped ZnO. The growth rate is estimated from the ratio of film thickness on the deposition time fixed at 12 min. As can be seen, the deposition rate increase considerably and varied non linearly with the doping concentration.

Generally, in the whole commonly used deposition techniques, film growth steps along nucleation, condensation and subsequent growth, which are mainly controlled by two major parameters: the substrate temperature and arriving species flux on the substrate; the first controls the species energy and motion onto the substrate and the second may be influence the nucleation only. In the case of spray pyrolysis, arriving species rate is controlled by the flow rate of the solution feeding the nozzle. It is worth noting that the substrate temperature is extensively studied in the literature, while, to our knowledge, the flow rate influence is less studied.

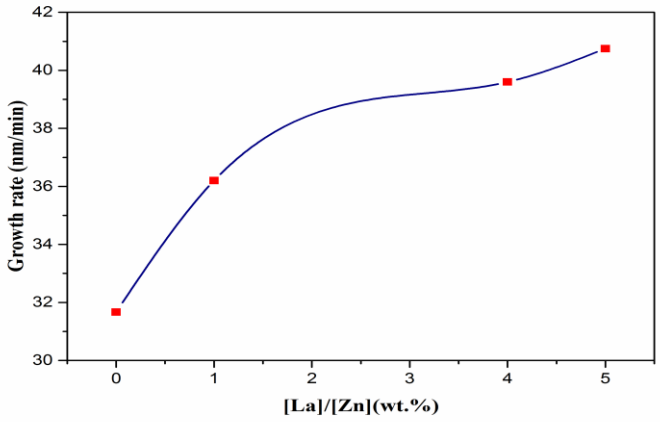

Fig 3. 13 Variation of growth rate as a function pure ZnO and La-doped ZnO.

3.5.2.2 Structural properties

In figure 3. 14, XRD patterns of prepared ZnO thin films at a constant substrate temperature of 375°C for 0-5 wt.%. La concentrations have been reported. For all samples, two important peaks which were observed at 34.5° and 36.29° corresponding to (002) and (101) diffraction planes. With increasing the lanthanum concentration, the dominant peak assigned to (002) became less intense. The crystallite size (D) of the ZnO was calculated using Scherrer's formula $D = 0.9\lambda/\beta\cos\theta$ [30], where λ is the wavelength (1.54 Å), β is the full-width at half maximum (FWHM), and θ is the angle at which (002) peak was observed. Further, the peak position deviation from the reference data of bulk ZnO (JCPDS 036-1451 card) was observed which confirms the presence of stress in the films.

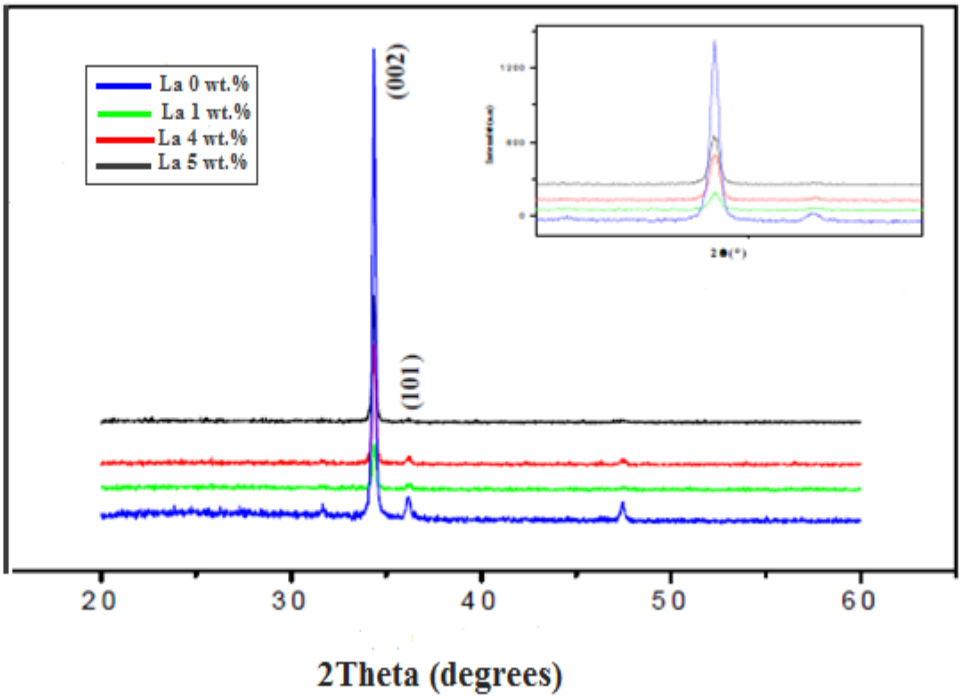

Fig. 3. 14. Evolution of the X-ray diffraction spectra of ZnO thin film for the chloride solution.

Based on the above XRD result it was remarked that the preferred orientation in the deposited ZnO thin films is effected by the variation of the lanthanum concentration as seen in figure 3. 16. The preferred growth of the (hkl) planes has been expressed in terms of the texture coefficient Tc(hkl) [5]. Quantitative information concerning the preferential crystallite orientation can been obtained from the texture coefficient Tc. Since two diffraction peaks were used (002) and(101), the maximum possible value Tc(hkl) is one. In our case, this value means 100% of the crystallites grew with a c-orientation perpendicular to the substrate plane.

The c-orientation as well know results from the minimum energy of the growth along the c-axis due to the highest atomic density found along the (002) plane being higher [31,32]. As the (002) ZnO plane has the lowest surface energy and is the most densely packed, continuous thin films tend to change into the (002) oriented films in order to lead to c-textured films. But in less compact films, crystallites may grow undisturbed along less densely packed (101) planes, leading to mixed crystallite orientations which was seen in the case of non doped sample. It has been proposed [33] that other growth processes depend on the initial substrate conditions.

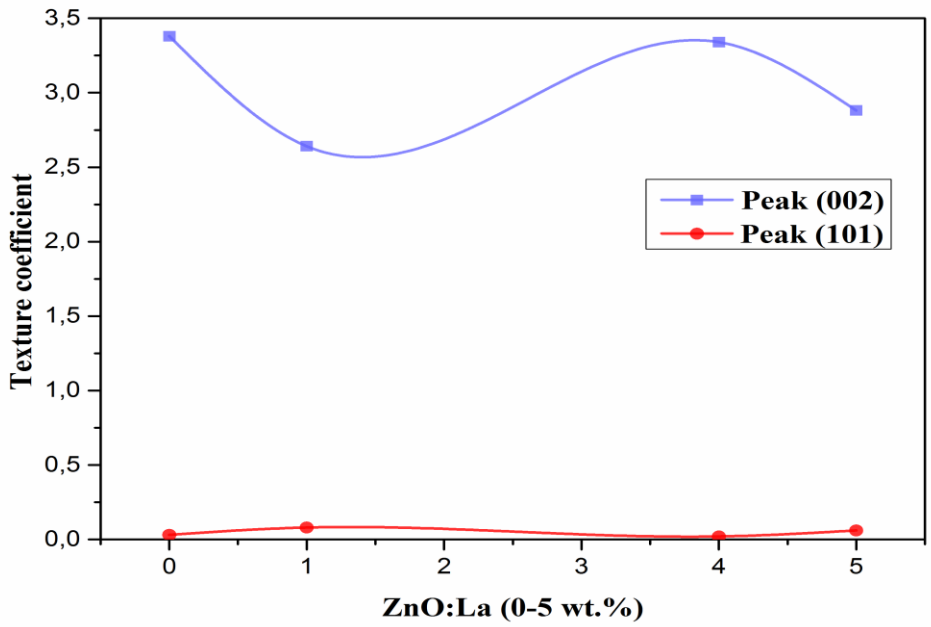

Fig. 3. 15 Variation of the texture coefficient for ZnO films elaborated with different :La (wt.%).

The estimated values of 2θ, FWHM, crystallite size, lattice parameter, strain and stress are given in Table 3. 5

The crystallite size of undoped and La-doped ZnO thin films is lying in 60.9-73.3nm domain, no extra phases involving chloride or lanthanum compounds were observed at the limit of detection.

Table 3. 5 . Estimation of structural parameters of ZnO thin films

Sample name	2θ (deg)	FWHM (deg)	D (nm)	Lattice parameter (Å)	Strain ($\times 10^{-4}$)	Stress (GPa)
[La]/[Zn] 0%	34.512	0.1181	73.3	5.1932	4.29	-1.10
[La]/[Zn] 1%	34.48	0.1427	60.91	5.1911	5.19	-1.28
[La]/[Zn] 4%	34.47	0.1227	70.83	5.1915	4.46	-1.25
[La]/[Zn] 5%	34.54	0.1245	69.82	5.1869	4.24	-1.64

In the case of comparison between the non doped films elaborated by this method and the bulk of ZnO, the negative values of the stress indicate the presence of compressive stress [17]. This compressive stress occurs usually if there are native defects and distortions in the lattice. Whereas if one compares the doped samples to the non one it reveal that a decrease in the lattice parameters with an increase in the stress. Such decrease in (c) means a decrease in the inter planer distance which may be originated a from substitution of Zn^{+2} by La^{+3} where the later has less radii. Figure (3. 16) shows a well variation between grain size , strain and dislocation .This is due to what was previously mentioned in the explanation regarding zinc acetate and the presence of lanthanum chloride on the surface of ZnO particles and granules boundaries.

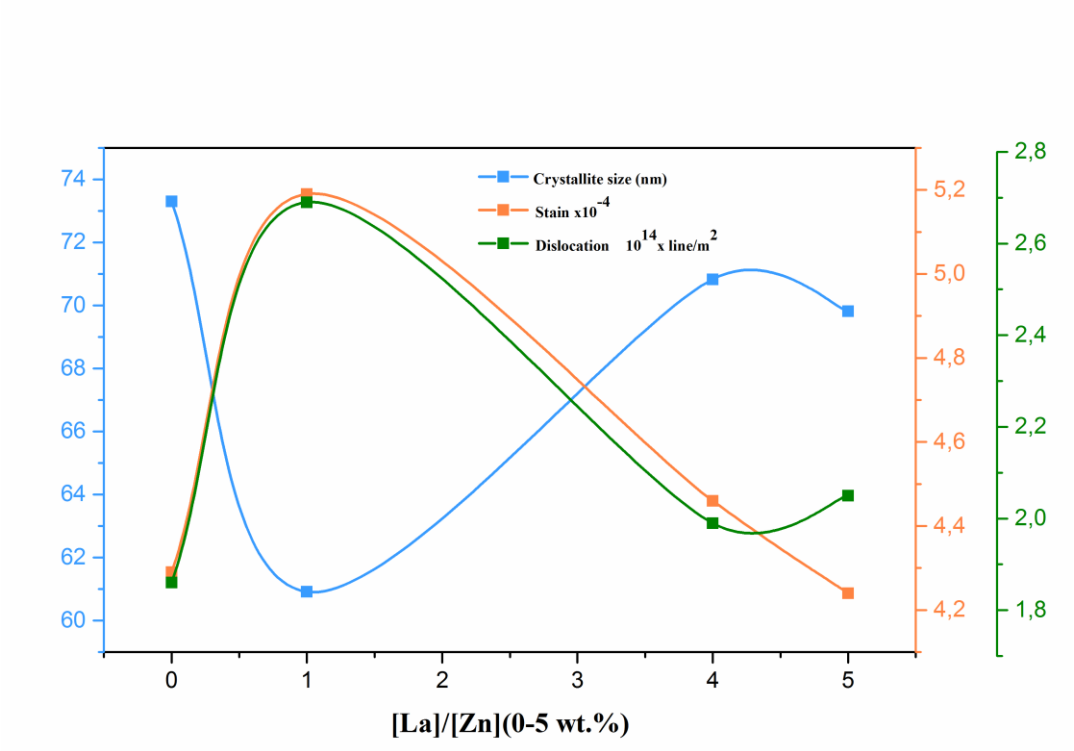

Fig. 3. 16. Variation of D,ε and ξ with La doping.

3.5.2.3 Surface morphology and composition

- **SEM analysis**

Figure 3. 17 shows the SEM images of doped ZnO with different concentrations of La^{3+} ions. As can be seen, there are no obvious differences in films morphology. This indicates that a doping with La^{3+} ions in ZnO does not affect the crystal morphology at the same temperature .The nucleation density of the micro crystallites increased in ZnO: La^{3+} thin films. Nucleation and growth rates were influenced by the presence of impurities, lowering the potential barrier for the formation of nuclei and slowing the growth velocities ,which were likely to be responsible for the decrease in grain size.

To get idea about the thickness of each samples, SEM images in cross section were made for the ZnO doped and undoped thin layers are exhibited in figure 3. 17, the estimated thickness of all samples is around 384-476nm.

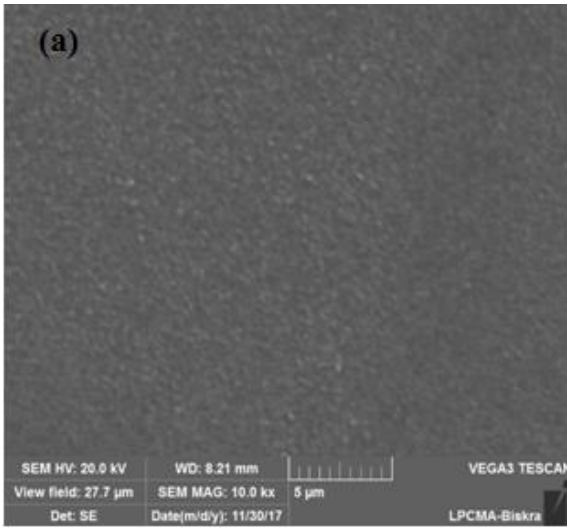

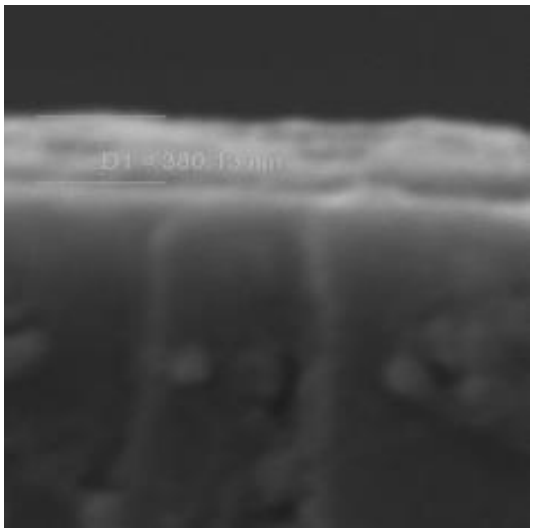

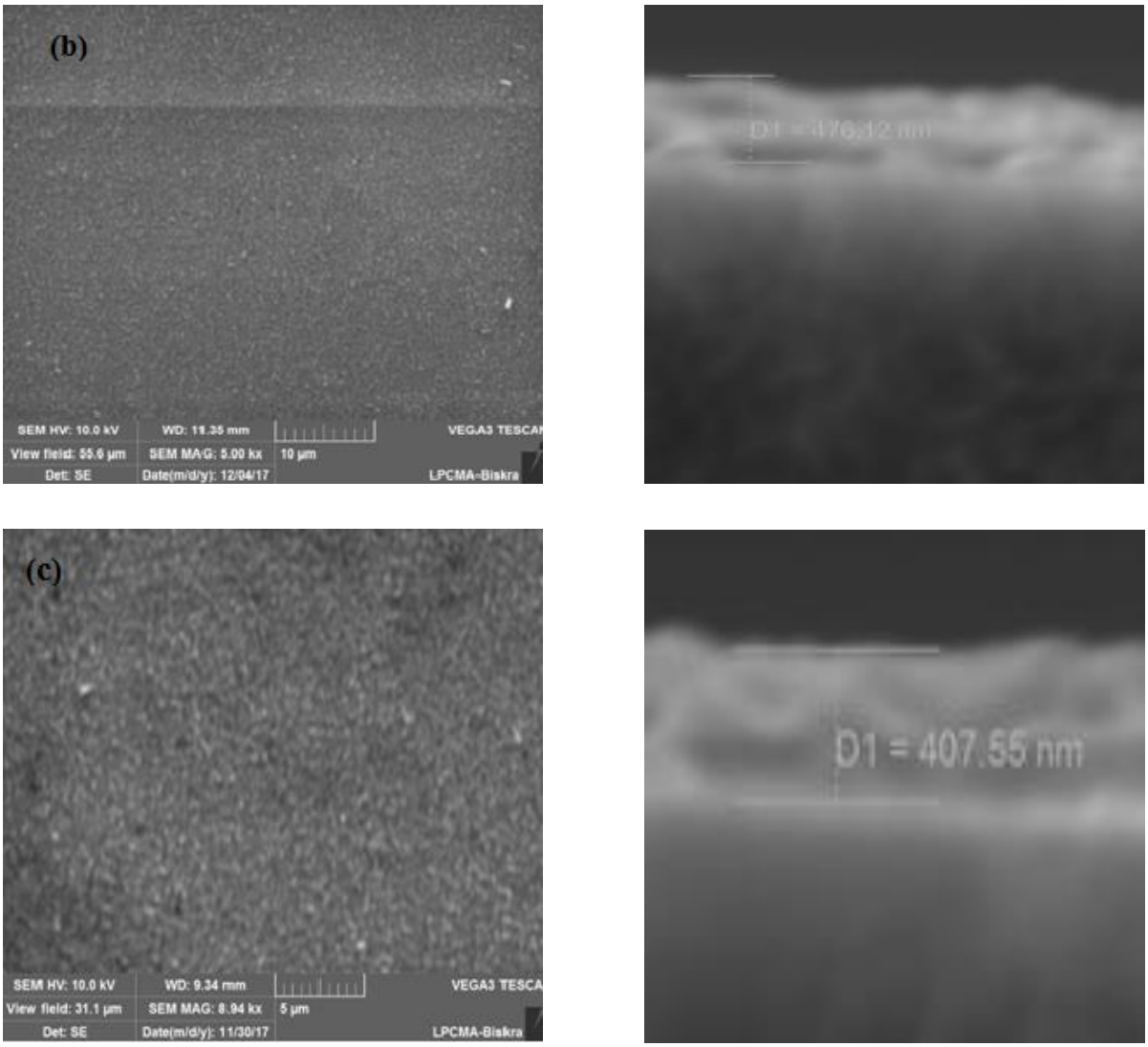

Fig. 3. 17 SEM images of ZnO films at 375 ˚C, (Left: front view and right: cross section):
a) [Zn]:[la] 0%, b) [Zn]:[la] 1%, and c) [Zn]:[la] 5%).

➢ EDAX analysis of as-synthesized La-doped ZnO

To evaluate the elemental composition of synthesized pure and doped ZnO thin films meanly La element, EDAX was recorded arbitrarily from the samples surfaces. In the preparation of La-doped ZnO, the successful doping of lanthanum ions into ZnO lattice was supported by EDAX spectra indicating the presences of La. Results of elements composition are shown in figure 3. 18 (a and b). In EDAX spectrum, numerous well-defined peaks were evident related to Zn, O and La which clearly support the synthesized products are made of Zn, O and La. No other peak related to impurities was detected in the spectrum which further confirms the purity of the thin layers. For instance the 5wt.% La doped sample, the atomic % of Zn, O and

La is 60.80, 38.72 and 0.48 respectively, which reveals deficiency of oxygen, such oxygen deficient materials useful for the photocatalysis which possesses more active centers.

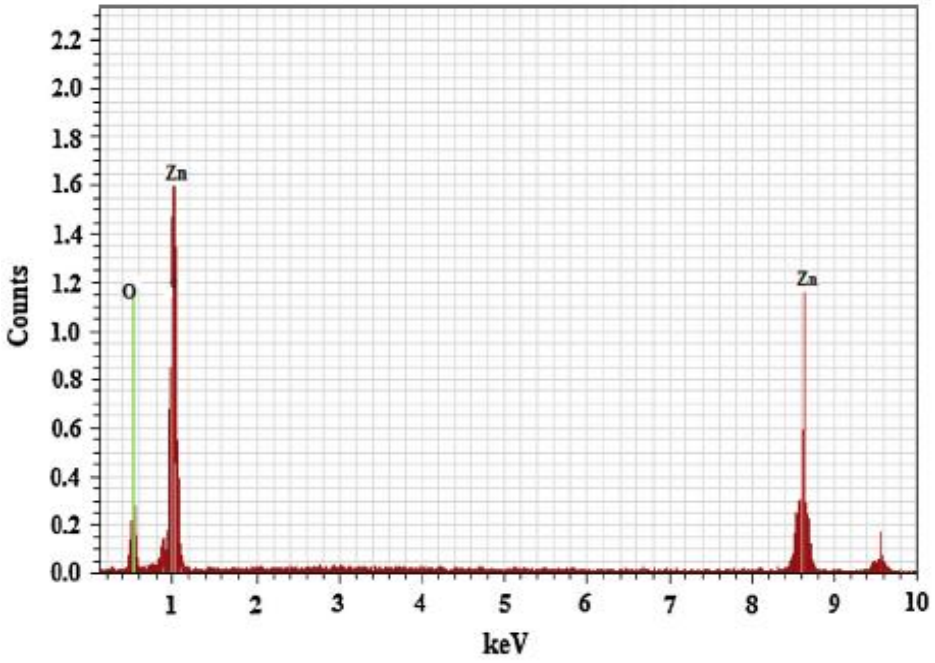

(a) EDAX spectra of pure ZnO.

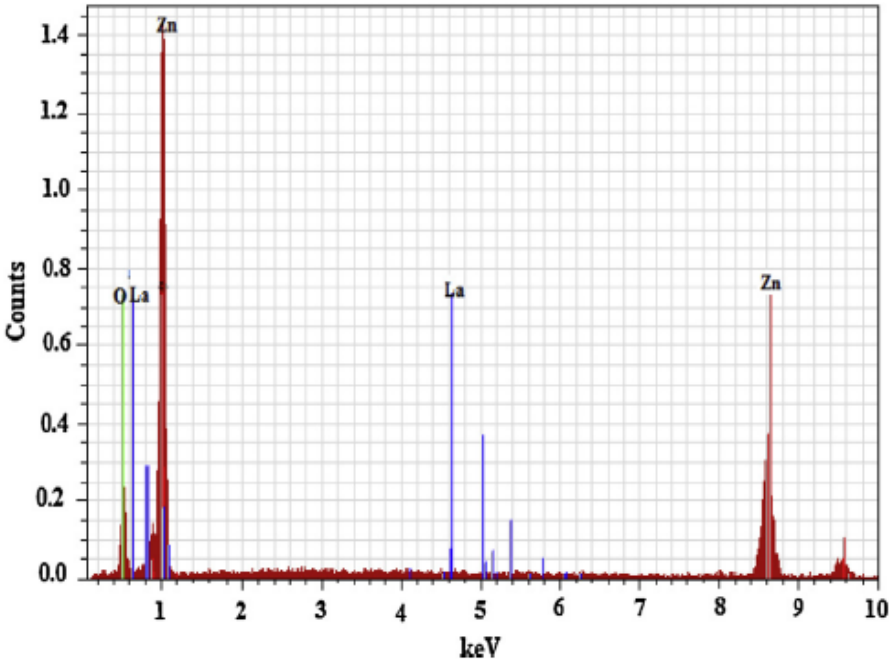

(b) EDAX spectra of 5 wt.% La-doped ZnO.

Fig. 3. 18. (a) EDAX spectra of ZnO and (b) La-doped ZnO thin layers.

3.5.2.4 Optical properties

The optical transmission T(λ) spectra of ZnO:La films in the wavelength region of 250-900nm are shown in figure 3. 19. Those spectra show that the prepared films exhibit a high transparency between 78 and 90 % with interference fringes in the visible domain revealing the smooth of the samples. The transmission is found to be maximal for ZnO :La 0% film and decreased with an increase in La content. This may be attributed to the increased scattering of photons by increase in roughness of surface morphology(see dislocation values of each samples in Table 3. 5). Those fringes are due to the multiple reflection on the two film interfaces.

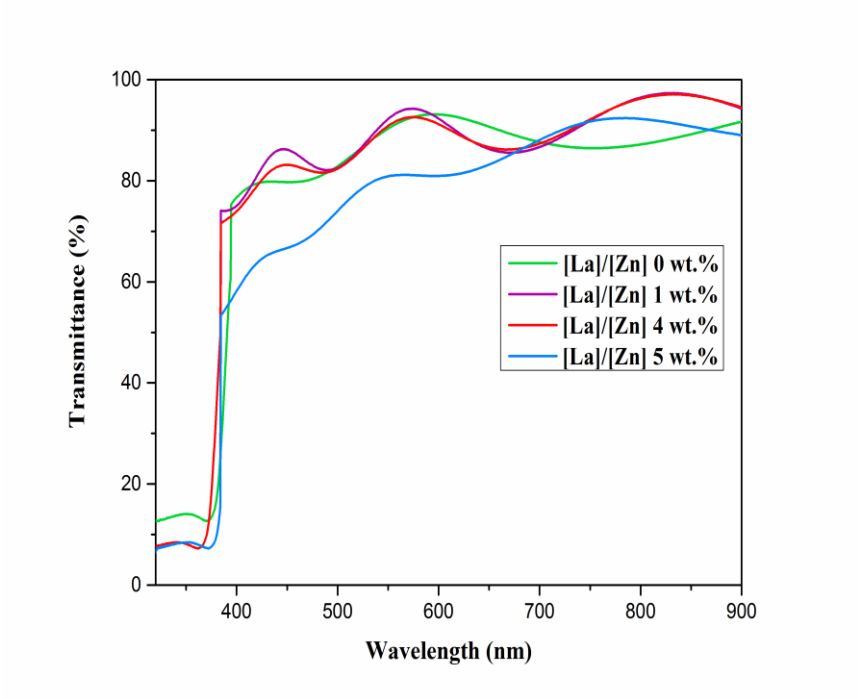

Fig. 3. 19 Transmittance spectra of 0-5wt.% La-doped ZnO thin films.

- ***Band gap energy***

Estimated values of optical band gap of lanthanum doped ZnO are summarized in Table 3. 6. It can be seen a decrease in optical band gap occurring with La doping.

Table 3. 6 Estimated band gap and Urbach energy values.

	ZnO:La 0%	ZnO:La 1%	ZnO:La 4%	ZnO:La 5%
E_g (eV)	3.281	3.269	3.276	3.271
E_{00} (meV)	78.6	106.5	105.3	105.9

The decrease in Eg values may be due to the increase in the concentration of defects in the crystals with doping. Such decrease originated from localized states under the conduction band as revealed by Urbach energy (see section below). The doping results in the rise of additional band tail states, leading to shrinkage of the band gap.

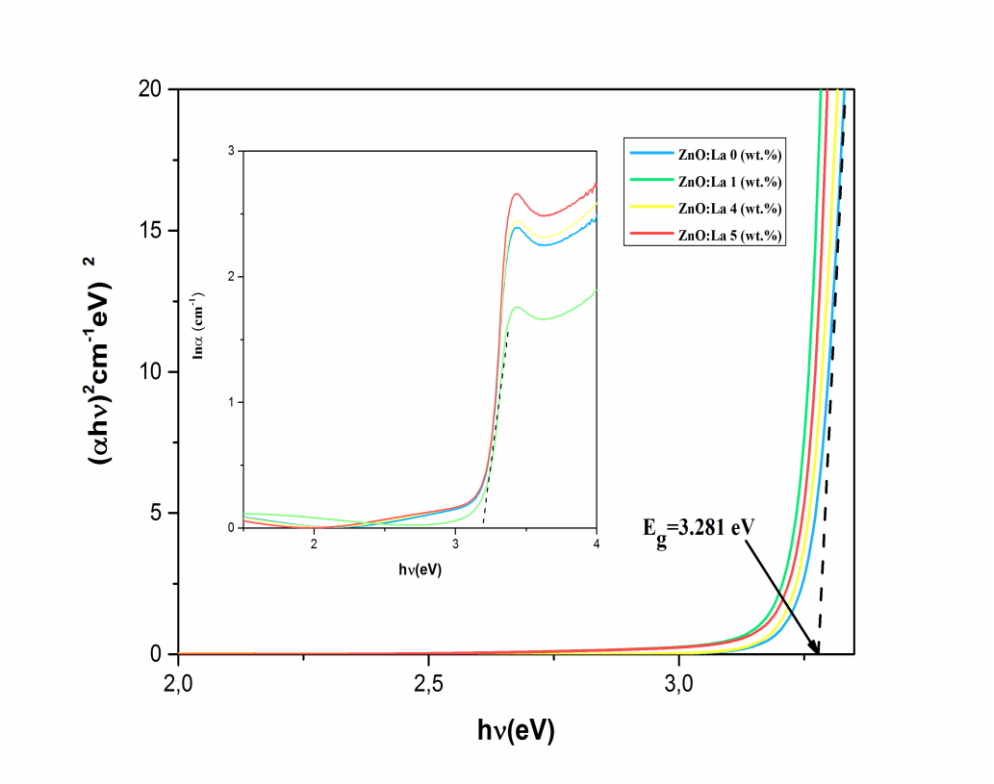

Fig. 3. 20: Band gap (E_g) estimation from Tauc relation of 0-5 wt. % La doped ZnO thin films Inset shows estimated (E_{00}) for doped and undoped ZnO.

- ***Urbach energy***

The disorder or Urbach energy (E_{00}), which characterizes the local defects under the band conduction. E_{00} values are deduced from the inverse of slop of ln(α) versus (hν) as depicted in the insert in figure 3. 20. The obtained values of Urbach energy are shown in Table 3. 6.

Based on that Urbach energy is associated to the micro structural lattice disorder, it can be suggested that the incorporation of La ions causes an increase in disorder and defects in the ZnO:La films since Urbach energy is greater for samples doped than the undoped one. Indeed, Figure 3. 21 shows a good correlation between the dislocation density and the Urbach energy.

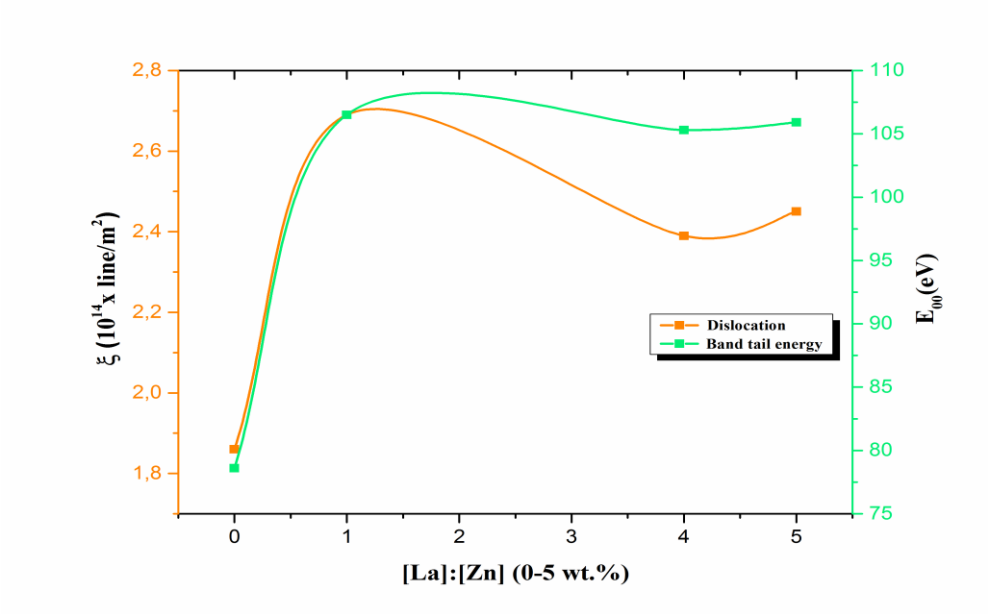

Fig.3.21: Variation of E_{00} and ξ with La doping.

The presence of a band tail for crystalline films indicates that the structural is inhomogeneous and disorder is significant. On the other hand, Figure 3. 22, giving E_{00} and Eg as a function of La concentration, shows that the variations of both Eg and E_{00} correlate very well: It is clear that the optical band gap is inverted to the disorder. As mentioned above, doping produce localized states in the energy band. As a result, both a decrease in the optical gap and a broadening of the Urbach tail occurred. This behavior indicates that the obtained optical band gap is governed with the disorder variation in the ZnO:La films.

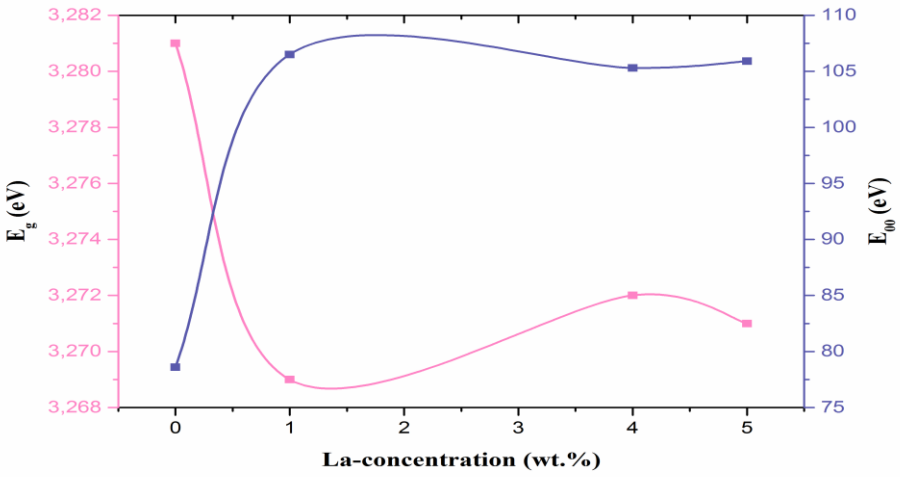

Fig. 3. 22. Correlation between Urbach energy and band gap with La doping.

3.6 Conclusions

In this chapter, the process of ZnO layers elaboration was described. Obtained morphological, structural and optical properties of the samples was shown.

ZnO thin films were prepared using zinc acetate and zinc chloride precursors by spray pyrolysis with moving nozzle technique on glass substrates at 375°C. Regardless of precursors, ZnO thin films are all in hexagonal structure. All deposited films have a preferred growth orientation along the c-axis (002) perpendicular to the plane of the substrate. SEM images show homogenous surface and no obvious differences in films morphology for the ZnO thin films whereas thickness of the films are around 210-350 and 384-476nm when zinc acetate and zinc chloride precursors were used, respectively. The optical measurements reveal that all films have an average 78-95% transmittance and the estimated optical band gap values ranged in 3.24-3.28eV for ZnO for different precursors which are very close to the band gap values of intrinsic ZnO crystal.

Bibliography

[1] R.R. Chamberlin, J.S. Skarman, *"Chemical Spray Deposition Process for Inorganic Films" ,* J. Electrochem. Soc. 113 (1966) 86.

[2] A.L. Patterson,*"The Scherrer Formula for X-Ray Particle Size Determination" ,* Phys. Rev. 56 (1939) 978.

[3] Meriem Touati tliba," *Etude des propriétés opto électronique des couches minces de ZnO élaboré par spray pyrolyses (Home made)*" Ph thesis of the Ouargla University, (2018) .

[4] G.K. Williamson, W.H. Hall, *"X-Ray Line Broadening From Filed Aluminium And Wolfram" ,* Acta Mater. 1 (1953) 22.

[5] C.S. Barrett, T.B. Massalski, "*Structure of Metals*", Pergamon, Oxford, (1980) 204.

[6] V. Bilgin, S. Kose, F. Atay, I. Akyuz, *"The effect of substrate temperature on the structural and some physical properties of ultrasonically sprayed CdS films " ,* J. Mater. Sci. 40 (2005) 1909.

[7] N.Benrguira, S.Bessaid, A. Akroune, A. Gue Chrian-Laidoudi ; INT. Cong. Mater. Sci Eng. USTHB (1999)27.

[8] M. Pinczlits, G. Spingholz and G. Bauer, Appl. Phys. Lett , 73(1998) 250.

[9] V.F. Drobny, D.L. Pulfrey, *"Properties of reactively-sputtered copper oxide thin films" ,* Thin Solid Films 61 (1979) 89.

[10] S. Kose, F. Atay, V. Bilgin, I. Akyuz, *"Some physical properties of copper oxide films: The effect of substrate temperature " ,* Mater. Chem. Phys. 111 (2009) 351.

[11] S. Muthukumaran, R. Gopalakrishnan," *Structural, FTIR and photoluminescence studies of Cu doped ZnO nanopowders by co-precipitation method*", Optical Materials, 34 (2012) 1946- 1953.

[12] J.Arnovich, A. Ortizand and R. H Bube, *"Optical and electrical properties of ZnO films prepared by spray pyrolysis for solar cell applications " ,* J. Vacuum Sci.Technol., 16 (1979) 994.

[13] P.K. Nair, M.T.S Nair, V.M. Gaecia, O.L Arenas, Y. Pena, A. Castillo, *"Semiconductor thin films by chemical bath deposition for solar energy related applications",* Solar Energy Mater and Solar Cells Soc. 313(1998) 52.

[14] S.T. Tan, B.J. Chen, X.W. Sun, X. Hu, X.H. Zhang, S.J. Chua, "*Properties of polycrystalline ZnO thin films by metal organic chemical vapor deposition*", J. Cryst. Growth 281 (2005) 571–576.

[15] S. Suwanboon, P. Amornpitoksuk, A. Sukolrat, N. Muensit, "*Optical and photocatalytic properties of La-doped ZnO nanoparticles prepared via precipitation and mechanical milling method*", Ceram. Int. 39 (2013) 2811.

[16] S. Anandan, A. Vinu, T. Mori, N. Gokulakrishnan, P. Srinivasu, V. Murugesan, K. Ariga, *"Photocatalytic Degradation of 2,4,6-Trichlorophenol Using Lanthanum Doped ZnO in Aqueous Suspension*", Catal. Commun. 8 (2007) 1377.

[17] R. Zamiri, A.F. Lemos, A. Reblo, H.A. Ahangar, *"Fabricating and characterising ZnO–ZnS–Ag_2S ternary nanostructures with efficient solar-light photocatalytic activity* ", J.M.F. Ferreira, Ceram. Int. 40 (2014) 523.

[18] V. Gupta, A. Mansingh, "*Influence of postdeposition annealing on the structural and optical properties of sputtered zinc oxide film Influence of postdeposition annealing on the structural and optical properties of sputtered zinc oxide film"*, J. Appl. Phys. 80 (1996) 1064–1073.

[19] T.P. Rao, M.C.S. Kumar, S.A. Angayarkanni, M. Ashok, "*Effect of stress on optical band gap of ZnO thin films with substrate temperature by spray pyrolysis*", J. Alloy. Compd. 485 (2009) 413–417.

[20] K. Ki, D. Kim, S. Kyu, S. Min, J. *Kyu, "Formation of ZnO nanoparticles by laser ablation in neat water"*, Chem. Phys. Lett. 511 (2011) 116–120.

[21] A. Boukhachem, S. Fridjine, A. Amlouk, K. Boubaker, M. Bouhafs, M. Amlouk, *"Study of nickel doping effects on structural, electrical and optical properties of sprayed ZnO semiconductor layers",* J. Alloys Compd. 501 (2010) 339.

[22] M.M. Hassan, A.S. Ahmed, M. Chaman, W. Khan, A.H. Naqvi, A. Azam, *"Influence of Iron Doping on Structural and Optical Properties of Nickel Oxide Nanoparticles ",* Mater. Res. Bull. 47 (2012) 3952.

[23] A. Mhamdi, B. Ouni, A. Amlouk, K. Boubaker, M. Amlouk, *"Study of nickel doping effects on structural, electrical and optical properties of sprayed ZnO semiconductor layers",* J. Alloys Compd. 582 (2014) 810.

[24] R. Zamiri, A.F. Lemos, A. Reblo, H.A. Ahangar, *"Fabricating and characterising ZnO–ZnS–Ag_2S ternary nanostructures with efficient solar-light photocatalytic activity* ", J.M.F. Ferreira, Ceram. Int. 40 (2014) 523.

[25] T. Chen, J. Wang, F. Zhang, G.A. Zhang, Z.G. Wu, P.X. Yan, *"The effect of La doping concentration on the properties of zinc oxide films prepared by the sol–gel method",* J. Cryst. Growth 310 (2008) 2627.

[26] W. Lan, Y.P. Liu, M. Zhang, B. Wang, H. Yan, Y.Y. Wang, Mater. *"Structural and optical properties of La-doped ZnO films prepared by magnetron sputtering",* Lett. 61 (2007) 2262.

[27] Faisal M, Ismail AA, Ibrahim AA, Bouzid H, Al-Sayari SA. "*Highly efficient photocatalyst based on Ce doped ZnO nanorods: controllable synthesis and enhanced photocatalytic activity*". Chem Eng J. 2013;229:225.

[28] Phuruangrat A, Thongtem T, Kuntalue B, Thongtem S. "*Microwave- assisted synthesis and characterization of rose-like and flower-like zinc oxide nano structures"*. J Ovonic Res. 2011;7(6): 107.

[29] Yayapao O, Thongtem S, Phuruangrat A, Thongtem T. "*Sonochemical synthesis, photocatalysis and photonic properties of 3 % Ce-doped ZnO nanoneedles"*. Ceram Int. 2013;39(S1):S563.

[30] Yang L, Tang Y, Hu A, Chen X, Liang K, Zhang L." *Raman scattering and luminescence study on arrays of ZnO doped with* Tb^{3+}". Phys B. 2008;403(13–16):2230.

[31] A.J.C. Langford, J.I, Wilson, "*Seherrer after Sixty Years: a Survey and Some New Results in the Determination of Crystallite Size*", J. Appl. Cryst. 11 (1978) 102–113.

[32] L. Znaidi, G.J.A.A. Soler Illia, S. Benyahia, C. Sanchez, A.V. Kanaev," *Surface and Interface Geometric and Electronic Structure",* Thin Solid Films 428 (2003) 257.

[33] J. Hong, H. Helming, X. Jiang, B. Szyszka, *"Texture analysis of Al-doped ZnO thin films prepared by in-line reactive MF magnetron sputtering",*Appl. Surf. Sci. 226 (2004) 378.

4 Characterization Of CuO Thin Films Prepared By Chemical Bath

Chapter 4

Characterization Of CuO Thin Films Prepared By Chemical Bath

4.1 Introduction

Copper ion (Cu^{2+}) is one of the heavy metal ions causing environmental pollution specifically in water. Different methods have been used to remove Cu^{2+} from water such as adsorption. For this purpose different adsorbents were used [1-3]. One of the good adsorbents for removal of heavy metal ions is zinc oxide powder [4,5]. However, the powdered adsorbents are difficult to be separated from solution. Thus, these systems need extra processing after adsorption, including long time centrifugation or fine filtration [6].

The purpose of the present work is to removal of copper ions from aqueous solution by thin films of zinc oxide prepared on glass using spray pyrolysis. The advantages of the prepared adsorbents in the present work are high adsorption capacity for Cu^{2+} and also ease of separation from the reaction medium. After annealing the slides at different temperatures (200 to 350°C) for 1hour. We see that both blades are covered with black and brown (CuO / Cu_2O) colored layers .

For this, we have characterized the microstructure and optics of our layers by different techniques: scanning electron microscopy (SEM), and X-ray diffraction (DRX) to obtain information on the directions of crystallographic growth and a spectrophotometer (UV-Visible) to obtain information on the transmittance, the energy of gap and the disorder of the deposited layers.

4.2. Experimental methods

4.2.1. Preparation of standard copper solutions

The aqueous solution of copper is prepared by the dissolution mass of ($CuCl_2$) copper chloride in a volume of distilled water in order to obtain concentration of C=0.05mol /L, for the purpose of using them in the dilutions successive steps required to establish the calibration

curve (see Figure. 4. 1)From this mother solution, the derived solutions are prepared a concentrations listed on the following table:

Table 4. 1 The derived concentrations from mother solution of copper metal ions .

Samples	**S_0**	**S_1**	**S_2**	**S_3**	**S_4**	**S_5**	**S_6**
Concentration 10^{-3} mol/L	C_0=50	C_1=25	C_2=16.6	C_3=12.5	C_4=10	C_5=8.33	C_6=7.14

4.2.2 The adsorption experiment

The prepared slides of La-doped ZnO/glass slides were used for adsorption of copper ion ($CuCl_2$) in aqueous solution with a concentration of 20molml^{-1}. The concentration of Cu^{2+} was determined using UV/visible spectrophotometer (Shimadzu 3101PC double beam) in the range of wavelength 200-900 nm.

The adsorption experiments were carried out from equilibrium . Each film was immersed in 15 ml of the copper ion solution under the natural sunlight for 4 hours at ambient temperature .After four hours the residual concentration of Cu^{2+} in solution (C_e) was determined by spectroscopic method in each sample . The removal percentage of copper ion in the aqueous solution was calculated by (Eq. 4. 1):

$$\boldsymbol{R}(\%) = \left(\frac{\boldsymbol{C_0 - C_e}}{\boldsymbol{C_0}}\right) \times \mathbf{100} \qquad \textit{(4. 1)}$$

where C_0 and C_e are the initial and the equilibrium concentration of Cu^{2+} after 4 hours. of copper ion (mol/L) and V is the solution volume (L)

4.3 Results and discussion

4.3.1. Absorption of standard copper solutions

UV-Visible absorption spectroscopy plays a very important role to investigate the optical properties of aqueous solution [7]. The optical property of copper ions solution was analyzed by the cited technique, which is Shimadzu apparatus (Shimadzu-1800 working in the wavelength range 200-900nm). The analysis was performed in a quartz cell, using distilled water as a reference solvent.

Before starting the removal of copper ions, a calibration of different synthetic solutions current was proceed and curve of which is obtained by plotting the absorbance peaks of absorption spectroscopy versus fixed standard concentrations of copper chloride. The UV-Vis spectra of copper metal ions at different concentrations in aqueous solution shown in (figure. 4. 1). As can be seen from this figure, one peak of maximum absorption are exhibited. this peak is strong at about 505nm , which are attributed to the formation of copper metal ions. A decrease in the intensity of the peaks with the concentration decrease is observed. This may be due to the decreasing number of copper ions in aqueous solution [8].

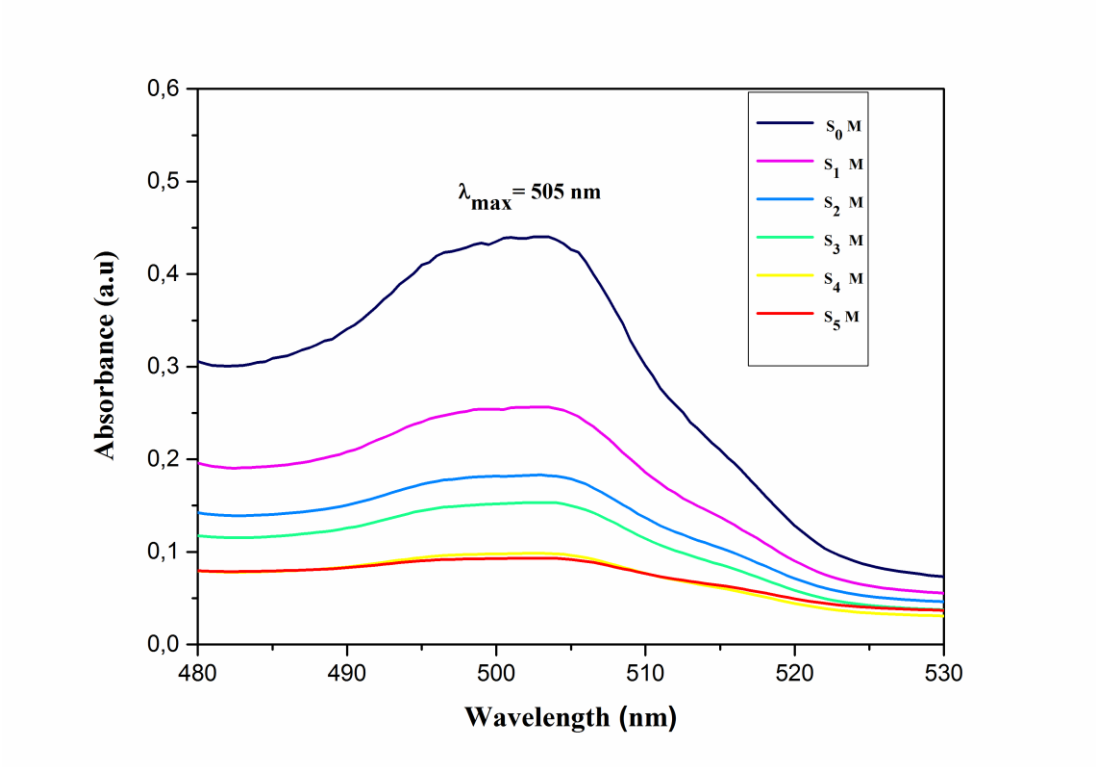

Fig. 4. 1. Absorption spectra of copper metal ions at different concentrations in aqueous solution .

4.3.2 Adsorption studies

The performance of the prepared ZnO/glass slides for removal copper ion from aqueous solution was tested by adsorption experiments. Figure 4. 2, shows the photograph of ZnO/glass slide before and after adsorption of copper ions. Change of slide color from white to blue clearly indicates the potential of ZnO thin films for removal of Cu^{2+} from aqueous solution.

Fig. 4. 2. Photogragh of ZnO/glass slide: (a) before and (b) after adsorption of copper ions .

4.3.2.1 Adsorption of copper ions from a solution under natural sunlight by ZnO:La thin films

- ***Zinc Acetate***

The calibration curve of the absorbance , versus the standard concentrations of copper, is shown in figure 4. 3. In order to determine the residual unknown concentration of copper in solution after each sheet immersion, absorption spectroscopy was also preceded and recorded in the wavelength range 480 to 530nm.

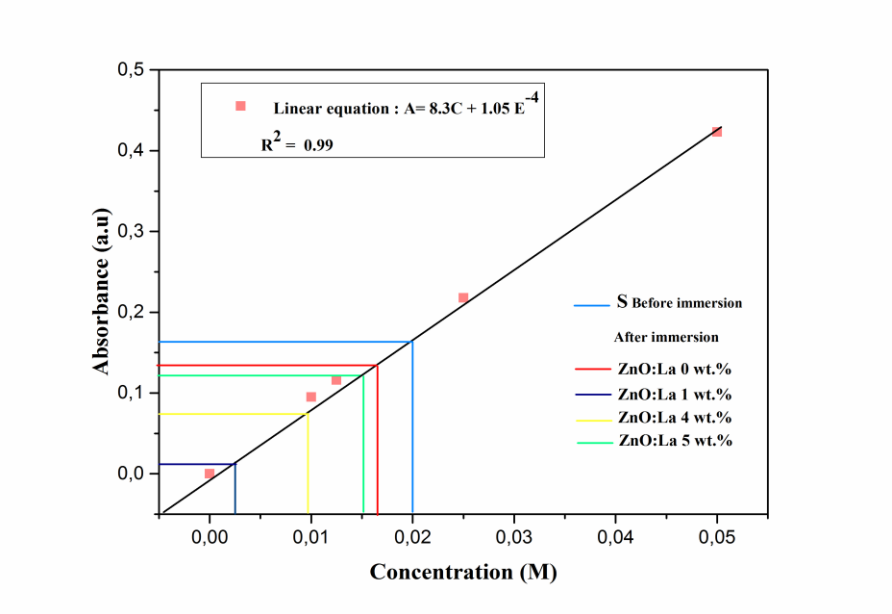

Fig. 4.3. Calibration curve of absorbance of Cu^{2+} versus standard concentrations of copper and absorbance of residual solutions upon 0-5wt.% La doped ZnO immersed.

Figure.4.4 shows the recorded absorption spectroscopy before and after each immersion. Before immersion , as can be seen one peaks more intense was observed approximately at 505nm. After immersion ,a decrease in the intensity of the peaks with the concentration decrease is observed. This may be due to the decreasing number of copper ions in aqueous solution because is absorbed by the substrate of ZnO/glass slide.

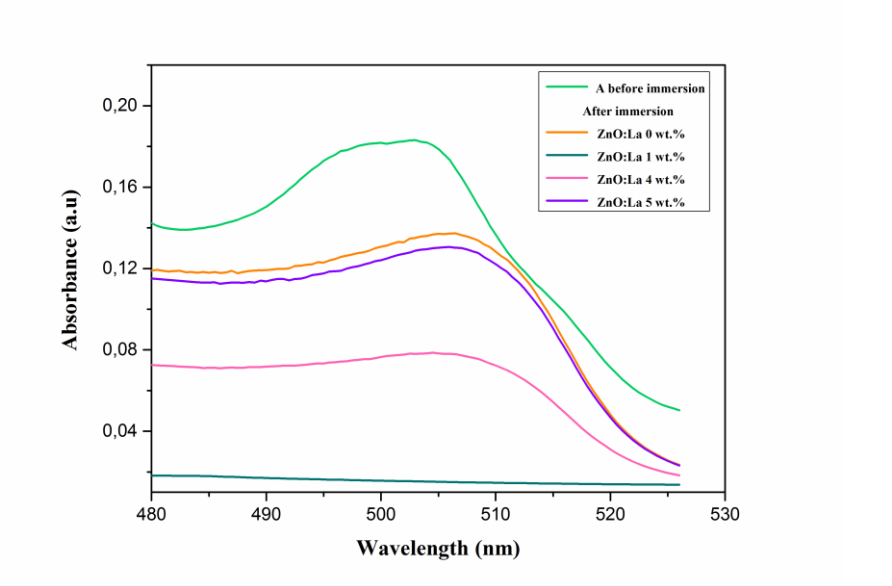

Fig. 4. 4. Absorption spectra of copper ions in aqueous solution at 0.02M, for 0-5 wt.% La doped ZnO sheets before and after each 4 hours of immersion.

The absorbance of the initial Cu^{2+} ions in a solution containing 0.02 mol/ml of $CuCl_2$ is 0.201 before immersion and decreases until 0.018 after having immersed 1wt% La doped sample for 4 hours. Absorbance values, before and after immersion, are listed in Table 4.2. Residual concentrations of Cu^{+2} ions (it means $CuCl_2$), in solution, were obtained by intercepting its absorbance the concentration axis in mol/ml via the calibration curve as plotted in figure 4.3

Table 4.2. Measured absorbance, concentrations ,mass and removal percentages of copper Cu^{+2} ions from aqueous solution with La level doped ZnO.

Samples (wt.%)°	Absorbance (a.u)	Concentration (mol/ml)	Mass (mg)	Percentage of removal (%)
Before immersion	**0.201**	**20**	**40.33**	**//**
After immersion	**(20 mol/ml) in aqueous solution of copper ions for 4 hours**			
ZnO:La 0	**0.134**	**16.6**	**33.471**	**17**
ZnO:La 1	**0.018**	**2.5**	**5.041**	**87**
ZnO:La 4	**0.076**	**9.6**	**19.36**	**52**
ZnO:La 5	**0.124**	**15**	**30.25**	**25**

Percentage removal of copper as a histogram and the grain size are drawn in figure. 4. 5. Based on removal equation of Cu^{+2} ions and its associated histogram, it becomes clear that, in general, adsorption of copper on sheets (or removal efficiency) of La-doped ZnO thin films has higher removal than undoped ZnO. The removal efficiency of ZnO increases from 17.% to 87% after La doping exhibiting the higher percentage removal of copper ions at 1wt.% La doping than undoped and the others La-doped ZnO thin films. Beyond 1wt. % La doping, removal of copper ions decreases to arrive at the minimum value of about 25.% with 5wt.% La doping level. Removal values were illustrated in Table 4. 2. Correlating the adsorption results with the crystallite size corresponding to 1wt.% La doped ZnO, it reveals that a link, between the removal and the surface area of samples, exists: the smallest grain size, as it was revealed in XRD study, provides great surface area (*i.e* decrease in grain size leads to sensitive nanostructure on the surface), yielding to more Cu^{+2}adsorption on the surface of the samples. This behavior may be credited to the presence of more active adsorption sites on the La-doped ZnO thin film surface [9]or also to the substitution of Zn^{+2}cation by La^{+3} hence 5 wt.% La doped sample has big crystallite size compared to the undoped one but it exhibits more Cu^{+2}removal, as seen in figure. 4. 5. This further removal may be attributed to the increase in the permanent dipole toward *c* direction in the ZnO matrix attracting Cu^{+2} from the solution.

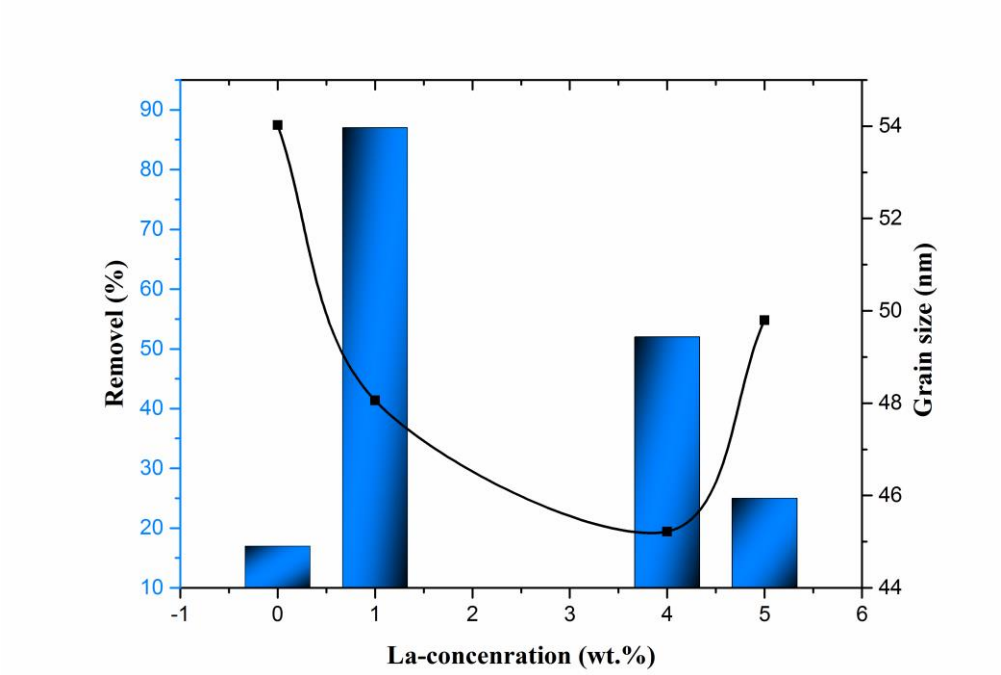

Fig. 4. 5. Drawn of a histogram in with the grain size of La doped ZnO on the removal of Cu^{+2} ions from aqueous solution.

Both of the tow conceptions improving the removal of Cu^{+2} ions may be explained as follow: The first one is the effect of the littleness in grain size mainly at lower level of doping (0-4 wt.% La) where the removal follows the decrease in grain size as seen in figure. 4.5. As it is well known that the ZnO is polar material along *c* direction; the second conception is the effect of La doping in intensifying the permanent dipole along *c* direction. At 5 wt. % La doping, it is very important to mentioned that even though the grain size increases, the removal increases too. This means that the insertion of La in Zn site increases the permanent dipole toward the *c* direction as shown in figure 4. 6. The insertion is confirmed by XRD studies where the shift of the peak towards the lower angles is more significant in the case 5 wt.% la doped sample. The permanent dipole intensification may be understood as follow: the insertion of La in ZnO matrix augmentains the lattice parameter ($ć=c+\Delta c$) and the local ionic charge yielding to an augmentation in the local permanent dipole ($\mu+\Delta\mu$) as illustrated in figure 4. 6; the augmentation in the local permanent dipole lets the sample surface more attractive (adsorptive) toward Cu^{+2}. As results, the adsorptive ability of thin films increases after La doping. Those results are in good agreement with similar results reported in the literature [9-11]which were obtained with Silver, Lanthanum and Gallium doped ZnO.

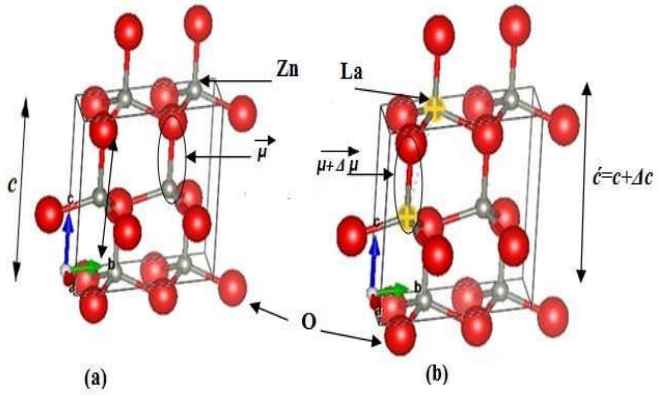

Fig. 4. 6. Effect of La in intensifying the permanent dipole toward the c direction:

a) μ before doping, b) (μ+Δμ) after doping.

➢ ***Zinc chloride***

To see the effect of the nature of the substrate which may be involved in the phenomenon of copper adsorption in solutions of water synthesized by lanthanum-doped ZnO, we prepared a series of solutions at a concentration of 0.02M ions of copper by dissolving $CuCl_2$ in 15mL of double distilled water in the same way as the case of the zinc acetate substrate. Each ZnO sample was immersed for 4 hours under natural sunlight and then removed from the solution.

Figure. 4. 7 shows the recorded absorption spectroscopy before and after each immersion. Before immersion , as can be seen one peaks more intense was observed approximately at 505 nm .After immersion ,a decrease in the intensity of the peaks with the concentration decrease is observed.

The absorbance of the initial Cu^{2+} ions in a solution containing 0.02mol/ml of $CuCl_2$ is 0.201 before immersion and decreases until 0.056 after having immersed 1wt% La doped sample for 4 hours. Absorbance values, before and after immersion, are listed in Table 4. 3. Residual concentrations of Cu^{+2} ions (it means $CuCl_2$), in solution, were obtained by intercepting its absorbance the concentration axis in mol/ml via the calibration curve as plotted in figure 4.8

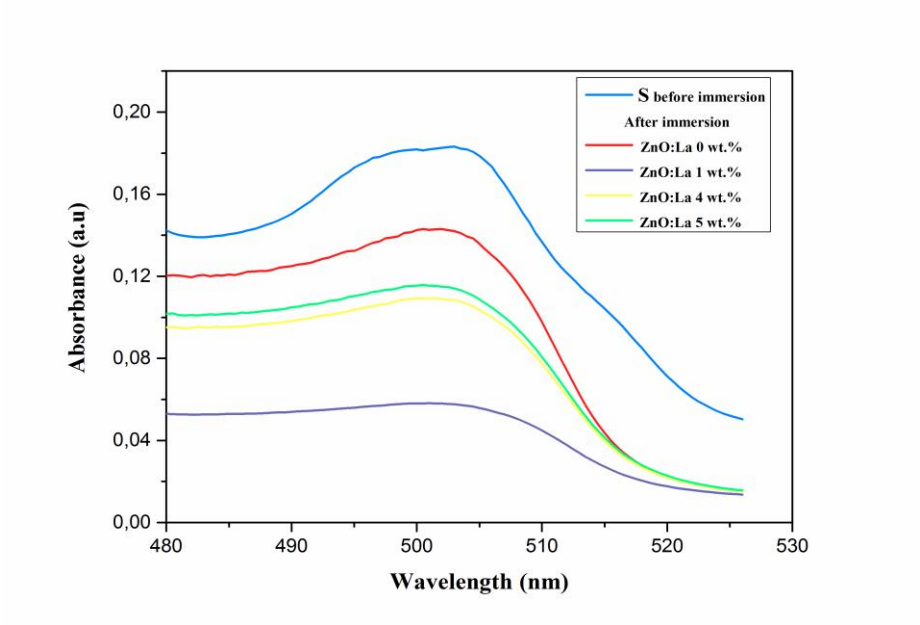

Fig. 4. 7. Absorption spectra of copper ions in aqueous solution at 0.02M, for 0-5 wt.% La doped ZnO sheets before and after each 4 hours of immersion.

The calibration curve of the absorbance , versus the standard concentrations of copper, is shown in figure 4. 8. In order to determine the residual unknown concentration of copper in solution after each sheet immersion, absorption spectroscopy was also preceded and recorded in the wavelength range 480 to 530nm.

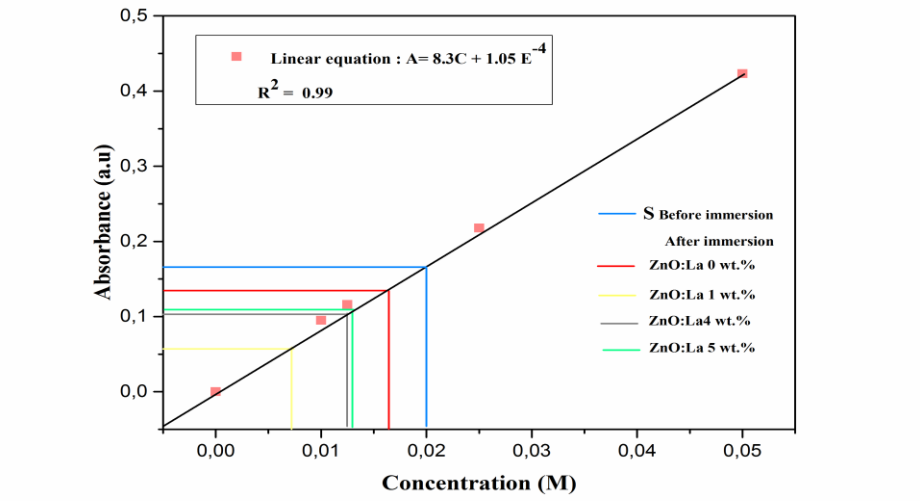

Fig. 4. 8. Calibration curve of absorbance of Cu^{2+} versus standard concentrations of copper and absorbance of residual solutions upon 0-5wt.% La doped ZnO immersed.

The efficiency of elimination of Cu^{+2} by ZnO increases from 20% to 65% after doping with lanthanum by 1.% by weight La / Zn showing the doping effect on the elimination of copper ions compared with undoped ZnO and the other lanthanum-doped ZnO (1, 4, 5% weight) (See figure. 4. 9). Beyond 1.% by weight of lanthanum doping, the elimination of copper ions decreases to reach a value of approximately 35.% With 5.% by weight La/Zn; an illustration of these values has been given in the table 4. 3. If the adsorption results are compared with the size of the crystallites corresponding to 1.% of ZnO doped with lanthanum, a correlation was observed between the percentage of copper removal from the solution and the surface, moreover small grain size, as revealed in the DRX study, which has a larger active surface, which leads to more adsorption on surface of ZnO doped with lanthanum (1weight.%). This behavior can be attributed to the presence of more adsorption sites more active on the surface of the thin film ZnO doped with lanthanum.

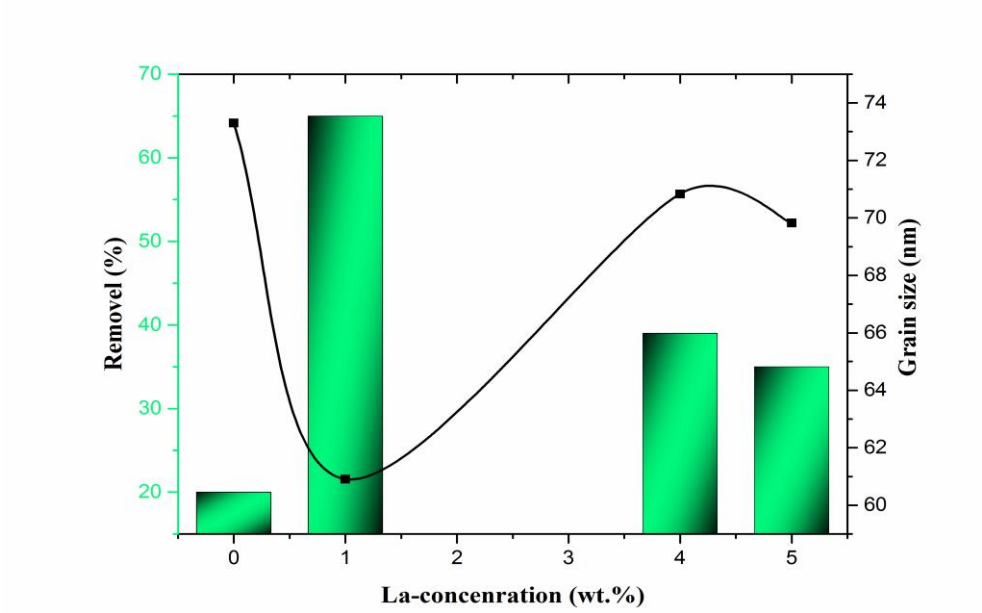

Fig. 4. 9. Drawn of a histogram in with the grain size of La doped ZnO on the removal of Cu^{+2} ions from aqueous solution.

Table 4.3. Measured absorbance , concentrations ,mass and removal percentages of copper Cu^{+2} ions from aqueous solution with La level doped ZnO.

Samples (wt.%)°	Absorbance (a.u)	Concentration (mol/ml)	Mass (mg)	Percentage of removal (%)
Before immersion	**0.201**	**20**	**40.33**	**//**
After immersion	**(20 mol/ml) in aqueous solution of copper ions for 4 hours**			
ZnO:La 0	**0.133**	**16**	**32.26**	**20**
ZnO:La 1	**0.056**	**7.00**	**14.11**	**65**
ZnO:La 4	**0.101**	**12.2**	**24.66**	**39**
ZnO:La 5	**0.105**	**13.0**	**26.21**	**35**

The adsorbent results confirm that the precursor type and the molarity play an important role in the physicochemical and adsorbent properties of ZnO films. The type of precursor, the solvent and their molar concentration resulted in changes in crystallinity, stress, porosity, types of nanostructures morphology and particle size.

In addition, varying the molar level of precursors acetate, ZnO/La wt. 1% showed better adsorbent activity than 0, 4 and 5 wt.%. We can attribute this higher activity to the non-uniform morphology created and to the lowest band-to-band recombination, indicating that a higher number of photo-generated electrons are able to interact with the surrounding molecules. In this film, hexagonal plates are randomly oriented. Similarly, zinc chloride precursors, ZnO/La 1wt.% showed better adsorbent behavior than the other respective molar levels, coinciding in that both have the smallest particle size of each set.

4.3.3 Copper oxide thin films

In this section, we present the results of CuO films prepared on substrate of ZnO:La 1wt.% with tow precursors namely: copper chloride ($CuCl_2..2H_2O$) and copper acetate $Cu(CH_3COO)_2$ at various substrate temperatures in order to investigate the effect of this parameter

4.3.3.1.Chopper chloride

Copper chloride is used as copper source with molarity equal to 0.02 M. The samples were deposited with various substrates temperature ranged from: 200-350°C.

4.3.3.1.1 Growth rate

In figure 4. 10 the growth rate variation was reported as function of the substrate temperature. As can be seen, the film thicknesses decrease with the increase in substrates temperature. The films deposition rate starts with 47.11nm/min at the beginning for the lower substrates temperature (200 °C) and decrease when substrate temperature rise to reach 16.65nm/min for CuO films deposited at higher temperature (350 °C). It is well known, that the increase of the substrate temperature improves the surface kinetic reaction of the substrate, which lead to thicker thin films. However, for CuO deposited thin films the thicknesses turn to reduce with increasing substrate temperature. In fact the deposition rate depends on the quantity of adsorbed copper ions as reactive species reaching the top of surface substrate. The increases in the substrate temperature enhance the evaporation of incoming species causing thin films thickness reduction. [12]

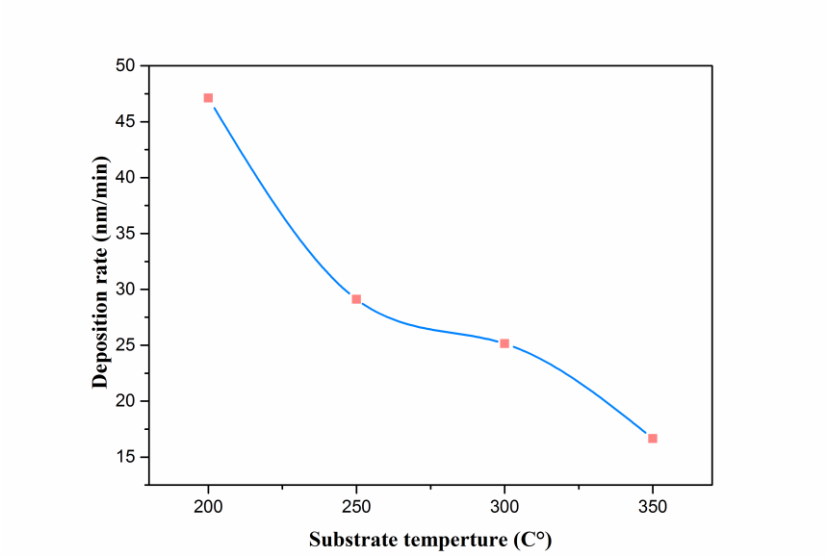

Fig. 4. 10 Variation of deposition rate as a function of substrates temperature.

4.3.3.1.2 Structural properties

The X-ray diffraction (XRD) patterns of copper oxide thin films annealed at different temperatures are illustrated in figure 4. 11. The observed XRD patterns match well with monoclinic phase of CuO (JCPDS 45-0937 and JCPDS 80-0076) [13,14]. No peaks corresponding to metallic Cu or Cu_2O phases were detected in the XRD patterns. Annealing the CuO films in air at various temperatures shows an improvement in crystallinity.

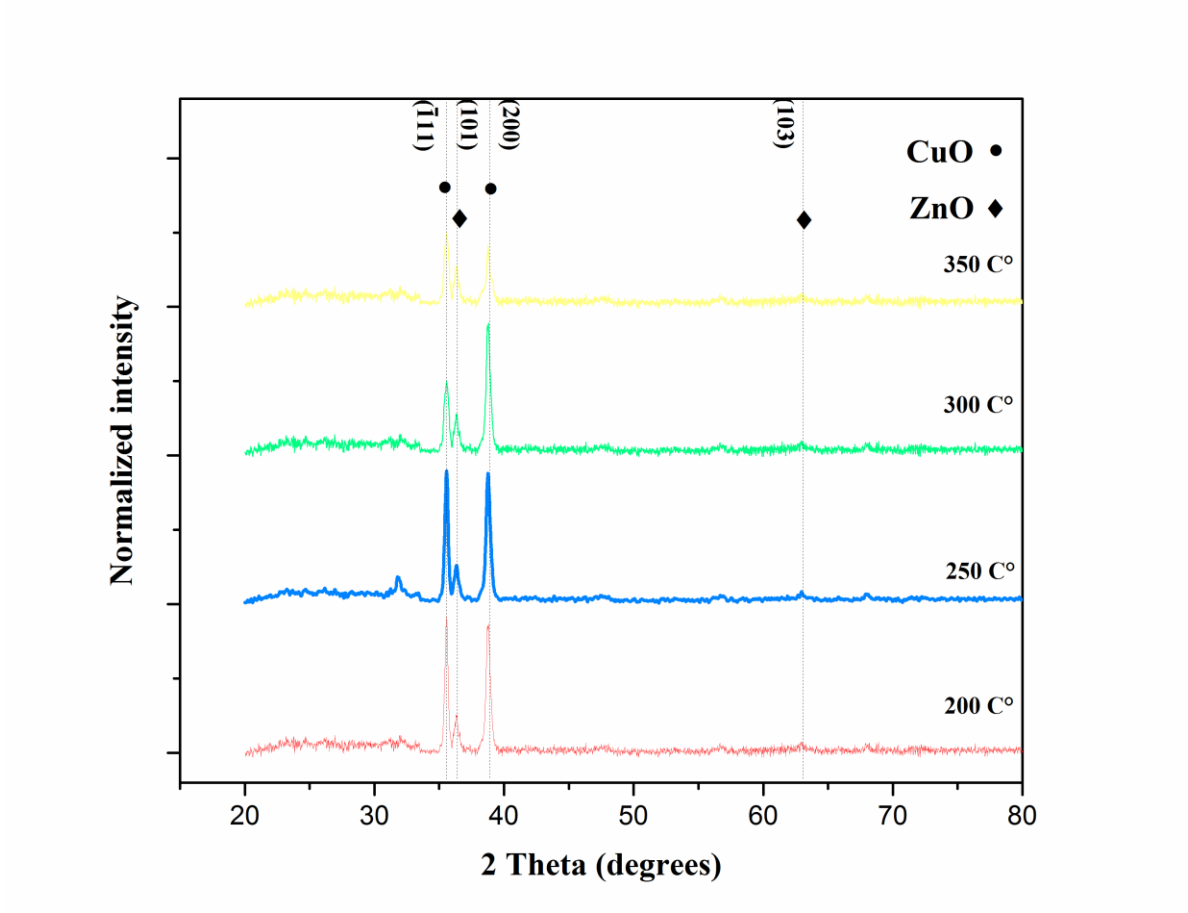

Fig. 4. 11. X-ray diffraction patterns of CuO thin films annealed at different temperatures

The films crystallites size was estimated from the most intense peak namely ($\bar{1}11$) and (200) by using the Scherer equation. In figure 4. 12 we have reported the variation of crystallite size as a function of substrates temperature. It is evident from the figure that the films crystallites size is reduced with increasing the substrate temperature. This variation can be explained in terms of the decrease in film thickness. Akaltun [15] have investigated the effect of thickness on the structural proprieties of CuO thin films prepared by bath chemical and he found increase of crystallite size from 8 to 18 nm for film thicknesses varied from 932 to 332nm.

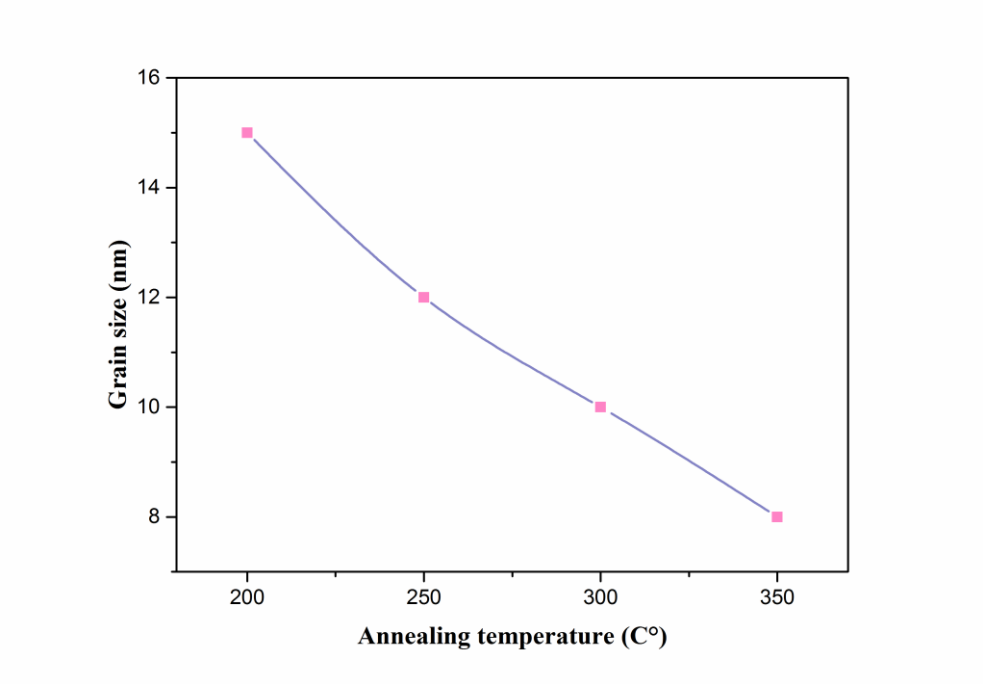

Fig. 4. 12. Plot of grain size versus annealing temperature of CuO thin films.

As can perceive from the XRD spectra, the intensity of this peaks are affected by the change in substrate temperatures. To describe the structure and preferred orientation of the deposited CuO thin films in detail, the texture coefficient (T_C) . In figure 4. 13 we have reported the variation of the texture coefficient estimated for the two prominent peaks namely ($\bar{1}11$) and (200) as function of substrate temperatures. As can be seen, the texture coefficient of the two atomic plans increase with increasing in substrate temperature to 300°C. Above this temperature the texture coefficient is reduced considerably. The decrease in the *Tc* value with substrate temperature shows that films obtained have more randomly oriented grains. The T_C of the (200) plan is higher than the T_C of the ($\bar{1}11$) plan in the investigated temperature, this indicated that all sample have preferred (200) orientation. Thus, it was clear from the calculated T_C that CuO films deposited at 300°C have best crystallization level and preferred (200) orientation.

We emphasize that no peak corresponding to Cu_2O has been appeared in the XRD pattern of films deposited at various substrate temperature. While some authors have reported the presence of both CuO and Cu_2O phase for spray deposited CuO films [16,17]. Maruyama [18] has observed a mixture of Cu_2O and CuO phase in CVD grown copper oxide films prepared at a substrate temperature of 300°C. Yoon et al. have observed a dominant CuO phase in copper oxide thin films prepared using ion beam sputtering at a substrate temperature varied from 25 to 400 °C. It is important to note that films deposited with bath chemical technique, copper

oxide thin films with a predominant CuO phase has been successfully grown with substrates temperature of 200-350°C.

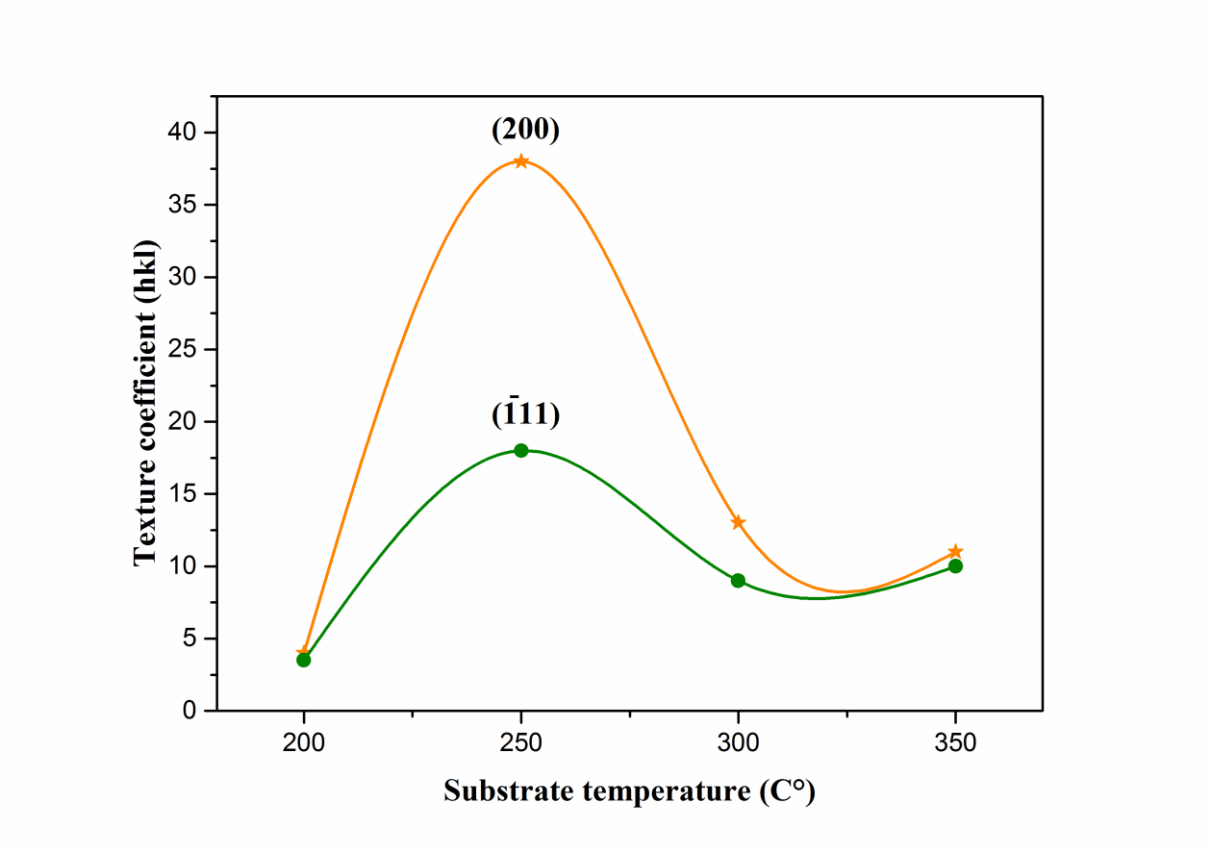

Fig. 4. 13. Variation of texture coefficient as various substrate temperatures.

In table 4. 4. we have regrouped the values of strain (ε) for CuO deposited films at various substrate temperatures. This structural parameter was also calculated from Hall–Williamson equation. The strain values varied from 0.0215 to 0.0593 in the studied temperature range . As can be seen, the maximum strain value found for the films deposited at 250°C. This can be explain by the appearance of all (hkl) plans characteristics of CuO phase in the same time which create a competition in the growth between this atomic plans and involve an augmentation of the strain in thin layer. Therefore, at higher substrate temperature the strain is found to decrease. This can be explained also by the disappearance of the (hkl) peaks as shown in XRD diffraction patterns.

A positive slope has been observed in the Hall equation plot for CuO films deposited at 200, 300°C, which confirms the presence of tensile strain in the crystal lattice. However, for CuO thin films deposited at higher temperature (350°C) a negative slope has been noticed

indicating the presence of compressive strain in the crystal lattice. As can be seen, variation of the substrate temperature leads also to change in the type of strain.

Table 4. 4 Values of strain of the as-prepared CuO thin films with different substrate temperature.

Substrate temperature (°C)	Strain
200	0.0421
250	0.0593
300	0.0215
350	-0.0219

4.3.3.1.3 Surface morphology and composition

- **SEM analysis**

The films surfaces were studied by scanning electron microscopy. The observations by SEM indicate the film surface homogeneity, the shape of the grains and aggregates of grains boundaries. SEM micrographs were taken for CuO films deposited with substrate temperature equal to 200 and 300 °C are embedded in figure 4. 14. The SEM micrographs show that deposited films are homogenous, dense and compact. However, the films deposited with higher temperature are smoother than the films deposited with lower temperature. This can be related to the decrease in film thicknesses. This confirms the extinction of interference fringes in transmittance spectra.

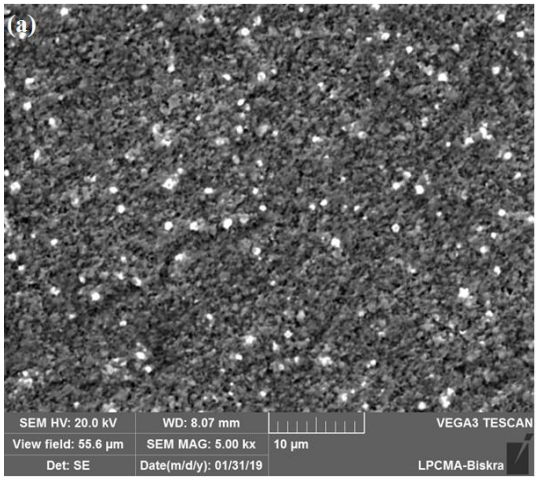

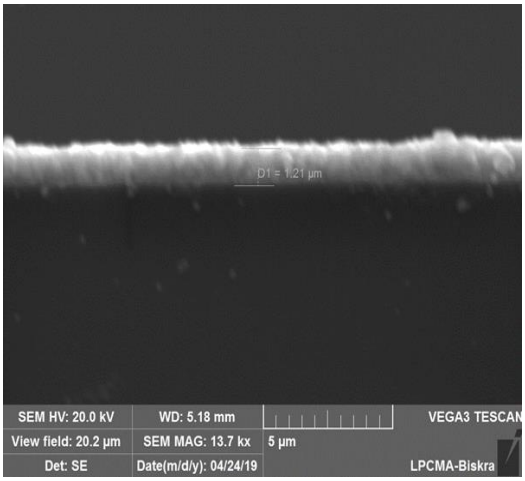

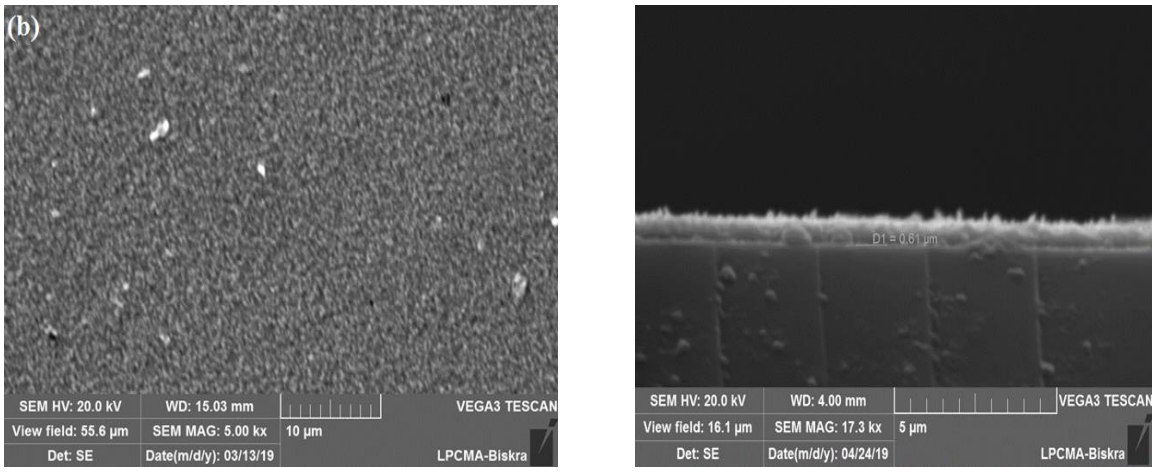

Fig.4 .14. SEM images of CuO thin films and their cross sections on substrate of ZnO:La 1wt.% .(a: 200℃, b: 300 ℃)**.**

➢ Film thickness measured using SEM

The SEM image in cross section made for the cupric oxide thin layer is illustrated in figure 4.14, the estimated thickness of which is around 1200-600nm.

➢ EDAX analysis

The chemical composition of the CuO thin film was determined by the energy dispersive analysis X-ray spectra. Figure 4. 15 shows the EDAX spectra obtained for sample of CuO on substrate of ZnO doped with 1% lanthanum.

For this sample ,the elements identified in the thin layer of CuO are copper and oxygen also the presence of other elements in the spectrum originated from the substrate glass. The EDAX analysis does not reveal the presence of the other peaks which are at the origin of the impurities. This proves that the synthesized CuO is pure. Do not take into account the peak of carbon present in the air .

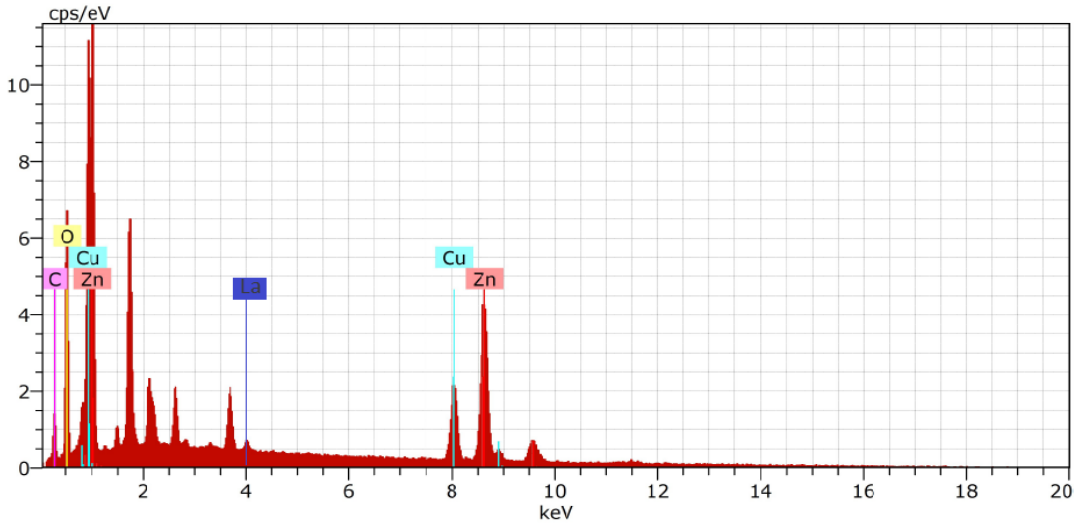

Fig. 4. 15. EDAX spectrum of CuO thin layers on substrate of La-doped ZnO 1wt.%.

4.3.3.1.4 Optical properties

The optical properties of the films were studied by measuring the transmission in the visible region. Figure 4. 16 shows the transmission spectra of CuO thin films annealed at various temperatures for a duration of one hour. It is clear that the deposited films exhibit a relatively high absorption ranged from 40 to 60 % for wavelengths greater than 600nm. The reduction of the transparency in this range with the substrates temperature is due to film thickness increasing.

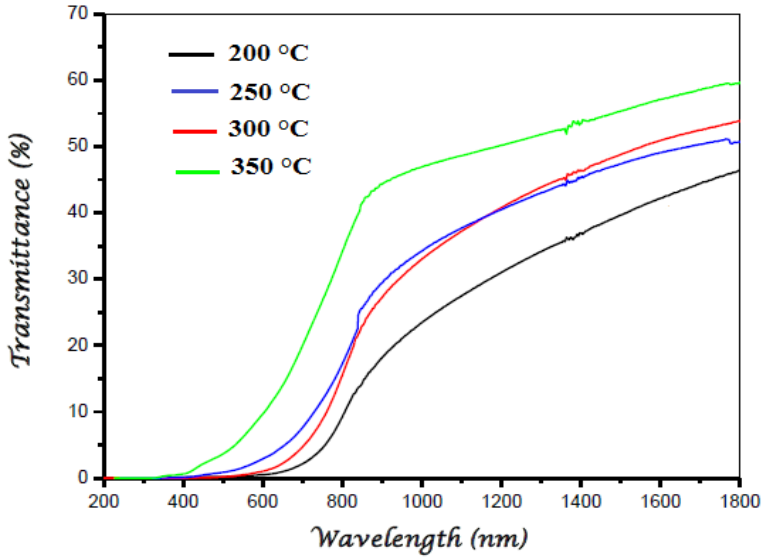

Fig. 4. 16. Optical transmission spectra of bath chemical CuO thin films annealed at different temperatures.

➢ *Band gap energy calculation*

The optical energy band gaps (E_g) of CuO thin films can be estimated using Tauc equation . The allowed direct band gap of CuO is found from the Tauc plot (Figure. 4. 17) [19].

The straight line intercept on energy axis at $(\alpha h\nu)^2$ equal to zero in the $(\alpha h\nu)^2$ versus hν plot will give the direct band gap of CuO films. The direct band gap of CuO films are observed to increase with annealing temperature

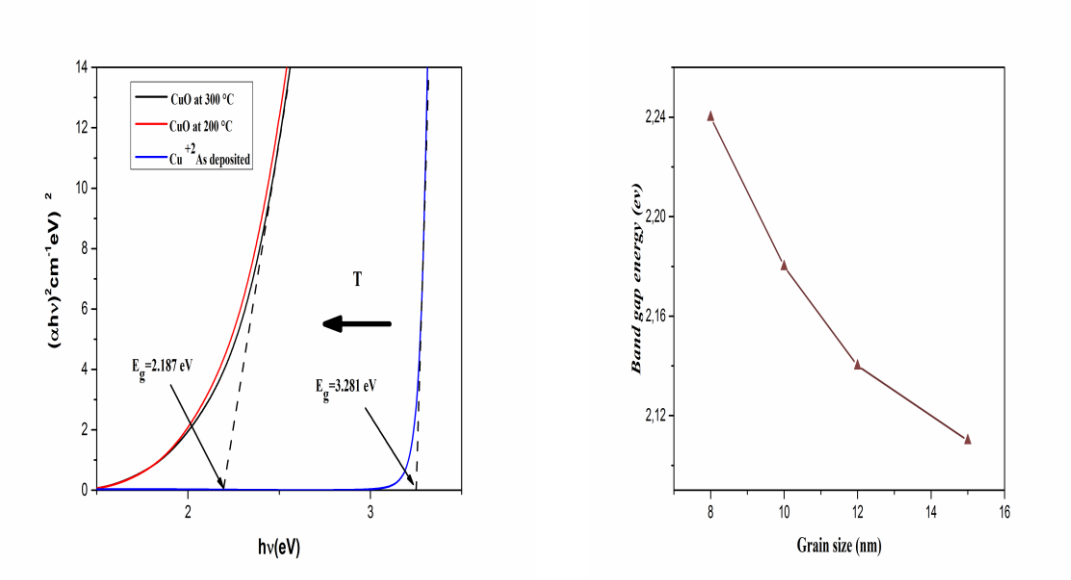

Fig. 4. 17 (a) The Tauc plots $(\alpha h\nu)^2$ versus hν showing direct band gap**, (b)** Plot shows band gap energy versus grain size of CuO thin films.

from the table 4.5, it is observed that as the annealing temperature increases the grain size as well as the film thickness decrease.

Table 4.5. The calculated band gap and Urbach energy values.

Samples	Thickness (nm)	Band gap energy (eV)	Urbach energy (meV)
200°C	1200	2.115	95
250°C	890	2.146	87
300°C	784	2.187	74
350°C	600	2.241	65

The increase in the values of band gap energy with decrease in grain size is attributed to the increase in crystallinity of CuO phase in the films [20].

The estimated band gap values of CuO thin films for direct transitions in the present study are consistent with the reported Eg values of copper oxide thin films [20-22].

4.3.3.1.5 FTIR spectroscopy analysis

The FTIR spectra were recorded on a PerkinElmer RX spectrometer with KBr as a diluting agent and operated in the wave number range of 400-1800cm^{-1} with 4cm^{-1} resolution .The products were diluted with potassium bromide in the ratio of 1:100 for FTIR analysis.

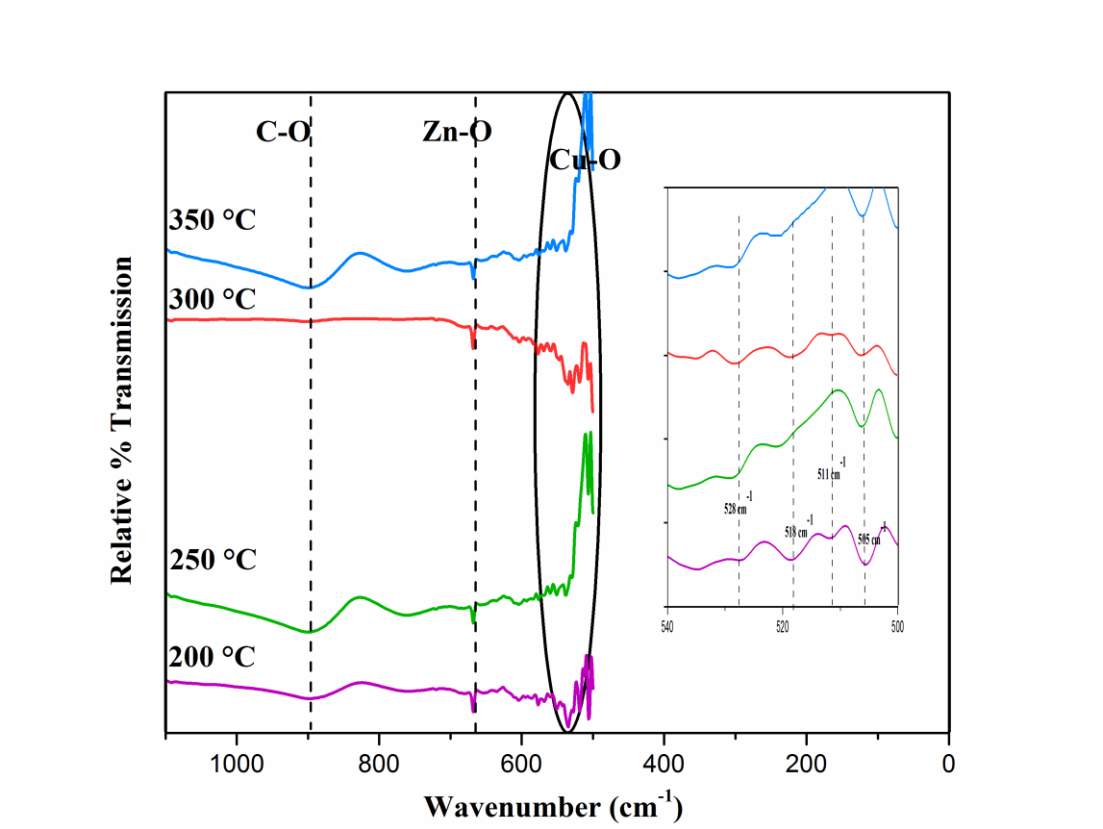

Fig. 4. 18 FTIR spectra of CuO synthesized by bath chemical method on substrate of ZnO doped La .

Figure 4. 18 shows FTIR spectra of CuO thin films at different temperature on substrate of La-doped ZnO products. Figure 4. 18 shows FTIR spectra of CuO thin films at different temperature on substrate of 1wt.% La-doped ZnO products. The absorption bands at 500 and 618cm^{-1} correspond to the stretching vibration of Cu-O bond in monoclinic CuO [23] as seen in the inset of figure 4.18. It is worth noting that the absorption band of Cu-O becomes greater than those obtained from the as synthesized of copper oxide films revealing that the annealing treatment ameliorates the oxide copper thin layers .but other absorption bands correspond to the stretching vibration of Zn-O bond wurtzite hexagonal type ZnO crystal [24,25].

4.3.4.2 Copper acetate

In this part, copper acetate is used as copper source with molarity equal to 0.02 M. the used samples study are deposited with various substrates temperature ranged from : 200- 350°C.

4.3.4.2.1 Growth rate

In figure 4. 19, Also the growth rate variation was reported as function of substrate temperature. As can be seen, the deposition rate diminish from 14 to 10nm/min in the investigate temperature range. Increasing in substrate temperatures causes to reduce of the quantity of reactive species and deteriorate the surface kinetic reaction of the substrate, which lead to decrease film thicknesses. We noted that films thickness condense with increasing in substrate temperature for the deposited CuO films with the two precursor salt namely: copper acetate and chloride. As result this behavior is mostly and particularly attributed to the films deposited by bath chemical deposition and annealing at higher substrate temperature which may be affected by the presence anions salts (Cl^- or CH_3COO^-) and incoming pieces with adsorbed Cu^{++}.

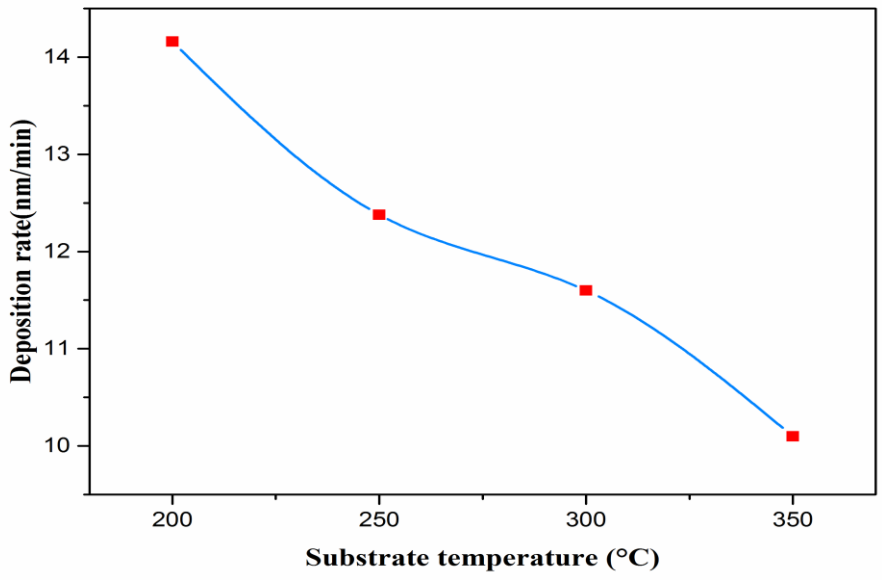

Fig. 4. 19. Variation of growth rate as function of substrate temperatures.

4.3.4.2.2 Structural properties

The XRD spectra of different films are reported in figure 4. 20. The influence of the deposition temperature on films structure can be divided as following:

- For substrate temperature varied from 200 to 300°C: Two most prominent peaks can be clearly seen at 2θ value 35.54° and 38.72° corresponding to atomic planes ($\bar{1}11$) and (111), respectively of CuO phase. No peak corresponding to Cu_2O phase of copper oxide has appeared in the XRD pattern indicating the formation of pure CuO films. However the intensity of these two important peaks changed with the variation of the substrate temperature.
- For the films deposited at 350°C: The DRX shows the presence of single (111) atomic planes located at 38.73° and the peak ($\bar{1}11$) disappears.

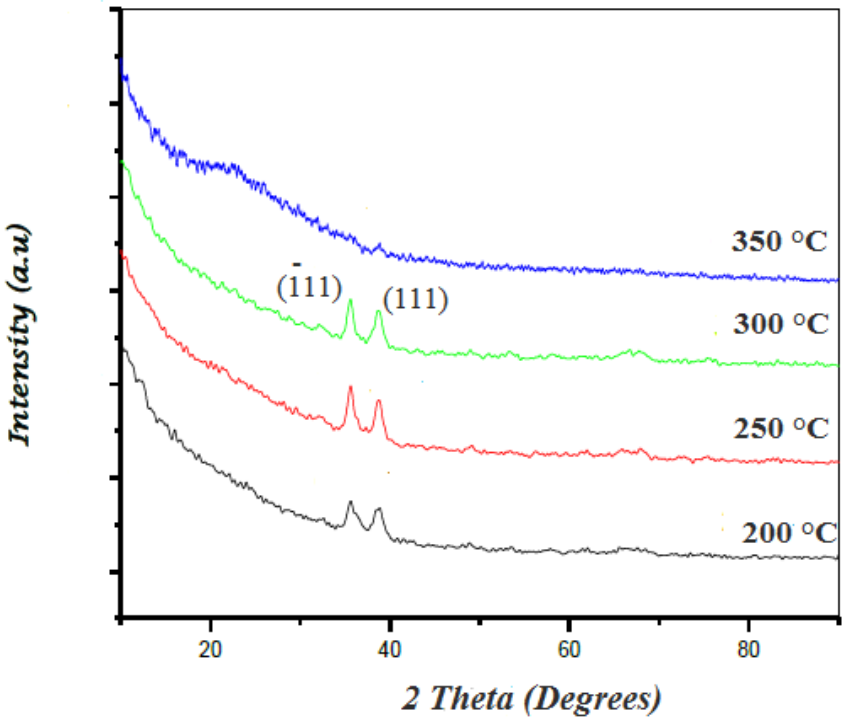

Fig. 4. 20. XRD diffraction patterns of CuO films prepared with different substrate temperatures.

To determine the preferential orientation in CuO films from the XRD data, the texture coefficient was calculated. The texture coefficient (*Tc*) for the ($\bar{1}11$) and (111) atomic planes at various substrate temperature is showing in figure 4. 21. As can be seen, the Tc of the two atomic plans have the same behavior, it is maximum for substrate temperature equal to 250°C

For the films prepared at 200°C, the samples show a (111) preferred orientation. With increasing substrate temperature the *Tc* of the two atomic plans equalized indicates a random distribution of grains in the film. At substrate temperature equal to 300°C, the preferred orientation of the CuO films change from (111) to ($\bar{1}$11). As result, for lower substrate temperature, the films showed a (111) preferred orientation and a ($\bar{1}$11) preferred orientation for the sample deposited at higher substrate temperature. All films are polycrystalline and the calculated texture coefficient shows that the CuO films elaborated at 250°C have the best crystallinity.

It is remarkable to note from the comparison of our observed and their reported from the XRD analysis that, the nature of salt solution used as Cu source for deposition CuO film by bath chemical technique might be responsible in change of copper oxide phases and the variation of structural proprieties of single phase CuO.

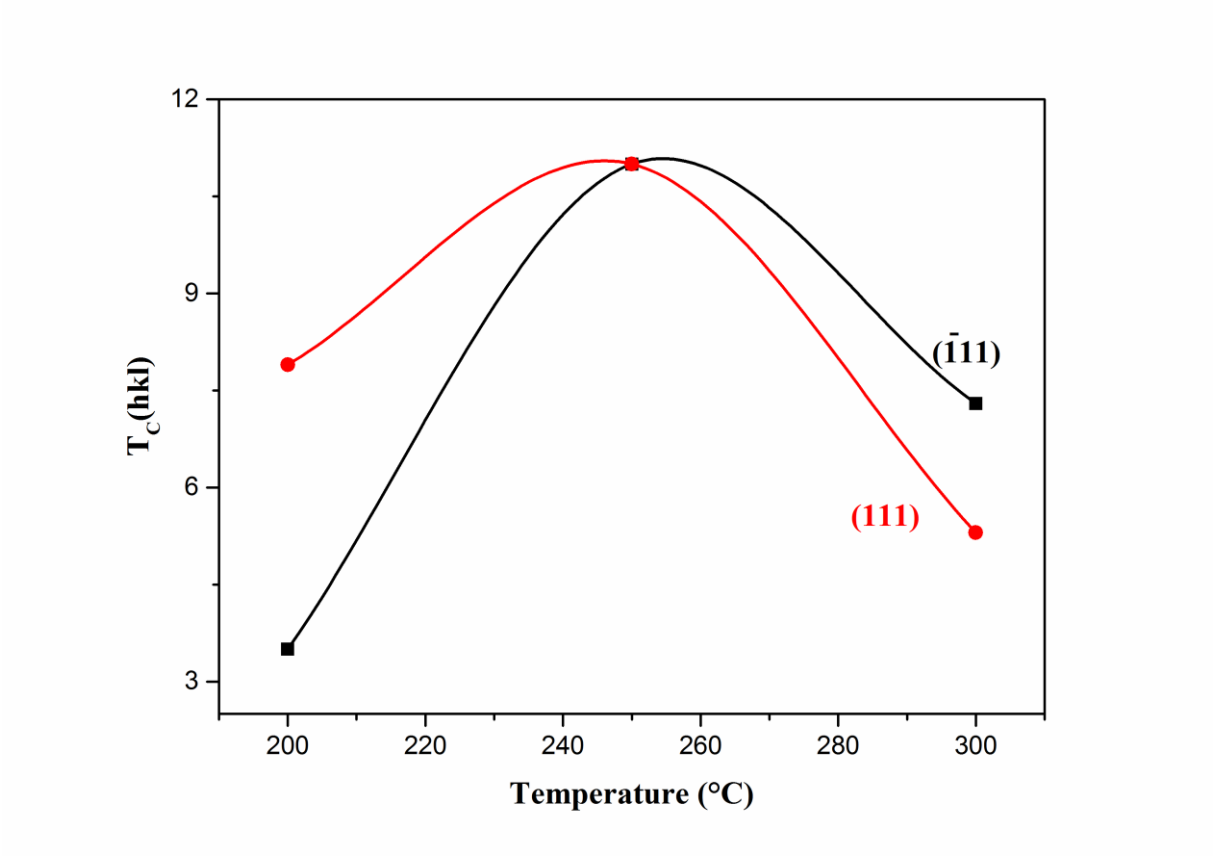

Fig. 4. 21. Variation of texture coefficient as function of substrate temperatures.

The films crystallites size was estimated from the most intense peak namely ($\bar{1}$11) and (111) by using Debye Scherrer formula (see chapter 3). In figure 4. 22 we have represented the variation of the crystallites size as function of the substrate temperature. It is clear from this figure that crystallites size increase with increasing substrate temperature. The calculated

crystallites size enlarges from 11 to 35 nm in the investigated temperature range. It is well know that the increase in substrate temperature improve the crystallinity and leads to the formation of bigger crystallites size. The nucleation step is highly sensitive to the substrate temperature. At hot surface substrate, atoms have larger kinetic energy which leads to wide nucleation and higher condensation of atoms in consequence growth of bigger crystallites size. Therefore, at low substrate temperature the nucleation center are fewer with less kinetic energy this leads to the growth of small crystallites size. In the same figure 4. 22 we have represented the variation of strain with various substrate temperatures. It is evident from this figure that the strain is reduced with increasing the substrate temperature. As can be noted the increase in substrate temperature improves the crystallinity and so the amount of the defects in the films. On other hand the increase in the crystallites size correlates well with the strain reduction in films. This indicates clearly that the obtained strain film is controlled by the value of the calculated crystallites size. In additional, the growth of lager crystallite size leads to grain boundaries reduction and consequently the reduction of defects in the structure. Grain boundaries are 2D defect in the crystal structure; it tends to decrease the film crystallinity. So, the reducing in crystallite size is a common way to improve the strain in films, as described by the Hall–Petch relation. It can be deduced an increase in the crystallite size causes the reduction in the strain.

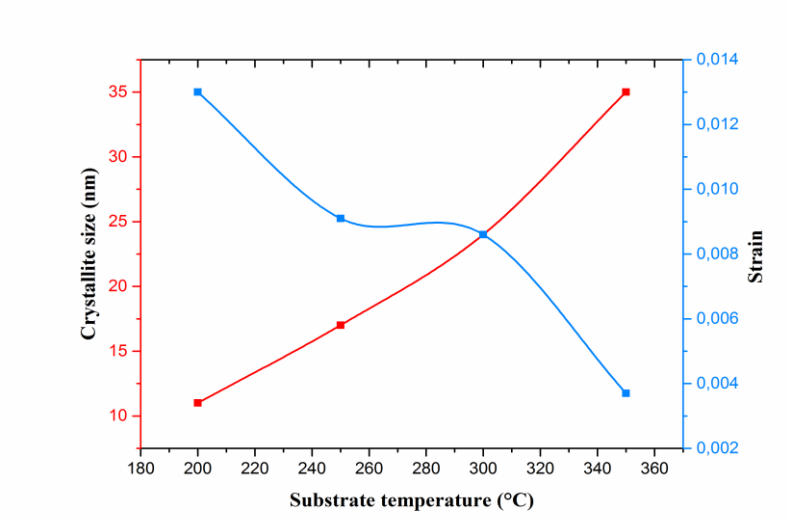

Fig. 4. 22. Variation of crystallites size and strain as function of substrate temperature.

4.3.4.2.3 Optical properties

In figure 4. 23 we have represented the diverse spectrum of transmittance in the UV-VIS-NIR range with different substrate temperatures. The films transparency varied wildly, in the investigated temperature range. It is seen that the films become more transparent with the increase in substrate temperatures. For wavelength above 800nm the transmittance of the whole films is ranged from 30 to 65%. This variation is in same rage reported in the literature [25]. CuO thin films are used as an absorber layers in solar cells. The high absorption of this layer in visible range is one of the required proprieties devices. The film transparency increases with increasing substrate temperature. This behavior is due to the decrease in films thicknesses.

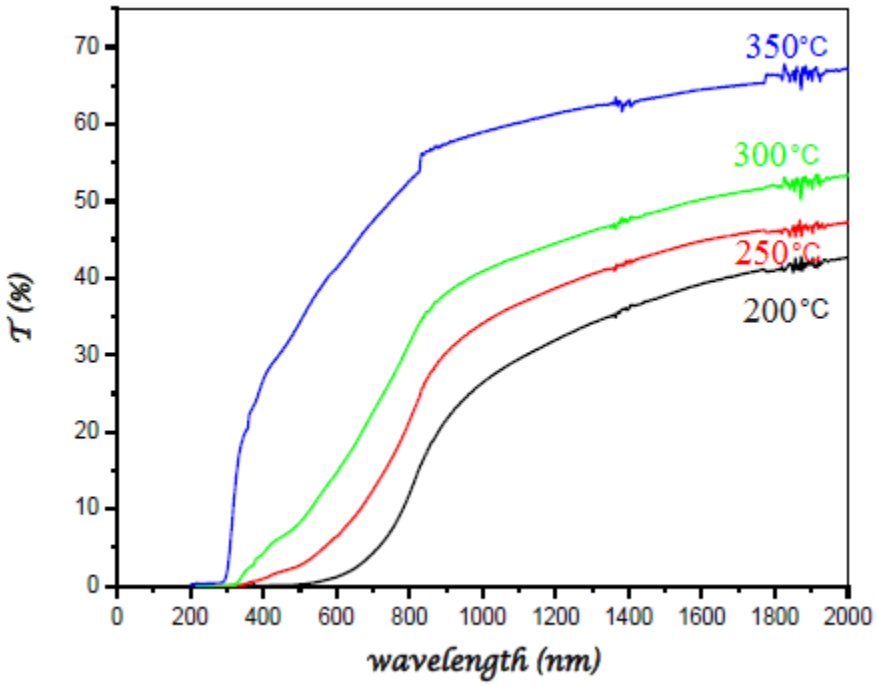

Fig. 4. 23. Transmittance spectrum in UV-VIS-NIR range of CuO films deposited with various substrate temperature.

The optical band of films is deduced from the transmittance spectra (as mentioned in chapter 3). The obtained results are shown in figure 4. 24. As can be seen, the optical band gap enlarges with increasing substrate temperature. It is varied from 1.23 to 1.46eV for substrate temperature ranging from 200 to 350°C. In figure 4. 24 we have represented the variation of the disorder (E_{00}) as function of substrate temperatures. As mentioned above the variation of optical band gap is related to the variation of disorder. The increase in optical band gap corroborates well the disorder reduction in films network. This confirms also the increase in

optical band gap with substrate temperature increasing. The increase in the gap energy indicates that the disorder in films is reduced with substrate temperature. This is consistent with the decrease is the values of the defects of the strain calculated from XRD patterns. In this case, the variation of the optical gap is governed by the film disorder .

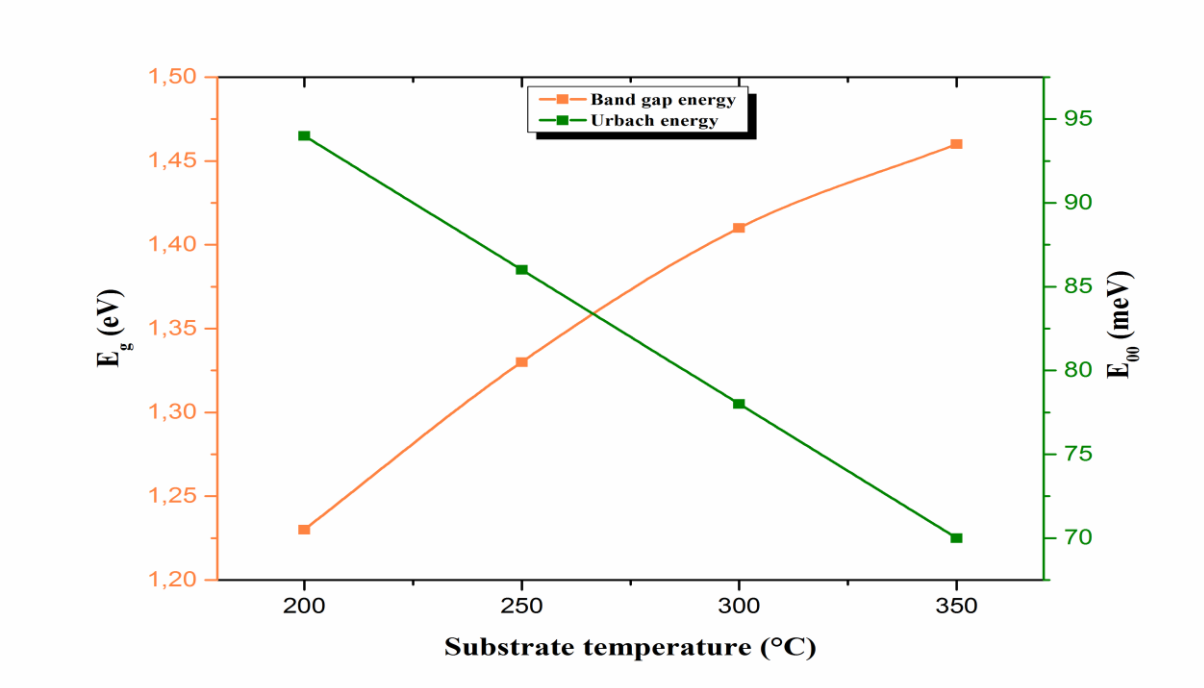

Fig. 4. 24. Variation of optical band gap and Urabch enery as function of substrate temperature.

Bibliography

[1] A. Roy, J. Bhattacharya, Chem. Eng. J. 211-212 (2012) 493.

[2] M. Imamoglu, O. Tekir, Desalination 228 (2008) 108.

[3] M. Sarioglu, U¨.A. Atay, Desalination 181 (2005) 303.

[4] C.S. Barrett, T.B. Massalski, "*Structure of Metals"*, Pergamon, Oxford, (1980) 204.

[5] S. Singh, K. Barick, D. Bahadur, Int. J. Nanosci. 10 (2011) 1001.

[6] X. Wang, W. Cai, Y. Lin, G. Wang, C. Liang, J. Mater. Chem. 20 (2010) 8582.

[7] L.Esteben, F. Malpartida, A. Esteban, C. Peccharoman, J.S. Moya, Nanotechnology20(8), 085103 (2009).

[8] N. Ahmad,S. Sharma, Green and Sustainable Chemistry2, 141 (2012).

[9] T. Wu, Y. Ni, X. Ma, J. Hong, Materials Research Bulletin48, 4754 (2013).

[10] S. Azizian, M. Bagheri, Journal of Molecular Liquids196,198 (2014).

[11] I. Ghiloufi, J. El Ghoul, A. Modwi, L. El Mir, Materials Science in Semiconductor Processing42, 102 (2016).

[12] P.K. Nair, M.T.S Nair, V.M. Gaecia, O.L Arenas, Y. Pena, A. Castillo. Solar Energy Mater and Solar Cells Soc. 313(1998) 52.

[13] K. Mageshwari, R. Sathyamoorthy, " *Physical properties of nanocrystalline CuO thin films prepared by the SILAR method* ", Mater. Sci. Semicon. Proc. 16 (2013) 337-343.

[14] F.A. Akgul, G. Akgul, N. Yildirim, H.E. Unalan, R. Turan, " *Influence of thermal annealing on microstructural, morphological, optical properties and surface electronic structure of copper oxide thin films* ", Mater. Chem. Phys. 147 (2014) 987-995.

[14] J. Moralesa, L. Sa´ncheza,, F. Martı´nb, J.R. Ramos-Barradob, M. Sa´nchezb Thin Solid Films 474 (2005)133.

[16] S. Kose, F. Atay, V. Bilgin, I. Akyuz, Mater. Chem. Phys. 111 (2009) 351.

[17] G.K. Williamson, W.H. Hall, Acta Mater. 1 (1953) 22 .

[18] T. Maruyama, Jpn. J. Appl. Phys. 37(1998) 4099.

[19] E.R. Kari, K.S. Brown, Choi, Chem. Commun 23 (2006) 3311.

[20] T. Ishihara, K. Kometani, Y. Nishi, Y. Takita, Sens. Actuators B 28 (1995) 49.

[21] L.S. Huang, S.G. Yang, T. Li, B.X. Gu, Y.W. Du, Y.N. Lu, S.Z. Shi, J. Cryst. Growth 260 (2004) 130.

[22] N. Serin, T. Serin, S. Horzum, Y. Celik, Semicond. Sci. Technol. 20 (2005) 398.

[23] J. Xia, H. Li, Z. Luo, H. Shi, K. Wang, H. Shu, Y. Yan, Journal of Physics and Chemistry Solids 70, 1461 (2009).

[24] V.Safarifard, A.Morsali, UltrasonicsSonochemistry19, 823 (2012) .

[25] P.C. Nagajyothi, P. Muthuraman, T.V.M .Sreekanth, H. K. Doo, S.Jaesool, Arabian Journal of Chemistry10(2), 215 (2017) .

Conclusion and Future Works

Chapter 5

Conclusion and Future Works

CuO thin films were deposited on substrate of zinc oxide by bath chemical. The CuO films are deposited with different deposition conditions in order to optimize these parameters for elaborate a CuO films with good quality which can be used in several applications such as: solar cells and gas sensor. The investigated parameters in this study were nature of substrate; substrate temperature, molarity and nature of salt. These layers have been characterized by different methods; X-ray diffraction (XRD) and scanning electron microscopy (SEM) for the observation of the microstructure, and UV-visible-IR spectroscopy for the study of optical properties.

The aim of the research is to elaborated and characterized they substrates of undoped and doped lanthanum zinc oxide and thin films of copper oxides. This study was therefore carried out in three parts.

In the first part of this work we have elaborated a series of deposition of ZnO thin films were deposited on substrate a glass by spray pyrolysis with moving nozzle at constant temperature 375°C with different parameters to study the effect of the lanthanum doping and the nature of the precursor, (in this case Zinc acetate and Zinc chloride) on structural and optical properties.

From the X-ray diffraction analysis we have concluded that the thin films of ZnO obtained are crystallized in a hexagonal wurtzite structure indicates that the structures of doped ZnO are not altered by the incorporation of La. It is also worth noting that no peaks related to lanthanum oxide are found in these spectra, which may be due to the low La content, with a preferential orientation (002) along a c axis perpendicular to the substrate for the precursors zinc acetate and chloride of zinc respectively. The crystallite size decreases from 54 to 45nm in the investigated a different lanthanum doping rates for the precursors zinc acetate. But for zinc chloride the crystallite size of undoped and La-doped ZnO thin films is lying in 73 to 60nm domain, no extra phases involving chloride or lanthanum compounds were observed .

A good correlation between the results obtained by scanning electron microscope (SEM) and the spectra obtained by X-ray diffraction was observed and made it possible to demonstrate the good quality of the thin layers prepared.

For zinc acetate precursor the optical transmission spectra of ZnO:La films were prepared films exhibit a high transparency lying around 95 % in the visible domain. The optical band gap increases with the doping concentration from 3.24 to 3.27eV, these are related to the decrease in the film disorder from 56 to 84meV. But for zinc chloride the optical transmission spectra of the films exhibit a high transparency lying between 78 and 90 % and interference fringes in the visible domain. The transmission is found to be maximal for ZnO :La 0% film and decreased with an increase in La content. These fringes are due to the multiple reflection on the two film interfaces which indicates that the films prepared with these conditions are smooth . The decrease of Eg value may be due to the increase in the concentration of defects in the crystals with doping. The doping results in the rise of additional band tail states, leading to shrinkage of the band gap. This phenomenon, which causes the decrease in Eg, is generally in competition with another called: the Burstein Moss shift.
The existence of functional groups and the Zn-O chemical bond are confirmed by Fourier transform infrared spectroscopy (FTIR), where it has been observed in particular the Zn-O stretching vibration bonds in the ZnO lattice; the wavelengths of vibration are located at $\approx 445.42 cm^{-1}$, we also observed the presence of the vibrations of elongation O-H, C-O, C-H, and a symmetrical bond C-H, of bending O-H, the vibration of elongation asymmetric of the carboxyl group have been assigned.

In the second part of this work is to removal of copper ions from aqueous solution by thin films of zinc oxide prepared on glass using spray pyrolysis with moving nozzle. The advantages of the prepared adsorbents in the present work are high adsorption capacity for Cu^{2+} and also ease of separation from the reaction medium. the elimination rate is 87 and 65% to 1.% by weight (La/Zn) under natural sunlight for the precursors acetate and zinc chloride respectively. Lanthanum is a good quality dopant to increase the adsorption capacity of ZnO thin films by increasing the active surface of the sample. After annealing the slides at different temperatures (200 to 350C °) for 1hour. We see that blades are covered with black and brown (CuO/Cu_2O) colored layers.

In the third part of this work have been characterized the layers after annealing by different techniques. From the investigation of substrate temperatures using copper chloride as precursor, the deposition rate decrease with increasing the substrate temperature; this is due to the evaporation of reactive species droplets and the thermal convection. The films structure reveals that all deposited films crystallize in monoclinic structure. The calculated texture coefficient reveals that CuO films deposited at 200 to 350°C have best crystallization level along preferred orientation (200). The crystallite size decreases from 18 to 8nm in the investigated substrate temperature. The SEM micrographs show that deposited films are homogenous, dense and compact. However, the films deposited with higher temperature are smoother than the films deposited with lower temperature. This can be related to the decrease in film thicknesses . the estimated thickness of which is around 1200-600nm.

The chemical composition of the CuO thin film was determined by the energy dispersive analysis X-ray spectra ,the elements identified in the thin layer of CuO are copper and oxygen also the presence of other elements in the spectrum originated from the substrate glass. The EDAX analysis does not reveal the presence of the other peaks which are at the origin of the impurities. This proves that the synthesized CuO is pure.

The transmission spectra of CuO thin films is clear that the deposited films exhibit a relatively high absorption ranged from 40 to 60 % for wavelengths greater than 600 nm.

The optical band gap increases with substrate temperature from 2.11 to 2.24eV, this is related to the decrease in the film disorder from 65 to 95 meV. The FTIR spectra of CuO thin films at different temperature on substrate of 1wt.% La-doped ZnO products .The absorption bands at 500 and 618cm-1 correspond to the stretching vibration of Cu-O bond in monoclinic CuO . It is worth noting that the absorption band of Cu-O becomes greater than those obtained from the as synthesized of copper oxide films revealing that the annealing treatment ameliorates the oxide copper thin layers .but other absorption bands correspond to the stretching vibration of Zn-O bond wurtzite hexagonal type ZnO crystal .

the films deposited with copper acetate at higher substrate temperature films grows with low deposition rate. The XRD analysis indicates that the obtained films have a monoclinic structure. The calculated texture coefficient shows that at lower substrate temperature, the films growth along (111) preferred orientation, contrary to preferred orientation ($\bar{1}11$) found for that deposited at higher substrate temperature. The best crystallinity is found for films prepared at 250°C. The increase of crystallite size and the decrease in strain confirms the crystallinity improvement of films deposited with increasing the substrate temperature.

The films transparency varied wildly, in the investigated temperature range. It is seen that the films become more transparent with the increase in substrate temperatures. For wavelength above 800 nm the transmittance of the whole films is ranged from 30 to 65 %.
The increase in optical band gap corroborates well the disorder reduction in films lattice .This confirms also the increase in optical band gap with substrate temperature increasing. The increase in the gap energy indicates that the disorder in films is reduced with substrate temperature.

Recommendations for Future Work

As there are still numerous opportunities for expending the research in alignment with the outcomes presented in this thesis, the author presents the following as the future outlook of this dissertation:

- It will be beneficial to investigate the films characterization of the different materials used for fabricated the heterojunctions such as: zinc oxide (ZnO) and cupric oxide (CuO) and the IV characteristic of the solar cells.

- For the measurement of the current-voltage characteristic of the fabricated p-CuO/n-ZnO heterojunctions as well as their performance.

- The result in this PhD thesis of CuO films characterization . It is possible application as sensitive layer and , the gas sensing performance of CuO based sensor towards organic vapor.

- CuO is a promising photo-catalyst that is used in many chemical processes, such as organic contamination degradation and water splitting under visible–light irradiation owing to their small band gap and low cost.

Publication

Defect and Diffusion Forum
ISSN: 1662-9507, Vol. 397, pp 206-212

Submitted: 2019-04-18
Revised: 2019-06-21
Accepted: 2019-06-22
Online: 2019-09-24

Effect of La Doping on ZnO Thin Films by Spray Pyrolysis

Allag Nassiba[1,3,a*], Ben Haoua Boubaker[2,b], Saied Chahnez[3,c], Barani Djamel[1,d], Segueni Leila[4,e] and Gasmi Brahim[3,f] , Achour Rahal[2,g], Atmane Benhaoua[2,h] and Abdelkader Hima[1,i]

[1]Faculty of Technology, Univ. El Oued, 39000 El Oued, Algeria

[2]Unité de Développement des Energies Renouvelables dans les Zones Arides (UDERZA), Univ. El-Oued, 39000 El Oued, Algeria

[3]Laboratoire de Physique des Couches Minces et Applications (LPCMA), Univ. Biskra, 07000 Biskra, Algeria

[4]Faculty of Exacts Sciences, Univ. El Oued, 39000 El Oued, Algeria

[a*]nousseiba_allag@yahoo.fr, [b]benhaouab@yahoo.com, [c]chahnez71@yahoo.fr, [d]djamel.chim@gmail.com , [e]segueni-laila@univ-elouded.dz , [f]brahim_gasmi@yahoo.fr , [g]rahalachour@yahoo.fr , [h]atmanbenhaoua@yahoo.fr , [i]abdelkader-hima@univ-eloued.dz

Keywords: Zinc, thin films, XRD, UV-Visible, Spray, oxide, Pyrolysis.

Abstract. In this study, Zinc oxide (ZnO) undoped and Lanthanum doped (ZnO: La) thin films were deposited on 400°C heated glass using spray pyrolysis technique with moving nozzle. The components (Zn $(CH_3COO)2$, $2H_2O$) and ($LaCl_3$, $7H_2O$) were used as sources to produce ZnO thin film and doped Lanthanum, respectively. Effects of dopant on the optical and structural properties of undoped and 0, 2 and 4 wt. % Lanthanum doped ZnO thin films were studied. Optical transmittance spectra of the films showed high transparency of about 98% in the visible region. The optical gap for ZnO and 0, 2 and 4 wt. % La doped ZnO thin films were found to be in 3.25-3.28 [eV] range. The X-ray diffraction showed that the thin films have hexagonal wurtzite structure with a strong (*002*) as preferred orientation, whereas the crystalline size was ranged in 15.89-33.45 nm. The ZnO thin films are promising to be used a light emitting diodes, gas sensor and UV detectors applications.

Introduction

Recently, thin films and especially the transparent semiconductor oxides (TSOs) have been widely invested by the scientific community and applied by the industry for different optoelectronic devices, the most used TSO's such as In_2O_3, ZnO, and ITO show considerable interest due to their unique optical, electronic and piezoelectric properties. ZnO offers a wide range of applications such as solar cells [1], diluted magnetic semiconductors [2] nanopiezotronics [3], UV detectors [4], gas sensors [5], light emitting diodes [6], etc. ZnO is a direct band gap semiconductor (Eg = 3.37 eV at room temperature) and has a large exciton binding energy (60 meV) [7]. ZnO is an n-type II-VI semiconductor most stable when crystallized in wurtzite structure. ZnO has the richest range of morphologies. Additionally, it has been found to display good photoconductivity and high transparency in the visible region. Various physical and chemical routes were used to synthesize RE+3-doped nanostructure material: electrochemical deposition [8], hydrothermal method [2, 4, 6], chemical vapor deposition (CVD) [3], sol-gel method [5, 10, 11], precipitation [9], solution combustion [12], and magnetron sputtering [13]. In this research, a facile route of spray pyrolysis of La-doped ZnO thin films at low temperature was created. A possible mechanism on the growth of La-doped ZnO thin films was explained. In the end, the photocatalytic performance of pure ZnO and La-doped ZnO was investigated. It was found that La-doped ZnO showed better photocatalytic performance than pure ZnO.

Experimental Methods

Solutions and thin films preparation

ZnO thin films were deposited on 400°C heated glass substrates using a spray pyrolysis method. By dissolving (1M) zinc acetate dihydrate (Zn (CH3COO)2, $2H_2O$) in the solvent containing equal volumes of double distilled water and absolute methanol solution (purity: 99.995%), undoped ZnO thin films solution was ready. Few drops of the concentrated acetic acid solution were added to the prepared solution as a stabilizer. The mixture solution was stirred at 50°C for 2 hours to have a clear and transparent solution. For Lanthanum doping, ($LaCl_3$, $7H_2O$) with the appropriated ratio of La/Zn (0, 2 and 4wt. %) was added to the precedent solution. Each solution, with the appropriated ratio of La/Zn, became homogeneous and clear after stirring for 2 hours too. For non-doped and La-doped ZnO thin films, the resulting solutions were sprayed on the heated substrates. The deposition of ZnO thin films was performed for 10 min with keeping the moving nozzle-substrate distance equal to 7cm. The substrates are microscope glass with compressed air.

Characterization

Optical transmittance spectra were carried out using a UV-Visible spectrophotometer (Shimadzu, Model 1800) operating in the range of 200-900 nm. Structural characterizations are implemented using X-Ray diffractometer (BRUKER - AXS type D8) under Cu Kα (λ = 1.5405 A˚) radiation while the full scanning range of (2θ) was between 10° and 80°. Fourier transforms infrared (FTIR) spectra of the powders (were recorded using a Fourier transform infrared spectrometer (Perkin Elmer) in the range of 4000–400 cm^{-1} with a resolution of 1 cm^{-1}.

Results and Discussion

Optical properties

All the ZnO thin films were n-type and films have an optical transmission of about 95% in the visible region Fig. 1 shows the transmission spectrum of a ZnO thin film with a different dopant.

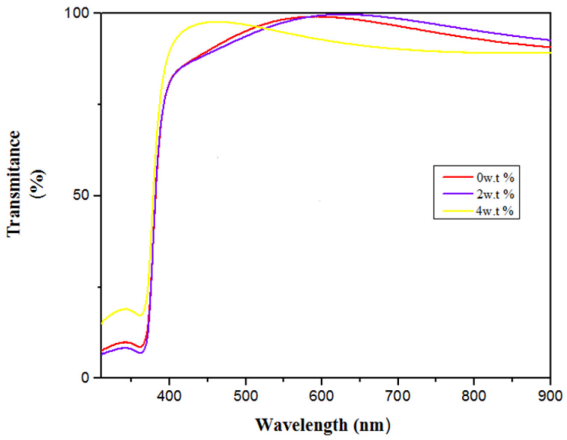

Fig. 1 Optical transmission spectra of spray pyrolysis doped and undoped La- ZnO thin films at 400C°.

The optical energy band gap (E_g) of ZnO thin films was 3.25-3.28 [eV] (inset of Fig. 2) as estimated from Tauc plot (Eq. (1)).

$$(\alpha h\upsilon)^2 = A(h\upsilon - E_g) \quad (1)$$

where α is absorption coefficient,$h\nu$ is the photon energy, A is a constant, E_g is the optical band gap. For E_g values were deduced from the transmission by extrapolating $(\alpha h\nu)^2 = 0$. The optical band gap values as in Table I.

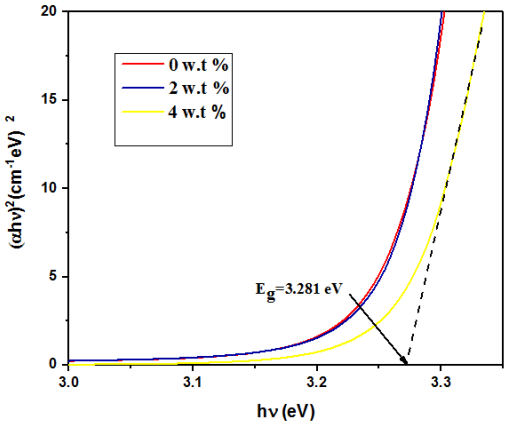

Fig. 2 The optical band gap of doped and undoped La- ZnO thin films.

Fig. 2 shows a plot of the variation in band gap energy with a different dopant and it is observed increases the band gap energy of ZnO after doping. The increase in the values of band gap energy with different dopant is attributed to the decrease in crystallinity and grain size of ZnO films [14].

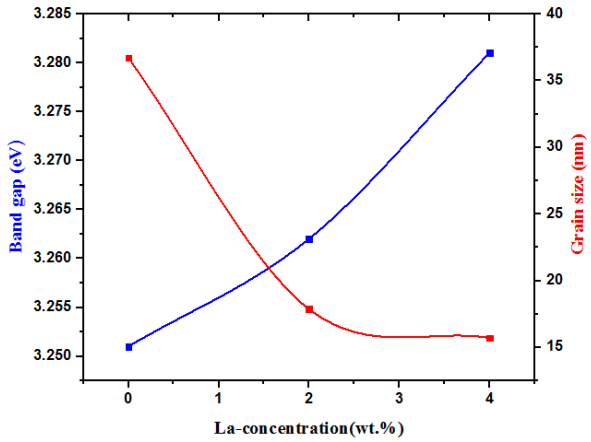

Fig. 3 Plot of grain size and band gap versus La- concentration of ZnO thin films.

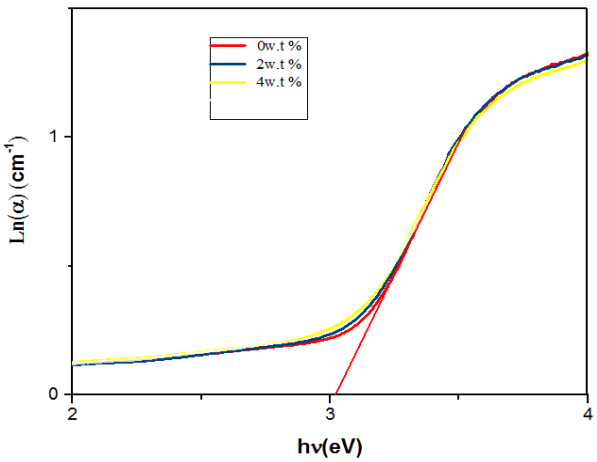

Fig. 4 Urbach energy (E_g) of La doped ZnO thin films.

Table 1 Optical parameters of 0-4wt % La-ZnO thin films: optical transmittance, band gap and Urbach energy.

Material	*Transmittance T (%)*	E_g *[eV]*	E_{Urbach} *[meV]*
ZnO: La (0 wt.%)	96	3.251	84.85
ZnO: La (2 wt.%)	97	3.262	80.42
ZnO: La (4 wt.%)	97	3.281	76.35

As Fig. 4 displays, Urbach energy (E_u) of ZnO thin films with different La doping levels, the E_u reflects the disorder in the thin film network; it is related to the absorption coefficient by the following relation (Eq. (3)) [15]:

$$a = a_0 \exp\left(h\nu / E_u\right) \tag{2}$$

where a_0 is a constant; E_u is the Urbach energy. The values of Urbach energy in these thin films varies from 76.35 to 84.85 meV.

Structural properties

The XRD patterns of ZnO thin films with different dopant are shown in Fig. 5. The diffraction peaks correspond to the wurtzite ZnO having a hexagonal structure (JCPDS No. 36-1451) [16]. The crystallinity of the films decreases after doping. The average crystallite size as calculated from XRD by Scherer equation (Eq. (3)) [17] is found to increase doping (Fig. 5).

$$D = \frac{K\lambda}{\beta \cos\theta} \tag{3}$$

where D is the crystallite size, K is the shape factor lying between 0.95 and 1.15 depending on the shape of the crystals and in the present study the value is assumed to be 1, β is the full width at half maximum (FWHM) of the diffraction peak in radians, θ is the Bragg angle of the diffraction peak and λ is the wavelength of X-rays [18]. The average crystallite size was found to be 33, 17 and 15 nm respectively for the La-ZnO films at 0, 2 and 4 wt%.

The texture coefficients $TC(hkl)$ have been based on the following formula [19]:

$$TC(hkl) = \frac{I(hkl)/I_0(hkl)}{N^{-1}\sum_n^N I(hkl)/I_0(hkl)} \tag{4}$$

where $TC(hkl)$ is the texture coefficient of the plane (hkl), $I(hkl)$ is the measured intensity, $I_0(hkl)$ is the standard intensity, N is the reflection number and n is the number of diffraction peaks. The preferred crystallographic orientation of the undoped and La-doped thin films was along (*002*). For the calculation of lattice parameter c and the inter-planer spacing d_{hkl}, we have used the following formulas [13]:

$$\frac{1}{d_{hkl}^2} = \frac{4}{3}\left(\frac{h^2 + hk + k^2}{a^2}\right) + \frac{l^2}{c^2} \tag{5}$$

where d_{hkl} is the distance between two adjacent parallel planes of the family hkl, (hkl) are the Miller indexes and 'a', 'b' and 'c' are the lattice parameters. The standard and calculated lattice parameters have been summarized in Table II. The increase in lattice parameter c of La-doped ZnO may be due to the large difference between the substitute ionic radius of La^{+3} (1.15 Å) with Zn^{+2} (0.74 Å) into the ZnO lattice and its decrease may be attributed to the loss in the substitutional position of La^{+3} ion in the ZnO lattice [20].

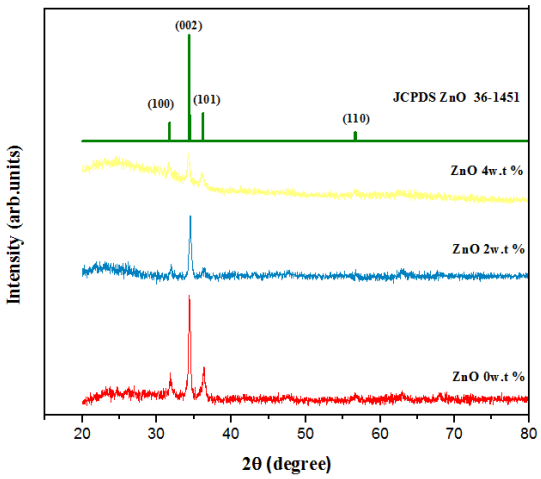

Fig. 5 XRD patterns of 0,2 and 4 wt. % La doped ZnO films.

Table 2 Lattice parameters *a*, *c*, of 0, 2 and 4 wt. % La doped ZnO.

ZnO: La	*LATTICE PARAMETERS*			
	a=b[A°]	***c[A°]***	***D[nm]***	***Stress[10^9 Pa]***
0 wt. %	3.246	5.202	33.12	-0.28
2 wt. %	3.262	5.213	17.43	-1.32
4 wt. %	3.268	5.244	15.21	-1.57

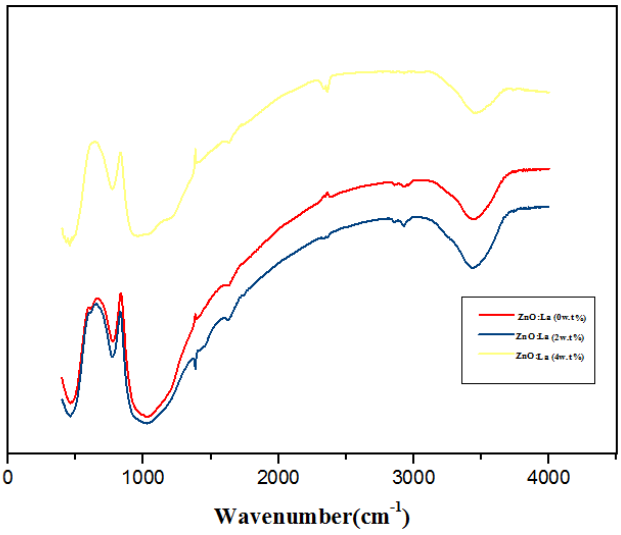

Fig. 6 FTIR spectra of pure ZnO and La-doped ZnO thin films by spray pyrolysis.

Fig. 6 shows FTIR spectra of 0 wt%,2.0 wt% and 4wt% La-doped ZnO products. The strong absorption bands at 426 and 565 cm^{-1} are attributed to the Zn–O stretching vibration of wurtzite hexagonal type ZnO crystal [21, 22], belonging to the oxygen sublattice (E2H) vibration and oxygen vacancies of wurtzite ZnO crystal, respectively [23]. The broad absorption bands at 3013–3633 cm^{-1} are the O–H stretching vibration of adsorbed water on the ZnO surface [24].

Summary

La-doped ZnO thin films with different dopant rates were deposit by spray pyrolysis on heated glass substrates. Effects of dopant on the structural, optical of 0, 2 and 4 wt. % lanthanum doped ZnO thin films were studied. The optical transmittance in the visible region was more than 96% for all thin films. The optical band gap for undoped ZnO and La-doped ZnO thin films increases from 3.25eV to 3.28 eV. The X-ray diffraction appeared that all the thin films the wurtzite ZnO having a

hexagonal structure. The preferential orientations of undoped and doped ZnO was along (*200*) planes. The crystalline sizes for undoped and La-doped ZnO thin films were in the range between 33.63 nm and 15 nm. La-doped ZnO has an excellent photocatalytic activity than pure ZnO for degradation of MB under UV irradiation. This research may provide guidance for the treatment of organic pollutants.

Acknowledgment

This study was supported in part by RERUAZ Renewable Energy Research Unit in Arid Zones El-Oued University. X-ray diffraction data in this work were supported by the University of Biskra. We thank Prof. Abdelouahed Chala and Touhami hanane (Biskra University) for the XRD characterization.

References

[1] P.S. Reddy, G.R. Chetty, S. Uthanna, B.S. Naidu, P.J. Reddy, Optical properties of spray deposited ZnO films, Solid State Common 77 (12) (1991) 899–901.

[2] I. Djerdj, G. Garnweitner, D. Arcon, M. Pregelj, Z. Jaglicic, M. Niederberger, Diluted magnetic semiconductors: Mn/Co-doped ZnO nanorods as case study, J. Mater.Chem. 18 (2008) 5208–5217.

[3] J. Volk, T. Nagata, R. Erdelyi, I. Barsoni, A.L. Toth, I.E. Lukacs, Z. Czigany, H. Tomimoto, Y. Shingaya, T. Chikyow, Highly uniform epitaxial ZnO nanorod arrays for nanopiezotronics, Nanoscale Res. Lett. 4 (2009) 699–704.

[4] A. Bechen, M. Durr, L.P. Nostro, P. Baglioni, Synthesis and characterization of zinc oxide nanoparticles: application to textiles as UV-absorbers, J. Nanoparticle Res. 10 (2008) 679–689.

[5] D.S. Bohle, C.J. Spina, Controlled Co(II) doping of zinc oxide nanocrystals, J. Phys. Chem. C 114 (2010) 18139–18145.

[6] M. Esro et al., "Solution processed SnO_2:Sb transparent conductive oxide as an alternative to indium tin oxide for applications in organic light emitting diodes," J. Mater. Chem. C, vol. 4, no. 16, pp. 3563–3570, 2016.

[7] Y. Jouane, S. Colis, G. Schmerber, P. Kern, A. Dinia, T. Heiser, Y.A. Chapuis, Room temperature ZnO growth by rf magnetron sputtering on top of photoactive P3HT: PCBM for organic solar cells, J. Mater. Chem. 21 (2011) 1953–1958.

[8] Bappaditya Pal, P.K. Giri, Roomtemperature ferromagnetismin Co doped ZnO nanoparticles, J. Nanosci. Nanotechnol. 11 (2011) 1–8.

[9] D. P. Joseph, P. Renugambal, M. Saravanan, S. P. Raja, and C. Venkateswaran, "Effect of Li doping on the structural , optical and electrical properties of spray deposited SnO_2 thin films," Thin Solid Films, vol. 517, no. 21, pp. 6129–6136, 2009.

[10] Bappaditya Pal, P.K. Giri, Roomtemperature ferromagnetismin Co doped ZnO nanoparticles J. Nanosci. Nanotechnol. 11 (2011) 1–8..

[11] J. Tauc, The optical properties of solids, (J. Tauc, ed.), Academic Press, New York (1966) 277.

[12] C. S. Barret, T. B. Massalski, Structure of Metals, Pergamon Press, Oxford,1980.

[13] C. Marcel, N. Naghavi, G. Couturier, J. Salardenne, J. M. Tarascon, J. Appl. Phys. 91 (2002) 4291.

[14] M.-M Bagheri-Mohagheghi, N. Shahtahmasebi, M.R. Alinejad, A. Youssefi, M. Shokooh-Saremi,"Fe-doped SnO_2 transparent semi-conducting thin films deposited by spray pyrolysis technique Thermoelectric and p-type conductivity properties",Solid State Sciences 11(2009) 233-239.

[15] M. Kurik, "Urbach rule," physica status solidi (a), vol. 8, pp. 9-45, (1971).

[16] P. Scherrer, Gottinger Nachrichten 2 (1918) 98.

[17] A. Rahal, A. Benhaoua, C. Bouzidi, B. Benhaoua, and B. Gasmi, "Effect of antimony doping on the structural, optical and electrical properties of SnO_2 thin films prepared by spray ultrasonic," SUPERLATTICES Microstruct., 2014.

[18] R. Mohan, K. Krishnamoorthy, S.J. Kim, Diameter dependent photo-catalytic activity of ZnO nanowires grown by vapour transport technique, Chem. Phys. Lett. 539–540(2012) 83–88.

[19] Nadia Febiana Djaja, Dionisius Agung Montja, Rosari Saleh, The effect of Co incorporation into ZnO nanoparticles, J. Adv. Mater.Phys. Chem. 3 (2013) 33–41.

[20] A. Moulahi, F. Sediri, ZnO nanoswords & nanopills: hydrothermal synthesis, characterization & optical properties, J. Ceram. Int. 40 (2014) 943–950.

[21] A. Sivagamasundari, R. Pugaze, S. Chandrasekar, S. Rajagopan, R. Kannan, Absence of free carrier and paramagnetism in Co doped ZnO nanoparticles synthesized at low temperature using citrate sol–gel route, J. Appl. Nanosci. 3 (2013) 383–388.

[22] Cristina D. Ghitulica, Mihaela Popa, Raluca Mereu, Adriana Popa,Traian Petrisor Jr., Mihai Gabor, Adrian Ionut Cadis, Bogdan S. Vasile, Synthesis, structural and morphological characteristics, magnetic and optical properties of Codoped ZnO nanoparticles, Ceram. Int. 40 (2014) 2835–2846.

[23] A. Manikandan, J. Judith Vijaya, J. Arul Mary, L. John Kennedy, A. Dinesh, Structural, optical and magnetic properties of Fe3O4 nanoparticles prepared by a facile microwave combustion method, J. Ind. Eng. Chem. 20 (2014) 2077–2085.

[24] Amalia Mesaros, Cristina D. Ghitulica, Mihaela Popa, Raluca Mereu, Adriana Popa, Traian Petrisor Jr., Mihai Gabor, Adrian Ionut Cadis, Bogdan S. Vasile, Synthesis, structural and morphological characteristics, magnetic and optical properties of Co doped ZnO nanoparticles, Ceram. Int. 40 (2014) 2835–2846.